AD-A035 960 KAMAN AEROSPACE CORP BLOOMFIELD CONN F/G 20/11
LABORATORY VERIFICATION OF FORCE DETERMINATION, A POTENTIAL TOO--ETC(U)
JAN 77 W G FLANNELLY, F D BARTLETT DAAJ02-75-C-0004
UNCLASSIFIED R-1457 USAAMRDL-TR-76-38 NL

1 OF 2
AD A035960

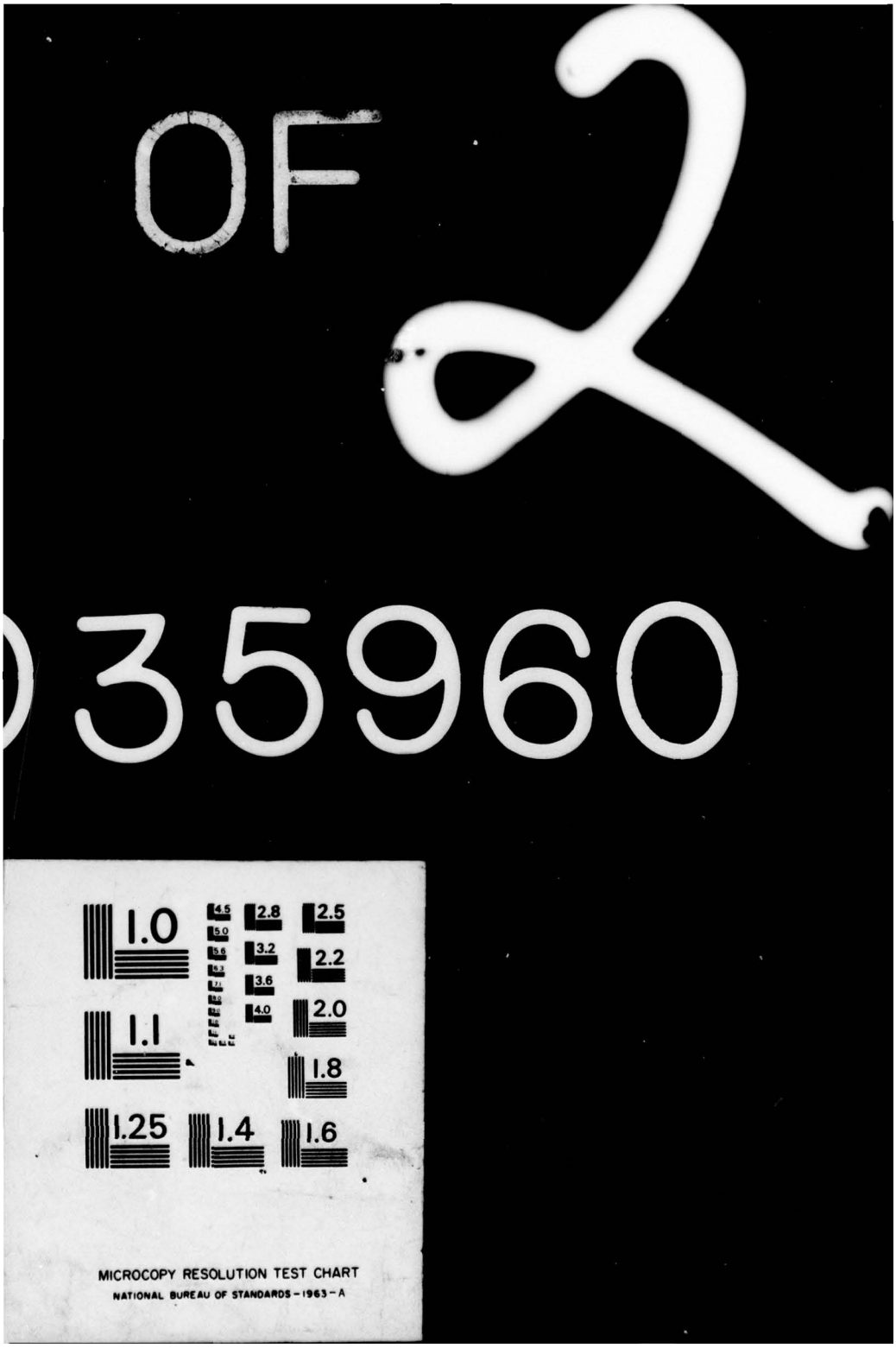
OF
035960
1.0
1.1
1.25
1.4
1.6
1.8
2.0
2.2
2.5
2.8
3.2
3.6
4.0
4.5
5.0
5.6
6.3
MICROCOPY RESOLUTION TEST CHART
NATIONAL BUREAU OF STANDARDS-1963-A

USAAMRDL-TR-76-38

LABORATORY VERIFICATION OF FORCE DETERMINATION, A POTENTIAL TOOL FOR RELIABILITY TESTING

Kaman Aerospace Corporation
Old Windsor Road
Bloomfield, Conn. 06002

January 1977

Final Report

Prepared for

EUSTIS DIRECTORATE
U. S. ARMY AIR MOBILITY RESEARCH AND DEVELOPMENT LABORATORY
Fort Eustis, Va. 23604

EUSTIS DIRECTORATE POSITION STATEMENT

A method for determining rotor hub loads (forces and moments) directly from measured fuselage accelerations was successfully demonstrated. The method, called Force Determination, was verified on a laboratory model representative of a helicopter in terms of mass and stiffness distributions, natural frequency, and structural damping. Following calibration of the 5-foot dynamic model, known vertical and lateral hub forces were applied simultaneously and the fuselage responses recorded. Using these responses and the calibration data, the hub forces were calculated using Force Determination. The overall accuracy was excellent. In general, the errors in the predicted hub forces were within the achievable accuracy limits of the instrumentation. The errors were on the order of 2-5% in amplitude and 2-4 degrees in phasing. In cases where the model was calibrated at a nominal gross weight and cg and then tested with force predictions made at a condition of extreme gross weight or cg, errors of 22-24% resulted. However, when calibrated for the tested gross weight and/or cg, the errors returned to the above-cited excellent results. This suggests that for actual aircraft use, calibration of the vehicle should not simply be done once but for a set of conditions representing the operational gross weight and cg range.

It has been concluded that Force Determination is a technique "in-the-bud" which, if successfully developed and implemented, could "blossom" into a technological breakthrough with far-reaching developmental and operational possibilities. The possibilities foreseen are: (1) Force Determination could expedite helicopter development. During flight test development hub loads over the mission profile could be determined. In turn, engineers could duplicate these loads on an actual helicopter in an accelerated, ground-based, simulated flight test to establish system and component reliability. Failures and their modes would be exposed much earlier in the development phase. Being ground-based, conditions pertinent to damage/failure modes could be easily observed, permitting timely, effective redesign prior to fleet introduction. And (2), operationally, "lead-the-fleet" endurance testing is foreseen. This would allow low-cost, highly-responsive reliability testing for detecting problems before they arise in the field and allow the evaluation of corrective redesigns before they are deployed in the field. With "lead-the-fleet" testing, it is envisioned that sensors, small units not encumbering vehicle utility, would be "planted" in aircraft delivered to the fleet to record in-flight responses; and hub loads, determined from these responses, could be used for accelerated endurance testing to induce failures before they occur in the fleet.

Demonstration of this new method on an Army inventory helicopter is planned.

This program was conducted under the technical cognizance of Joseph H. McGarvey, Military Operations Technology Division.

UNCLASSIFIED

SECURITY CLASSIFICATION OF THIS PAGE (When Data Entered)

REPORT DOCUMENTATION PAGE

READ INSTRUCTIONS BEFORE COMPLETING FORM

1. REPORT NUMBER: USAAMRDL TR-76-38
2. GOVT ACCESSION NO.:
3. RECIPIENT'S CATALOG NUMBER:

4. TITLE (and Subtitle): LABORATORY VERIFICATION OF FORCE DETERMINATION, A POTENTIAL TOOL FOR RELIABILITY TESTING

5. TYPE OF REPORT & PERIOD COVERED: Final Report

6. PERFORMING ORG. REPORT NUMBER: R-1457

7. AUTHOR(s): William G. Flannelly, Felton D. Bartlett, Jr., Thomas W. Forsberg

8. CONTRACT OR GRANT NUMBER(s): DAAJ02-75-C-0004

9. PERFORMING ORGANIZATION NAME AND ADDRESS: Kaman Aerospace Corporation, Old Windsor Road, Bloomfield, Connecticut 06002

10. PROGRAM ELEMENT, PROJECT, TASK AREA & WORK UNIT NUMBERS: 62209A 1F262209AH76 00 030 ER

11. CONTROLLING OFFICE NAME AND ADDRESS: Eustis Directorate, U.S. Army Air Mobility R&D Laboratory, Fort Eustis, Virginia 23604

12. REPORT DATE: January 1977

13. NUMBER OF PAGES: 109

14. MONITORING AGENCY NAME & ADDRESS (if different from Controlling Office)

15. SECURITY CLASS. (of this report): Unclassified

15a. DECLASSIFICATION/DOWNGRADING SCHEDULE

16. DISTRIBUTION STATEMENT (of this Report)

Approved for public release; distribution unlimited.

17. DISTRIBUTION STATEMENT (of the abstract entered in Block 20, if different from Report)

18. SUPPLEMENTARY NOTES

19. KEY WORDS (Continue on reverse side if necessary and identify by block number)

Force Determination	Testing	System Identification
Dynamics	Forces & Moments	Normal Modes
Helicopters	Shaking	Impedance, Mechanical
Shake Testing	Flight Testing	Vibrations

20. ABSTRACT (Continue on reverse side if necessary and identify by block number)

Results of laboratory tests on a helicopter dynamic model show that the external vibratory forces, such as those of main and tail rotors, acting on a helicopter can be accurately determined from flight tests using only accelerometers in the fuselage.

The contract was in three tasks: (I) Design and fabrication of a model representative of helicopters in terms of mass and stiffness distribution as well as natural frequency and structural damping; (II) Dynamically calibrate the model followed by exciting the hub with

DD FORM 1 JAN 73 1473 EDITION OF 1 NOV 65 IS OBSOLETE

UNCLASSIFIED

SECURITY CLASSIFICATION OF THIS PAGE (When Data Entered)

404362

20. ABSTRACT (Continued)

known forces and verify the method of Hub Force Determination by calculating what the forces must have been, using the measured fuselage accelerations and the dynamic calibration data as a basis; and (III) Dynamically calibrate the model by both direct hub excitation and single-point excitation at any other convenient point. This third task was to demonstrate that single-point excitation can yield fuselage accelerations which together with the methods of Modal Acceleration testing and Force Determination could be used as a viable structural dynamic test method, yielding the same results as if the structure had been excited at the hub. If successful, a considerable time and cost savings would be realized. It would no longer be necessary to shake the helicopter at the hub. Instead, shaking could take place with the excitation applied at any convenient point other than a node.

Following calibration of the 5-foot dynamic model, known vertical and lateral hub forces were applied simultaneously. Different flight speeds and maneuvers were represented by different magnitudes and phasings of the shaker forces at the hub. This was done for various "rotor speeds" (shaker frequencies) as well as a broad range of gross weight and CGs. For each flight condition the amplitudes and phasings of the twelve fuselage accelerometers were recorded. Using these recorded responses and the calibration data, the hub forces were calculated using Force Determination. A total of 81 test cases were run covering 54 combinations of vertical and lateral forces over phase angles ranging from 0^{o} to 180^{o}. The overall accuracy of Force Determination was shown to be excellent. In general, the errors in the predicted hub forces were within the achievable accuracy limits of the instrumentation. The errors were on the order of 2-5% in amplitude and 2-4 degrees in phasing. In cases where the model was calibrated at a nominal gross weight and cg and then tested with force predictions made at a condition of extreme gross weight or cg, errors of 22-24% resulted. However, when calibrated for the tested gross weight and/or cg, the errors diminished to the above-cited excellent results. This suggests that for actual aircraft use, calibration of the vehicle should not simply be done once but for a set of conditions representing the operational gross weight and cg range. These results were equally good whether the model was actually shaken at the hub or at some convenient fuselage station. Thus, the additional advantages of single-point excitation appear to be realizable.

PREFACE

The work of this contract was under the technical direction of Joseph H. McGarvey, Eustis Directorate, U. S. Army Air Mobility Research and Development Laboratory (USAAMRDL), Fort Eustis, Virginia. Dr. Felton D. Bartlett, Jr., a principal investigator on this project while employed by Kaman Aerospace Corporation, is now employed by Langley Directorate, USAAMRDL.

Force determination on the Bell UH-1H DAVI-equipped aircraft was done under the technical supervision of Robert Jones. Alex Berman served as analytical consultant and Nicholas Giansante as experimental consultant in the investigations. The helicopter dynamic model was constructed by Harry A. Cooke and W. T. Rhodes. Among those contributing to the instrumentation work were D. Stewart, I. N. Johnson, and R. F. Metzger. G. T. Neu was engineering editor of the final report.

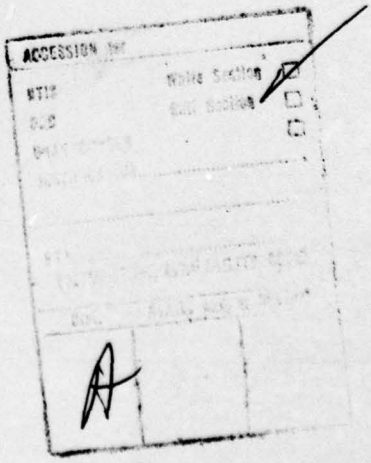

TABLE OF CONTENTS

TABLE OF CONTENTS (Continued)

LIST OF ILLUSTRATIONS

LIST OF ILLUSTRATIONS (Continued)

LIST OF TABLES

LIST OF TABLES (Continued)

INTRODUCTION

APPLICATION OF FORCE DETERMINATION TO RELIABILITY

Reliability and Vibration

The Army has a continuing goal of improving the reliability of its aircraft and particularly its helicopters. Although in recent years availability rates of helicopters have approached and sometimes exceeded those of fixed-wing aircraft, it has only been at a very high cost in maintenance man-hours, spares bought and stocked, and excessive depot overhaul of aircraft and components.

A fundamental cause of the high maintenance man-hours, the frequent component replacement, and the generally low helicopter reliability, is the high vibratory loads the machine experiences. In general, the highest vibratory loads are generated by the rotor and occur at blade passage frequencies, although there are significant loads at other frequencies. All major helicopter manufacturers have published technical reports and papers outlining their efforts to reduce these vibrations and hence increase reliability. One study (Reference 1), performed by Sikorsky under contract to the Eustis Directorate of USAAMRDL, found very large increases in helicopter reliability resulting from the reduction in blade passage frequency forces transmitted to the fuselage.

There are three major technical thrusts in the industry for increasing the reliability of helicopters by reducing the vibratory forces and moments transmitted to the fuselage from the rotor: (1) improved rotor design; (2) rotating system dynamic absorbers (hub absorbers, blade absorbers); and (3) rotor isolation (antiresonant, conventional, and active). Excellent progress has been made in these areas in recent years in spite of technical problems.

Force Determination

A technique developed by Kaman Aerospace Corporation under contract to the Eustis Directorate, USAAMRDL, is a solution to many of the technical problems which frustrate continued progress in the three areas listed above.[2] This technique is called force determination. Force determination is a method for determining the magnitudes and phasings of vibratory

[1] Angelo C. Veca, VIBRATION EFFECTS ON HELICOPTER RELIABILITY AND MAINTAINABILITY, Sikorsky Division, United Technologies Corp.; USAAMRDL Technical Report 73-11, Eustis Directorate, U. S. Army Air Mobility Research and Development Laboratory, Fort Eustis, VA, April 1973, AD 766307.

[2] W.G. Flannelly and N. Giansante, EXPERIMENTAL VERIFICATION OF SYSTEM IDENTIFICATION, Kaman Aerospace Corporation; USAAMRDL Technical Report 74-64, Eustis Directorate, U. S. Army Air Mobility Research and Development Laboratory, Fort Eustis, VA, August 1974, AD 784190.

rotor forces and moments (and other external forces and moments) on a helicopter in flight through accelerometer measurements on the fuselage only.

Rotor Analysis Correlation and Vibration Effects of Proposed Rotors

In 1974, Dr. R. A. Ormiston of USAAMRDL conducted a comparative test of rotor loads analysis methods of the U. S. military helicopter industry.[3] "Large" to "very large" differences in root shears were found among the analytical methods of the industry but experimental data were not available for establishing the accuracy of any loads prediction method. Dr. Ormiston's findings raise disquieting questions on the validity of rotor model shear predictions.

A great deal of effort in the helicopter industry is devoted to improvements in the mathematical analysis of rotors. If analysts had at hand accurate in-flight measurements of the magnitudes and phasings of hub shears and moments in various maneuvers, they could then cheaply and conveniently correlate predictions from their mathematical rotor models over a range of forward speeds. This would enable them to select more rapidly the most suitable mathematical models for each case and thereby permit faster and more effective improvements in rotor analysis computer programs.

Although prediction of hub shears and moments is not the sole measure of rotor model accuracy, force determination allows these predictions to be checked against known flight loads. This check serves as a valuable indication of the model's overall validity and allows the engineer to weed out those models demonstrably unsuitable or select from among alternative models.

Having a rotor model whose validity has been verified within the flight regimes of interest will be of inestimable benefit. New rotors proposed for existing aircraft can be analyzed to evaluate the fatigue-producing vibratory loads. If the analysis shows improvement, the manager can move from design to hardware with much more confidence than heretofore possible. In short, force determination will permit the verification of mathematical formulations of rotors based on information gathered in flight in a manner that has not been possible previously.

Rotor Absorber and Isolator Design

The motions which a rotor absorber or a rotor isolator must undergo, and therefore the size of such devices, depend on the magnitudes and phasings of rotor shears and moments to which the absorber is subjected, and on

---

[3] R. A. Ormiston, COMPARISON OF SEVERAL METHODS FOR PREDICTING LOADS ON A HYPOTHETICAL HELICOPTER ROTOR, Proceedings of the Meeting of Specialists on Rotorcraft Dynamics, American Helicopter Society and Ames Research Center, Sponsors, 13-15 February 1974.

the mobility of the fuselage at its attachment points. The fuselage mobility also determines bandwidth for a given weight. Force determination provides both pieces of necessary information - excitation and mobility - from actual testing, thereby eliminating much of the trial and error in flight testing rotor isolator and absorber designs.

Rotor absorbers and isolators do not usually reduce all the rotor forces and moments transmitted to the fuselage, and even improved rotor designs may decrease some of the hub loads while increasing others. The engineer needs to know the phasing among the hub loads to decide which should be reduced to provide the lowest vibration at any given point on the ship. Reducing only the largest load may actually increase the total vibration at critical fuselage points, as V. Sankewitsch of Boeing Vertol once pointed out with, in essence, the following physical explanation:

The resultant vibration, say in g's, at any point on the fuselage is the resultant of the vector sum of the vibrations at that point due to each of the hub excitations. An accelerometer on the centerline of the helicopter shows the resultant of the accelerations due primarily to vertical hub shear, longitudinal hub shear, and hub pitching moment as shown hypothetically in Figure 1. If the longitudinal force, which has the largest effect in this hypothetical example, is eliminated, the resultant vibration gets significantly worse.

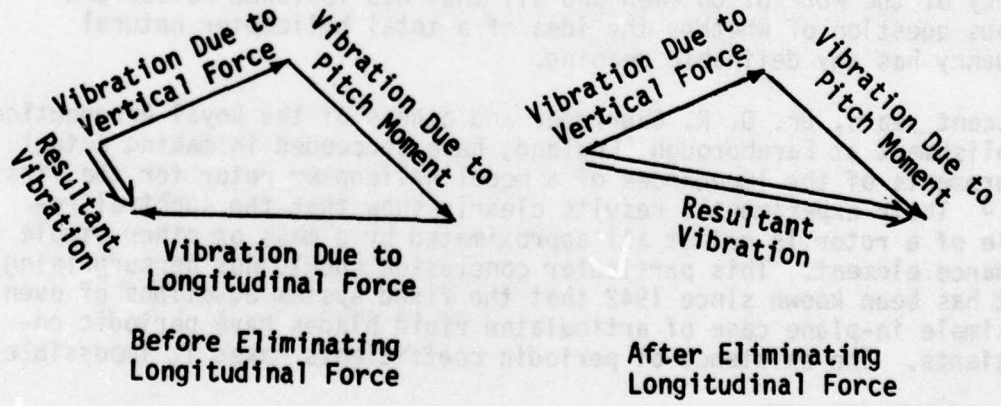

Figure 1. Effect of Eliminating a Force .

Removing only the largest hub force or moment can actually make the vibration worse because of the phasing of mobility and loads. Force determination testing would provide all the necessary decision-making information.

Rotor Mass in Shake Testing

With the results of force determination, flying, and the dynamic calibration in force determination ground testing, the engineer could predict the effects of changing any of the transmitted hub loads.

Shake tests of helicopters have had the unknown rotor impedances, which change the natural frequencies, "simulated" with purely conjectural lumped masses (sometimes equal to the rotor mass and sometimes half the rotor mass, depending on the preference of the individual engineer). The erroneous idea that some lumped mass is a practical approximation to rotor impedance probably originated with a misinterpretation of Coleman's pioneering work of the 1940's in mechanical instability, also known inaccurately but popularly as "ground resonance" from the early autogiro accidents.[4] Coleman used a lumped rotor mass at the hub for testing as a convenience because he approximated hub modal mass by shifts in the natural frequency with hub mass changes, a technique now known to be accurate only in a single degree of freedom system. However, Coleman accounted for the lumped mass in his analysis by coupling the hub response of the grounded fuselage with his in-plane rotor analysis of rigid hinged blades. He did not simulate hub impedance by a lumped mass.

A study of the work of Coleman and all that has followed raises the serious question of whether the idea of a total helicopter natural frequency has any definable meaning.

In recent years, Dr. D. R. Gaukroger and others of the Royal Aeronautical Establishment at Farnborough, England, have succeeded in making actual measurements of the impedances of a model helicopter rotor for the first time.[5] Their experiment's results clearly show that the spectral response of a rotor is not at all approximated by a mass or other simple impedance element. This particular conclusion should not be surprising as it has been known since 1942 that the fixed system equations of even the simple in-plane case of articulated rigid blades have periodic coefficients. The existence of periodic coefficients makes it impossible

---

[4] R.P. Coleman and A.M. Feingold, THEORY OF SELF-EXCITED MECHANICAL OSCILLATIONS OF HELICOPTER ROTORS WITH HINGED BLADES, National Advisory Committee for Aeronautics Technical Note 3844, February 1957.

[5] R. Cransdale, D.R. Gaukroger, and C.W. Skingle, A TECHNIQUE FOR MEASURING IMPEDANCES OF A SPINNING MODEL ROTOR, Royal Aircraft Establishment Technical Report 71092; Ministry of Defence, Farnborough Hants, England, May 1971.

to rigorously define a "lambda matrix" with roots (i.e., eigenvalues or characteristic values) so that, according to the Hamilton-Cayley Theorem (circa 1822), "natural frequencies" can be mathematically defined in the form in which we would like to use them in helicopter engineering. It seems reasonable to expect that no solutions to the problem will be found before the problem is defined.

DEFINING THE PROBLEM - FORCE DETERMINATION

What an engineer needs to know to make a helicopter shake test is not some value of the dubious abstract concept of "natural frequency" of the total system but the forces and the phasing of the excitations, how the helicopter responds to those excitations, and how those responses can be changed. Force determination divides the total problem into its definable and solvable parts, and gives the engineer information pertinent to dynamic evaluation.

The force determination approach divorces the unknown and undefinable classical dynamics of the rotor in the fixed system from the well-defined classical dynamics of the fuselage, thereby eliminating the situation and the problem mentioned above. Periodic coefficients or nonlinearities in the fixed system equations of the rotor are immaterial in force determination. The testing is rigorously correct when using zero hub mass because the response of the fuselage to rotor forces and moments is determined as the sum of products of the hub loads and the partial derivatives of the fuselage response with respect to the hub loads. The undefined question of "total helicopter natural frequencies" thus does not enter into the matter. It is replaced by more practical considerations of maximum fuselage response (roughly "fuselage natural frequencies") to rotor excitations and maximum actual rotor excitations from flight.

Full Ship Ground "Flight" Testing

Once having used force determination to find the magnitudes and phasings of the vibratory forces and moments acting on the aircraft in all the major flight conditions of the mission profile, engineers can reproduce these loads on an actual ship in a test bay. The reliability of the engine "motored" (turning slowly), the main and tail rotor transmission mounts and cases, the fuselage structure, the stabilization equipment, the secondary structure, the radios, the flight instruments, the navigation equipment, the external stores supports and other parts of the aircraft affected by the main and tail rotor induced vibration flight environment can then be evaluated by "ground flying" the ship 24 hours a day, 7 days a week.

Not only would this "ground flying" provide a very significant calendar time lead over actually flying aircraft to accumulate fatigue damage data, at the rate of up to eight thousand seven hundred flight hours per year, but, because the ship is on the ground, conditions pertinent to the damages can be easily observed. The opportunity to make such ground measurements as passive vibration surveys, acoustic emission monitoring

and electronic measurements with the ship in its flight vibration environment would open unprecedented possibilities for determining the causes of failures and for testing potential fixes long before the failures occur in flight.

The advantages of "ground flying" reliability testing apply to ships with a long service record as well as to new aircraft under development. Changes in mission profile and minor changes in aircraft equipment and structure often result in new reliability and maintainability problems, many of which could be prevented if the ship could be externally observed in its flight vibration environment. The kind of "ground flying" testing which force determination makes possible is by no means all-inclusive. The effects of main and tail rotor vibratory forces and the effects of other vibratory loadings on most of the helicopter components can be simulated, but ground flying does not include flight effects on the rotors. Rotating parts of the transmission, at least under torque load, are not accounted for, but the fatigue effects on the transmission case, which is a major load path, are simulated. The effects of the rotor-induced vibration environment on the actual engine can be ground-flight tested presuming that the engine is lubricated and motored, perhaps externally under no output load, to prevent false brinelling. Engines on helicopters have been shaken with the engine externally motored. In "ground flying", the helicopter would be under the steady flight 1.0-g download as, initially, the limit of interaction of steady and vibratory loadings. Eventually, using the Elastic Influence Coefficients to accurately simulate greater than 1.0 g-steady loads, engineers can further refine the total maneuver load simulation in "ground flying".

The inclusion of all main- and tail-rotor harmonics of rotor speed in "ground flying" is not beyond the state of the art, but insofar as simulating principal effects at reasonable cost, it should perhaps be left to eventual refinement.

How to "Ground Fly" a Helicopter

"Ground flying" a helicopter, even given the vibratory rotor loads from force determination, may not seem to be an entirely straightforward task, but it is quite within the state of the art. The first requirement is that we reproduce specific shears, moments and respective phase angles at the hub using shakers. For an arbitrary phase reference, say "A" blade passing zero azimuth, we have twelve variables for each harmonic at each hub: three forces, three moments and a phase angle associated with each. At the hub, this condition can be satisfied by six shakers properly arranged and properly controlled. The technology for the control of the phase and force magnitude of an electromagnetic shaker relative to any other electromagnetic shaker in a system is well established and equipment for doing this is commercially available; such equipment was used in this contract. The essential problem in "ground flight" testing is then seen to be that of using the mathematically-necessary six shakers in a manner that causes negligible interaction among the various coordinates in essentially reproducing the shears, moments and associated

phase angles found in force determination in flight.

Figure 2 shows a method of doing this. Essential to this particular method are relatively long cables and a lightweight pyramid which transmits forces to the hub. The long cables minimize interaction, and the lightweight three-dimensional truss construction of the force-transmitting pyramid minimizes drainage of the shaker forces to inertial space while retaining essential strength. The cables link the aircraft to the shaker with low spring-rate shock cord at both extremities beyond the shaker armature/aircraft connection. The armatures of the shakers are, of course, structurally integral with the cables. The cables are preloaded to static loads in excess of the vibratory forces produced by the shakers, thereby allowing the shakers, in the phraseology of freshman engineering, to "push on a rope". The low spring rate of the shock cord, or "bungee", extreme to the aircraft and the shakers, makes the mechanical impedance load of the tare on the shakers negligible compared to the mechanical impedance load of the aircraft on the shakers for all practical purposes. The spring rates of the cables do not diminish force transmission and are important only to the extent, in the frequency range of normal helicopter testing, that they are not so low as to not require excesses of the travel limitations of the shaker armatures. This matter is one of designer control, and solid steel straps with rod-end bearing connections might serve as well as cables.

The advantage of long cables, or straps, in minimizing interaction among the coordinates is best illustrated by example. With cables 20 feet long on either side of the pyramid preloaded statically to 3000 pounds, a hub vibration of 1.0 g at 10 cps produces a transverse interaction load of only 2.45 pounds. For a given frequency and g-loading at the hub, the transverse interaction load is inversely proportional to the equal cable length on either side of the ship. One would preload the cables to slightly greater than the maximum vibratory force to be transmitted to the hub. With a 20-foot half span in a static test bay, we should therefore expect at 1.0 g and 10 cps an interaction of something less than one part in a thousand.

In a teetering rotor helicopter, moments other than torque are negligible, and the setup for "ground flying" is somewhat simpler, as shown in Figure 3. For simplicity, the shakers, shock cord, tensioners and other devices have been eliminated in Figure 3.

The forces and phase angles for each shaker necessary to produce the desired moment, shear and associated phase angles are given by a simple 4 x 4 matrix inversion. With the distances x, y, and z measured from the hub center, the real and imaginary forces on shakers 1 and 2 to

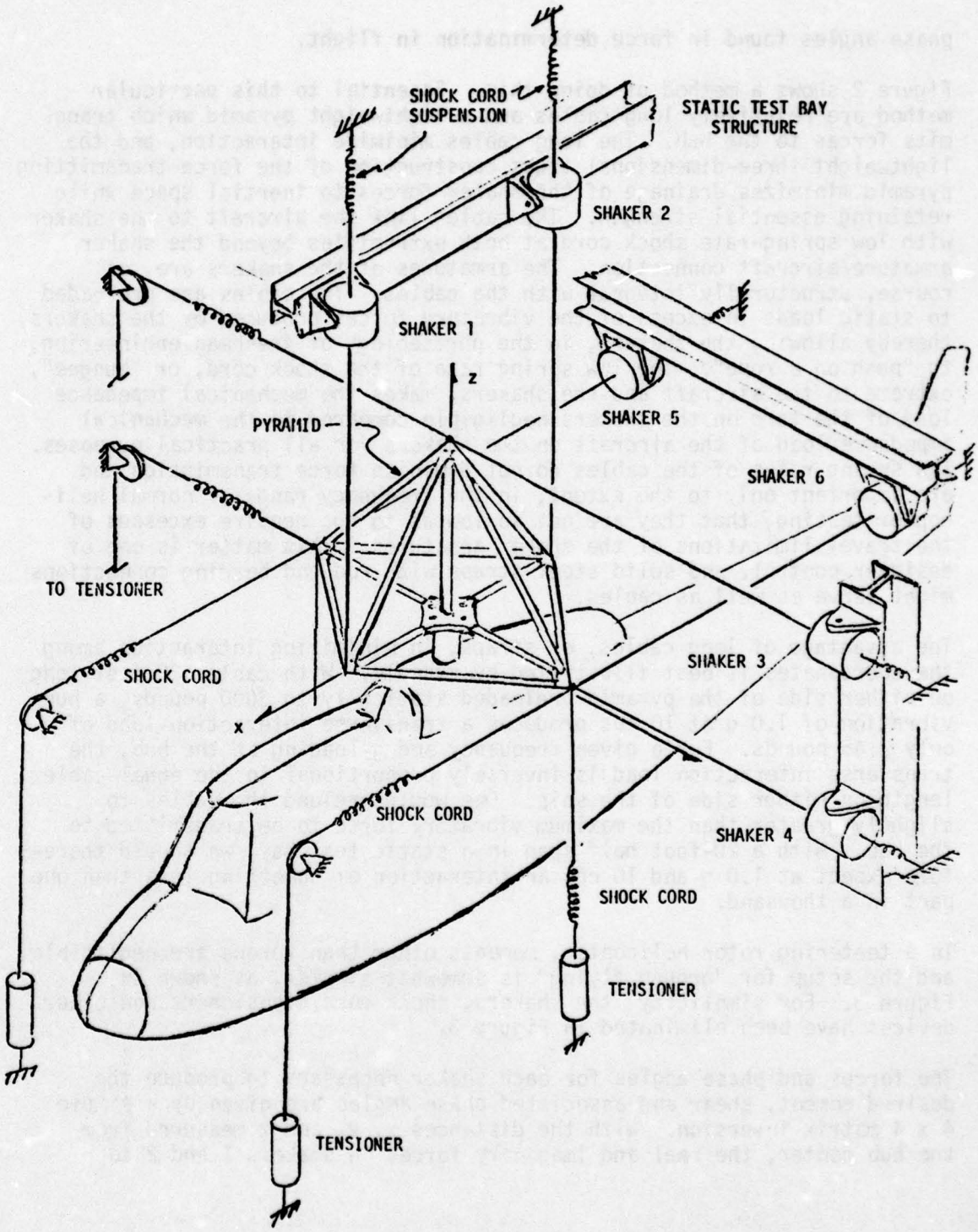

Figure 2. Method of Ground Flying a Helicopter With More Than Two Blades

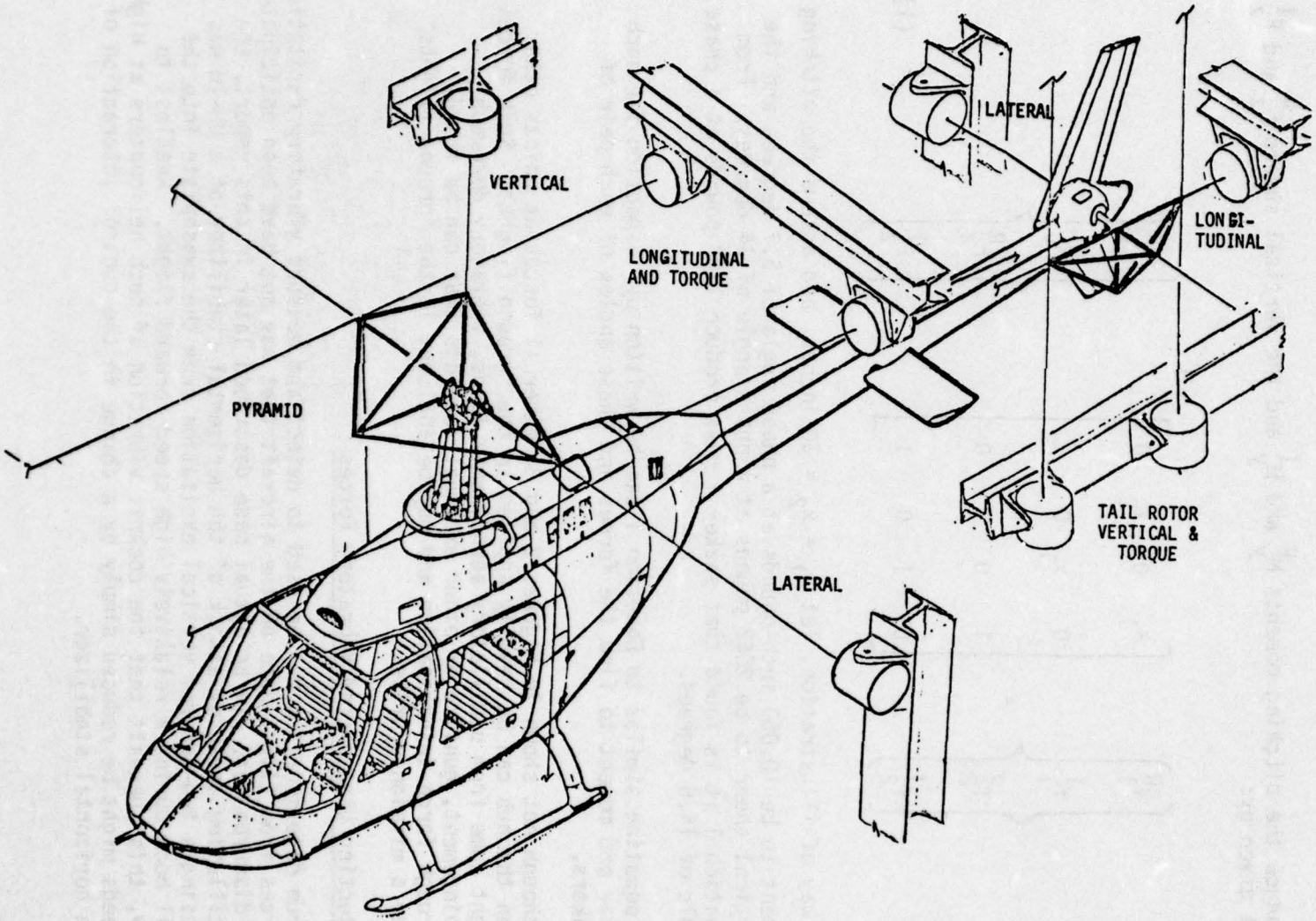

Figure 3. Method of Ground Flying a Two-Bladed Teetering Rotor Helicopter

produce the pitching moments M_y^R and M_y^I and the vertical shears F_z^R and F_z^I are given by:

$$\begin{Bmatrix} f_1^R \\ f_1^I \\ f_2^R \\ f_2^I \end{Bmatrix} = \begin{bmatrix} x_1 & 0 & x_2 & 0 \\ 0 & x_1 & 0 & x_2 \\ 1 & 0 & 1 & 0 \\ 0 & 1 & 0 & 1 \end{bmatrix}^{-1} \begin{Bmatrix} M_y^R \\ M_y^I \\ F_z^R \\ F_z^I \end{Bmatrix} \quad (1)$$

By way of illustration, let $x_1 = x_2 = 30$ inches, and assume the pitching moment to be 10,050 inch-pounds at a phase angle of 5.7 degrees and the vertical shear to be 2062 pounds at a phase angle of 14 degrees. From Equation 1 it is found that shaker 1 must produce 1197 pounds at a phase angle of 15.6 degrees.

An equation similar to Equation 1 can be written by inspection for each shear and moment to find the forces and phase angles of each pair of shakers.

Although not shown in Figures 2 and 3, external forces at points other than the hub can be readily applied in the "ground flight". Such forces might come from oscillatory aerodynamic loads, vibratory downwash impingement, gunfire or other external loadings that can be found through force determination and may be included in the "ground flights" over a mission profile.

Detecting Unsuspected Vibratory Forces

Force determination may be used to detect and measure vibratory excitation forces from flight data on the aircraft that may not have been anticipated as disturbances. In an actual case described later in this report, the oscillating angle of attack of the horizontal stabilizer of a UH-1H was passing a two-per-rev vertical excitation from the swashplate into the tail boom during a relatively high speed forward flight. Needless to say, this suggests that the cockpit vibration of such helicopters at high speeds might be reduced simply by a change in the control interaction of the horizontal stabilizer.

Force determination also offers the opportunity to do flight investigations of the vibration effects of downwash impingement on large surfaces close to the rotor, the effects of tail-rotor fuselage interference effects, harmonic forcing from aerodynamics on control surfaces, and the effects of other excitations that have never been measured.

PRINCIPLES OF FORCE DETERMINATION

BASIC APPROACH

The accelerations of a structure at any frequency are given by the product of the acceleration mobility matrix and the external forces acting on the structure.

$$\{\ddot{y}\} = [\ddot{Y}]\{f\} \tag{2}$$

The accelerations and the forces are, in general, complex; i.e., they have various phase angles, and therefore the acceleration mobility matrix is also complex. As used here, "forces" should be taken to include moments as well as shears.

If there are N external forces and moments to be determined, it is necessary to use at least N accelerometers so that there will be, in Equation 2, as many simultaneous equations as there are unknowns. These accelerometers will not be at the points of application of the external forces but will be distributed throughout the fuselage. The mobility matrix is obtained by shake testing the helicopter fuselage without the rotor. The terms in the mobility matrix are the real and imaginary ratios (partial derivatives) of the response of each accelerometer to each external force or moment, often expressed in units of g/pound.[2] If there are N forces and moments to be found in flight and N accelerometers on the ship, then the forces and moments would be given by:

$$\{f\} = [\ddot{Y}]^{-1}\{\ddot{y}\} \tag{3}$$

SOLUTION TO THE SIGNAL/NOISE PROBLEM

Although mathematically correct and substantially what has been attempted with hub strain gaging in the past, Equation 3 is not suitable for practical engineering application because it is sensitive to errors in the measurement of accelerations in flight and of mobilities in the ground shake test. As shown in Reference 6, matrices which are numerically well-conditioned may, because of errors in the measurement of their elements, give physical information which is meaningless when inverted.

---

[2] Flannelly and Giansante.

[6] W.G. Flannelly, A. Berman and N. Giansante, RESEARCH ON STRUCTURAL DYNAMIC TESTING BY IMPEDANCE METHODS, Kaman Aerospace Corporation; USAAMRDL Technical Report 72-63A, B, C, & D, U. S. Army Air Mobility Research and Development Laboratory, Fort Eustis, VA, November 1972, AD 756389, AD 756390, AD 756391, & AD 756392.

Further, one would have no way of determining from the use of Equation 3 whether the information obtained is physically meaningless.[6]

To eliminate this serious problem, we use the property of "redundancy", which has been employed so effectively in information theory and has been described as that property which "...makes language intelligible in the midst of noise".[8] To achieve a high degree of redundancy we should like to use many more accelerometers in the fuselage than there are forces to be determined. This would make the mobility matrix of Equation 2 rectangular, with many more rows than columns, giving us many more equations than unknowns. The problem now is how to invert a rectangular matrix.

In 1968, A. Berman of Kaman Aerospace Corporation discovered a matrix form with peculiar properties. It was later found that the same properties could be achieved with a process of matrix algebra known as the "pseudoinverse", "Moore's generalized inverse", or the "generalized reciprocal". Among the simplest properties of the pseudoinverse, discovered by E. H. Moore in 1920 but lost and rediscovered by R. Penrose in 1955, is that the inversion of a rectangular matrix of maximal rank amounts to a least-squares solution to a problem with more equations than unknowns.[9,10] The pseudoinverse was employed in dynamics in References 2, 6, and 11, and additionally in eigenvalue form for the first time in Reference 5, where a derivation is shown.

---

[2] Flannelly and Giansante.

[5] Cransdale, Gaukroger, and Skingle.

[6] Flannelly, Berman, and Giansante.

[8] Jagjit, Singh, GREAT IDEAS IN INFORMATION THEORY, Language and Cybernetics, New York, Dover Publications, 1966.

[9] E.H. Moore, GENERAL ANALYSIS, PART I, Social Security Administration, American Philosophical Society, Philadelphia, Pa., 1935.

[10] R. Penrose, A GENERALIZED INVERSE FOR MATRICES, Proceedings of the Cambridge Philosophical Society, 51, 1955, pp 406-413.

[11] A.L. Klosterman and J.R. Lemon, DYNAMIC DESIGN ANALYSIS VIA THE BUILDING BLOCK APPROACH, Shock and Vibration Bulletin, 42(4), January 1972, pp 97-104.

If we now use F accelerometers in the fuselage, where the number of accelerometers used is much larger than the H forces and moments at the hub (F >> H), then the square $[\ddot{Y}]^{-1}_{FH}$ inverse matrix of Equation 3 becomes a rectangular H x F pseudoinverse matrix $[Y]^{+}_{FH}$. The superscript "+" replaces the familiar "-1" to denote the pseudoinverse. We thus obviate the problem of inversion leading to meaningless information. and the signal-to-noise problem is solved. Then we have, from Equation 3:

$$\underset{Hx1}{\{F\}_H} = \underset{HxF}{[Y]^{+}} \underset{Fx1}{\{\ddot{y}\}_F} \qquad (F>>H) \qquad (4)$$

WRONG SIGNALS AND NOISE

The usefulness of the information from dynamic testing, or analysis, in the process of deciding how to improve a helicopter is obviously heavily dependent on the physical accuracy of the information. Hardware decisions based on false information from tests and analyses which cannot be or are not verified, and the large number of pointless dynamic tests conducted annually drain the limited budget of funds which could be more usefully applied elsewhere.

Although the signal-to-noise problem is fundamental both to dynamic testing and communication theory, dynamic testing differs from communication in that it involves the additional possibility of receiving "wrong signals". Wrong signals can come from many common causes: a mounting distortion of an accelerometer case, an accelerometer mounted upside down with respect to the physical meaning given to its signal, incorrect calibrations, and location errors. Electronic or statistical checks against noise cannot insure that a test signal is physically meaningful. The only way a wrong signal can be found is through checking the physics of the structure itself. Two ways to do this in helicopter dynamic testing are Maxwell's Reciprocity Theorem and the Rigid Body Acceleration Coefficient.

METHODS OF OBTAINING THE MOBILITY MATRIX

DIRECT SHAKING

The most direct method of obtaining the mobility matrix is to shake the helicopter at the locations of the excitation forces and measure the resulting accelerations per unit shaking force in the fuselage. In the determination of rotor forces and moments, this usually entails shaking at the hub with vertical, lateral, and longitudinal forces and moments one at a time.

Among the methods discussed in this report, direct shaking has the advantages of: providing the mobility matrix directly without any intervening techniques; exciting the fuselage at the sources of flight excitation, and thus allowing shake testing consistent with known dynamic testing practice. It has the disadvantages of: the customary expensive set-up costs; the problems and expense of minimizing tare dynamics in moment shaking; the necessity to accurately cross-control two shakers simultaneously to simulate moments; and the lack of opportunity to use smaller-than-usual shakers.

Although applicable to all types of helicopters, direct shaking is most easily applied to teetering rotor ships where the only significant vibration hub excitations are vertical, fore and aft, lateral shears and torque.

RECIPROCITY SHAKING

This is not only another method of obtaining the mobility matrix, but can and should be used to a limited extent with other methods as a physical check on the mobilities measured. The basis of this technique is the well-known reciprocity theorem of Maxwell. It states that in any linear system the acceleration at j due to a force at k (and only at k) is the same as the acceleration at k due to the same force at j. In mobility terms, $Y_{jk} = Y_{kj}$. If the reciprocity theorem is not confirmed by shaking at some accelerometer station, the engineer should carefully reexamine his work for either an error in the testing or structural nonlinearity, such as ankylosis, which can and should be accounted for.[12]

[12] R.A. Frazer, W.J. Duncan, and A.R. Collar, ELEMENTARY MATRICES, Cambridge, England, Syndics of the Cambridge University Press, 1938, reprinted 1965.

To obtain the mobility matrix by reciprocity shaking, the engineer would shake at each of the accelerometer stations and measure the responses (using rotational as well as translational accelerations) at the excitation's coordinates. The advantages of this method are that the suspension system is greatly simplified because there is no hub shaking and smaller shakers can be used if the fuselage accelerometers are placed at mobility antinodes (places of high fuselage response). The main disadvantage of this method is that it requires shaking at the many accelerometer locations. This requires not only much more testing time than direct shaking but, by presently proven methods, also requires large set-up costs in providing the many shaker hard-point attachments.

At this time it is difficult to envision reciprocity testing having an overall advantage as a primary method for obtaining the mobility matrix over the other two methods presented here. However, impact testing with Fast Fourier Transform equipment has made very significant strides in recent years. Should this technique be proven practical for helicopters, then reciprocity testing could become a very economical method for obtaining the mobility matrix. In the meantime, the limited use of reciprocity testing as a physical check on other methods is very valuable.

MODAL ACCELERATION TESTING

Modal acceleration testing (MAT) can define the total N x N mobility matrix, for N accelerometers, by shaking at only one point on the fuselage. This allows force determination to be done with only one shake test. The degree of flexibility inherent in the one-shake-test calibration allows the engineer to evaluate proposed modifications, such as the addition of missiles or other external stores and changes in rotors and rotor speeds, without repeating the shake test. MAT also yields the true undamped natural frequencies (as opposed to mobility peaks) and the actual normal modes (as opposed to mere mobility ratios). These two results are necessary for the comparison of finite element dynamics predictions with test results. MAT also provides the basic information necessary for system identification.[2,6]

In actual practice, MAT is used at several excitation points for a physical check on the test data and to take advantage of modal density reduction caused by near symmetry of the fuselage. Because the excitation can be at a mobility antinode, a minimum capacity shaker can be used. Because there need be only one to three excitation points, which may be conveniently chosen, an elaborate suspension structure or a hangar static test bay is not necessary. Consequently, very little attachment hardware

---

[2] Flannelly and Giansante.

[6] Flannelly, Berman, and Giansante.

need be designed or built. The entire set-up may consist of a fork lift and an A-frame with bungee connected to the hub. The setup costs of MAT are quite small, and the operational costs are minimal.

Because of the importance of modal acceleration testing, it will be described in detail in separate sections of this report.

MODAL ACCELERATION TESTING THEORY

MODAL ACCELERATIONS

Derivation of Basic Equation

The theory and application of analytical testing and system identification technology include many mathematical formulations which describe the dynamic behavior of linear structures having proportional structural damping.[13] At any frequency ω, the resulting equations of motion can be written as:

$$[K - \omega^2 M + igK] \{y\} = \{f\} \tag{5}$$

The terms in the matrix of Equation 5 are defined as the "displacement impedance" Z.[5] Similarly, the "acceleration impedance" $\ddot{Z}$ is defined as the matrix coefficients of the accelerations in the equations giving the forces

$$[\ddot{Z}]\{\ddot{y}\} = \{f\} \tag{6}$$

Note that $\ddot{Z}$ is not the second derivative of Z with respect to time, which is self-evident in the context it is used.

From Equation 6, the accelerations are given by

$$\{\ddot{y}\} = [\ddot{Z}]^{-1}\{f\} \equiv [\ddot{Y}]\{f\} \tag{7}$$

where the inverse of $\ddot{Z}$ is defined as the "acceleration mobility" $\ddot{Y}$. Unless otherwise specified, the use of the term "mobility" is taken to mean "acceleration mobility". Helicopters are generally shake-tested while suspended as free bodies, and "acceleration mobility" is finite at zero frequency. For this reason and others which become obvious from the following development, "acceleration mobility" is chosen as the most convenient "measurable" quantity.

---

[5] Cransdale, Gaukroger, and Skingle.

[13] W.W. Soroka, NOTE ON THE RELATIONS BETWEEN VISCOUS AND STRUCTURAL DAMPING COEFFICIENTS, Journal of the Aeronautical Sciences, Volume 16, No. 7, July 1949, p 409.

As seen from the matrix expressions of Equations 6 and 7, both impedance and mobility are properly partial derivatives. Acceleration impedance is the partial derivative of force with respect to acceleration, and acceleration mobility is the partial derivative of acceleration with respect to force.

The acceleration impedance is written:

$$\ddot{Z} = M - (1 + ig)K/\omega^2 \tag{8}$$

Premultiplying $\ddot{Z}$ by $\Phi^{-T}\Phi^{T}$ and postmultiplying by $\Phi\ \Phi^{-1}$ gives

$$\ddot{Z} = \Phi^{-T}\left[M_i^* - (1 + ig_i)K_i^*/\omega^2\right]\Phi^{-1} \tag{9}$$

From the definition of acceleration mobility,

$$\ddot{Y} = \Phi\left[M_i^* - (1 + ig_i)K_i^*/\omega^2\right]^{-1}\Phi^{T} \tag{10}$$

The response at j to a force at x, $\ddot{Y}_{jx}$, can be expressed in terms of normal modes, generalized mass and stiffness, and modal structural damping.[6]

$$\ddot{Y}_{jx} = \ddot{Y}^{R}_{jx} + i\ \ddot{Y}^{I}_{jx} \tag{11}$$

where

$$\ddot{Y}^{R}_{jx\omega} = -\sum_{i=1}^{N} A_{jxi}\frac{\omega^2}{\Omega_i^2}\frac{(1 - \omega^2/\Omega_i^2)}{[(1 - \omega^2/\Omega_i^2)^2 + g_i^2]} \tag{12}$$

and

$$\ddot{Y}^{I}_{jx\omega} = \sum_{i=1}^{N} A_{jxi}\frac{\omega^2}{\Omega_i^2}\frac{g_i}{[(1 - \omega^2/\Omega_i^2)^2 + g_i^2]} \tag{13}$$

---

[6] Flannelly, Berman, and Giansante.

and A_{jxi} is defined as the jx-th modal acceleration of the i-th mode.[2]

$$A_{jxi} \equiv \frac{\Phi_{ji}\Phi_{xi}}{\{\Phi\}_i^T[M]\{\Phi\}_i} \tag{14}$$

Letting

$$\ddot{F}^R_{i\omega} \equiv -\frac{\omega^2}{\Omega_i^2}\frac{(1 - \omega^2/\Omega_i^2)}{[(1 - \omega^2/\Omega_i^2)^2 + g_i^2]}$$

and

$$\ddot{F}^I_{i\omega} \equiv \frac{\omega^2}{\Omega_i^2}\frac{g_i}{[(1 - \omega^2/\Omega_i^2)^2 + g_i^2]}$$

Equations 12 and 13 may be written more concisely as

$$\ddot{Y}^R_{jx\omega} = \sum_{i=1}^{N} A_{jxi}\ddot{F}^R_{i\omega} \tag{15}$$

and

$$\ddot{Y}^I_{jx\omega} = \sum_{i=1}^{N} A_{jxi}\ddot{F}^I_{i\omega} \tag{16}$$

The modal acceleration, A_{jxi}, is a term which can be determined from the plot of mobility versus frequency for the acceleration at j due to a force at x.

It is more convenient to use the orthonormal mode ψ, defined as

$$\{\psi\}_i^T[M]\{\psi\}_i = [I] \tag{17}$$

---

[2] Flannelly and Giansante.

than the conventionally normalized normal mode Φ. For the i-th mode, then,

$$A_{jxi} = \psi_{xi}\psi_{ji} \tag{18}$$

For the accelerometer at the excitation point x, we determine A_{xxi} for each mode i and find

$$\psi_{xi} = \sqrt{A_{xxi}} \tag{19}$$

For any accelerometer j,

$$\psi_{ji} = \frac{A_{jxi}}{\sqrt{A_{xxi}}} \tag{20}$$

Suppose that the shaker is at station x in the shake tests and that we wish to know the response $\ddot{Y}_{jk}$ at accelerometer j if the ship were shaken at accelerometer k. From the $\ddot{Y}_{xx}$ plot, we find the modal accelerations A_{xxI}, A_{xxII}, A_{xxIII}, ...; from the $\ddot{Y}_{jx}$ plot, we find A_{jxI}, A_{jxII}, A_{jxIII}, ...; and from the $\ddot{Y}_{kx}$ plot, we find A_{kxI}, A_{kxII}, A_{kxIII},.... Using Equations 19 and 20, we determine the orthonormal mode elements ψ_{xI}, ψ_{xII}, ψ_{xIII}, ..., ψ_{jI}, ψ_{jII}, ψ_{jIII}, ... and ψ_{kI}, ψ_{kII}, ψ_{kIII},.... Then we construct

$$\ddot{Y}^{R}_{jk\omega} + i\ddot{Y}^{I}_{jk} = \sum_{i=1}^{N} A_{jki}(\ddot{F}^{R}_{i\omega} + i\ddot{F}^{I}_{i\omega})$$

$$= \sum_{i=1}^{N} \psi_{ji}\psi_{ki}(\ddot{F}^{R}_{i\omega} + i\ddot{F}^{I}_{i\omega}) \tag{21}$$

Using Equation 20, the engineer can construct the mobility relative to any two instrumented points. If we were determining the acceleration at j due to a moment at k in flight, then the plot $\ddot{Y}_{kx}$ of the shake test would be that of the rotational acceleration at k due to a shaker force at x.

As shown in References 2 and 6, and as can be seen from Equations 12 and 13, the higher the natural frequency of any mode above the frequency range of interest, the less effect it has on the mobility. Therefore, the number of modes which must be covered in the testing is relatively small. Usually, covering only two modes above the frequency of the force to be determined (N-per-rev in most rotor cases) is sufficient.

In an unrestrained system, such as a helicopter in flight, there are six "rigid-body" degrees of freedom. Some systems are not totally unrestrained, such as a beam with one pin end, and may have fewer than six, say z, "rigid-body" modes. Consistent with Reference 2, Equation 15 may be written

$$\ddot{Y}^{R}_{jx\omega} = E_{jx} - \sum_{i=Z+1}^{N} A_{jxi} \frac{\omega^2}{\Omega_i^2} \frac{1 - \omega^2/\Omega_i^2}{(1 - \omega^2/\Omega_i^2)^2 + g_i^2} \tag{22}$$

where E_{jx} is the rigid-body acceleration coefficient (RAC). At zero forcing frequency, the real acceleration mobility is equal to the RAC. The RAC has no effect on the imaginary mobility. The RAC can be accurately determined from weights data on the aircraft, and one of the checks on the physical validity of the mobility test data is to see whether the mobility asymptotically approaches the RAC at frequencies between the very low suspension modes and the first elastic mode of the fuselage.

Antiresonance Theory Representation

The following development is a completely mathematical formulation of Y_{jx} based entirely upon antiresonant eigenvalues of matrices.[14]

---

[2] Flannelly and Giansante.

[6] Flannelly, Berman, and Giansante.

[14] F.D. Bartlett, Jr., and W.G. Flannelly, APPLICATION OF ANTIRESONANCE THEORY TO HELICOPTERS, Journal of the American Helicopter Society, Volume 19, No. 1, January 1974, pp 11-15.

Mathematically, the jx-th acceleration mobility at frequency ω is defined as

$$\ddot{Y}_{jx} = \frac{\partial \ddot{y}_j}{\partial F_x} = \frac{(-1)^{j+x}|\ddot{Z}|_{jx}}{|\ddot{Z}|} \tag{23}$$

since $\ddot{Z}^{-1} = \ddot{Y}$ where $|\ddot{Z}|$ is the determinant of $\ddot{Z}$ and $(-1)^{j+x}|Z|_{jx}$ is the jx-th co-factor of $\ddot{Z}$.

The acceleration impedance from Equation 7 can be written as

$$\ddot{Z} = M\left[[I] + M^{-1}(1 + ig)K/\omega^2 \right] \tag{24}$$

The determinant of $\ddot{Z}$ is then seen to be

$$|\ddot{Z}| = |M||[I] + M^{-1}(1 + ig)K/\omega^2)| \tag{25}$$

which, when expanded, becomes

$$|\ddot{Z}| = |M|\frac{(-1)^N}{\Omega^2}\left\{\omega^{2N} - p_1\omega^{2(N-1)} - \ldots - (-1)^{N-1}|1 + ig|\frac{|K|}{|M|}\right\} \tag{26}$$

where N is the order of the matrix and

$$\frac{|K|}{|M|} = \prod_{i=1}^{N} \Omega_i^2$$

Ω_i are the eigenvalues of $M^{-1}K$ and Equation 26 is further simplified as

$$|\ddot{Z}| = \frac{|M|}{\omega^2}\prod_{i=1}^{N} \Omega_i^2\left[(1 + ig) - \omega^2/\Omega_i^2\right] \tag{27}$$

Similarly, the jx-th co-factor of $\ddot{Z}$ becomes

$$(-1)^{j+x}|\ddot{Z}|_{jx} = \frac{|M|_{jx}}{\omega^2}\prod_{i=1}^{N} a_{jxi}^2\left[(1 + ig) - \omega^2/a_{jxi}^2\right] \tag{28}$$

where a_{jx} are the eigenvalues of $|M|^{-1}_{jx}|K|_{jx}$ known as antiresonances. Reference 14 interprets the meaning of a_{jxi} both mathematically and physically.

In an unrestrained system, there are Z natural frequencies (Ω_i) which are zero, and Z-1 antiresonant frequencies (a_{jx}) which are zero. Combining Equations 27 and 28 gives

$$\ddot{Y}_{jx} = E_{jx} \frac{\prod_{i=Z}^{N-1} \left[(1 - \omega^2/a_{jxi}^2) + ig\right]}{\prod_{i=Z+1}^{N} \left[(1 - \omega^2/\Omega_i^2) + ig\right]} \tag{29}$$

$$E_{jx} = (-1)^{j+x} \frac{|M|_{jx}}{|M|} \frac{\prod_{i=Z}^{N-1} a_{jxi}^2}{\prod_{i=Z+1}^{N} \Omega_i^2} \tag{30}$$

From Equation 29 the mobility can be reproduced if E_{jx}, a_{jxi}, Ω_i, and g are known.

REMOVAL OF DAMPING

By definition, the natural frequencies and modal accelerations are undamped parameters of the system. In order to calculate these undamped modal parameters, the undamped mobility must be known. Since all measurements include damped real mobility, it is necessary to derive the appropriate relations for calculating undamped resonances. As a consequence of the development, a new expression for determining modal damping is included. This new result is valid for closely coupled modes and assumes $g_i^2 \ll g_i$.

Consider Equation 29 and rewrite as:

$$\ddot{Y}_{jx} = E_{jx} \frac{\prod_{i=Z}^{N-1} \left[(1 - \frac{\omega^2}{a_i^2})(1 - \frac{\omega^2}{\Omega_i^2}) + g_i^2 + ig_i(\frac{\omega^2}{a_i^2} - \frac{\omega^2}{\Omega_i^2})\right]}{\prod_{i=Z+1}^{N} \left[(1 - \omega^2/\Omega_i^2)^2 + g_i^2\right]} \tag{31}$$

where the j, k and x subscripts are left off a_i for clarity.

Reindexing the antiresonances to pair with the resonances, Equation 31 becomes

$$\ddot{Y}_{jx} = E_{jx} \prod_{i=Z+1}^{N} (R_i + iI_i) \tag{32}$$

Ignoring terms involving the products of the modal imaginaries in the expansion of Equation 31, the real mobility can be approximated as

$$\ddot{Y}^R_{jx} \cong E_{jx} \prod_{i=Z+1}^{N} \frac{\left[(1 - \frac{\omega^2}{a_i^2})(1 - \frac{\omega^2}{\Omega_i^2}) + g_i^2\right]}{\left[(1 - \omega^2/\Omega_i^2)^2 + g_i^2\right]} \tag{33}$$

where the j, k subscripts are left off a_i for clarity.

Expressing the numerator and denominator of the factors of Equation 33 in terms of the roots given,

$$\ddot{Y}^R_{jx} \cong E_{jx} \prod_{i=Z+1}^{N} \frac{(\frac{\omega^2}{\Omega_i^2} - \alpha_i^2)(\frac{\omega^2}{\Omega_i^2} - \beta_i^2)}{\left[\frac{\omega^2}{\Omega_i^2} - (1 + ig)\right]\left[\frac{\omega^2}{\Omega_i^2} - (1 - ig)\right]} \tag{34}$$

where

$$\alpha_i^2 = \frac{1}{2}\left(1 + \frac{a_i^2}{\Omega_i^2}\right)\left(1 - \sqrt{1 - \frac{4(1 + g^2)a_i^2/\Omega_i^2}{(1 + a_i^2/\Omega_i^2)^2}}\right) \tag{35}$$

and

$$\beta_i^2 = \frac{1}{2}\left(1 + \frac{a_i^2}{\Omega_i^2}\right)\left(1 + \sqrt{1 - \frac{4(1 + g^2)a_i^2/\Omega_i^2}{(1 + a_i^2/\Omega_i^2)^2}}\right) \tag{36}$$

If, for any mode i, the α_i and β_i roots are complex, then there will not be any zero mobility crossover for that mode. To have a zero crossover in the real mobility for the i-th mode, it is necessary and sufficient that, for a real antiresonance, the quantity under the radical of α_i and β_i be positive. This condition gives the range of a_i/Ω_i in terms of g_i for which a zero crossover in the real acceleration mobility exists. In other words,

$$\sqrt{1 + g_i^2} + g_i \leq \frac{a_i}{\Omega_i} \leq \sqrt{1 + g_i^2} - g_i \tag{37}$$

When there is a zero crossover for a real antiresonance, the crossover at $\omega_\beta = \beta_i \Omega_i$ is associated with, but not equal to, the resonance, and the crossover at $\omega_\alpha = \alpha_i \Omega_i$ is associated with, but not equal to, the antiresonance. An accurate approximation of the true undamped antiresonance is obtained by adding Equations 35 and 36.

$$a_i^2 \cong \omega_{\alpha_i}^2 + \omega_{\beta_i}^2 - \Omega_i^2 \tag{38}$$

Subtracting Equations 35 and 36 gives an approximation for modal damping:

$$g_i^2 = \frac{\omega_{\beta_i}^2 \, \omega_{\alpha_i}^2}{\Omega_i^2(\omega_{\alpha_i}^2 + \omega_{\beta_i}^2 - \Omega_i^2)} - 1 \tag{39}$$

Equations 38 and 39 assume that Ω_i is the undamped resonance.

The determination of the true undamped resonance can be performed as follows. If a constant K is subtracted from the real acceleration mobility, Equation 33 becomes, after simplification,

$$\ddot{Y}_{jk}^R - K \cong (E_{jk} - K) \prod_{i=Z+1}^{N} \frac{1}{\Omega_i^4} \; \frac{(\omega^2 - \omega_{\alpha_i}^2)(\omega^2 - \omega_{\beta_i}^2)}{\left[\left(1 - \frac{\omega^2}{\Omega_i^2}\right)^2 + g_i^2\right]} \tag{40}$$

where ω_{α_i} and ω_{β_i} are frequencies at which the mobility is equal to K. Let ω_{k_i} be the frequency at which the mobility equals K for no damping; then the roots may be expressed as

$$\omega_{\alpha_i}^2 = \frac{1}{2}(\Omega_i^2 + \omega_{k_i}^2)\left(1 - \sqrt{1 - \frac{4(1 + g_i^2)\omega_{k_i}^2/\Omega_i^2}{(1 + \omega_{k_i}^2/\Omega_i^2)}}\right) \tag{41}$$

$$\omega_{\beta_i}^2 = \frac{1}{2}(\Omega_i^2 + \omega_{k_i}^2)\left(1 + \sqrt{1 + \frac{4(1 + g_i^2)\omega_{k_i}^2/\Omega_i^2}{(1 + \omega_{k_i}^2/\Omega_i^2)}}\right) \tag{42}$$

Adding Equations 41 and 42 gives the frequency at which the mobility is equal to K when the damping is zero.

$$\omega_{k_i}^2 \cong \omega_{\alpha_i}^2 + \omega_{\beta_i}^2 - \Omega_i^2 \tag{43}$$

Similarly, subtracting the two equations gives the damping coefficient

$$g_i^2 \cong \frac{\omega_{\alpha_i}^2 \omega_{\beta_i}^2}{\Omega_i^2(\omega_{\alpha_i}^2 + \omega_{\beta_i}^2 - \Omega_i^2)} - 1 \tag{44}$$

Equations 43 and 44 are independent of K, which means that they are valid for and independent of the mobility at which the damped real mobility exists at adjacent frequencies. The calculation of the undamped mobility is based on a frequency shift of the damped mobility and does not yield undamped mobilities at levels where the damped mobility does not exist. Equations 41 and 42 can now be used to determine the undamped resonances. At a maximum or a minimum in the damped real mobility, Equations 41 and 42 are equal.

$$p_{2_i} = \omega_{\beta_i} = \omega_{\alpha_i} \tag{45}$$

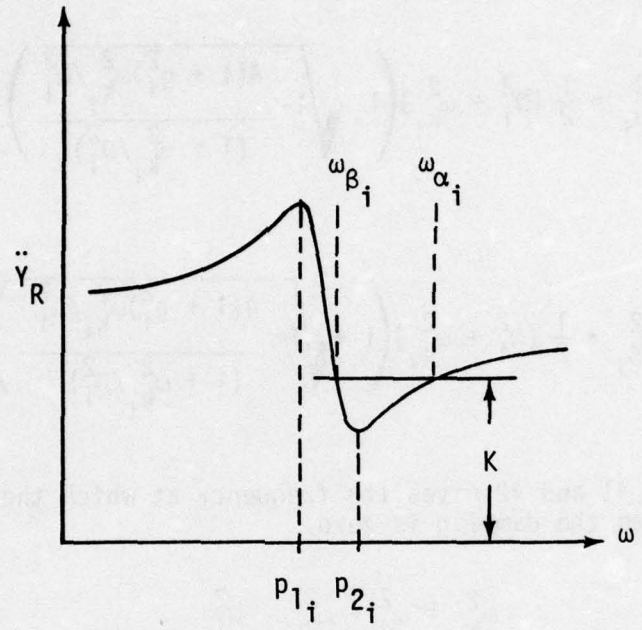

Figure 4. Real Mobility

This occurs when the term under the radical is zero.

$$(1 + \omega_{k_i}^2/\Omega_i^2) = 4(1 + g_i^2)\ \omega_{k_i}^2/\Omega_i^2 \tag{46}$$

There are two such frequencies for each mode (p_{1_i} and p_{2_i}) in the damped real mobility, as shown in Figure 4. From Equation 43 this gives

$$\omega_{k_{1_i}}^2 = 2p_{1_i}^2 - \Omega_i^2 \tag{47}$$

$$\omega_{k_{2_i}}^2 = 2p_{2_i}^2 - \Omega_i^2 \tag{48}$$

Equations 47 and 48 are substituted into Equation 46 to obtain

$$\left(\frac{2p_{1_i}^2}{\Omega_i^2}\right)^2 = 4(1 + g_i^2)\left(\frac{2p_{1_i}^2}{\Omega_i^2} - 1\right) \tag{49}$$

$$\left(\frac{2p_{2_i}^2}{\Omega_i^2}\right)^2 = 4(1 + g_i^2)\left(\frac{2p_{2_i}^2}{\Omega_i^2} - 1\right) \tag{50}$$

Dividing Equation 49 by Equation 50 gives, after simplifying,

$$\Omega_i^2 = \frac{2p_{1_i}^2}{\frac{p_{1_i}^2}{p_{2_i}^2} + 1} \tag{51}$$

Equation 51 relates the true undamped resonance in terms of the peak frequencies p_{1_i} and p_{2_i} independent of damping and mobility.

Substituting Equation 51 into Equation 44 similarly relates the damping solely in terms of these modal peak frequencies.

$$g_i^2 = \frac{1}{4}\left(\frac{p_{2_i}}{p_{1_i}} + \frac{p_{1_i}}{p_{2_i}}\right)^2 - 1 \tag{52}$$

or

$$g_i = \frac{(p_{2i}/p_{1i})^2 - 1}{2\ p_{2i}/p_{1i}} = \frac{1}{2}\left(\frac{p_{2i}}{p_{1i}} - \frac{p_{1i}}{p_{2i}}\right)$$

Equations 51 and 52 are both important in the applications of the E-MASS for reducing the data in terms of undamped modal accelerations.

RIGID BODY ACCELERATION COEFFICIENT CALCULATION

The following derivation, although shown in Reference 2, is presented here in the interest of completeness.

In Figure 5, x, y, and z are any orthogonal axes through the center of gravity of a body of mass M, with points x_i, y_i, and z_i, shown on the respective axes, having rotational accelerations $\ddot{\theta}_x$, $\ddot{\theta}_y$, and $\ddot{\theta}_z$.

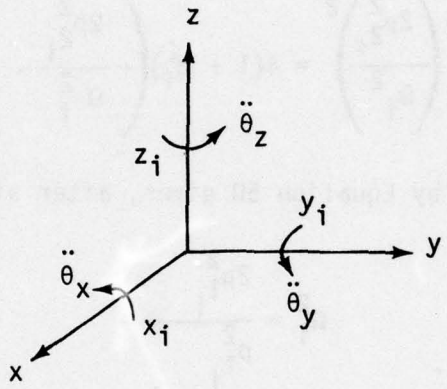

Figure 5. Axis System

The moments M_x, M_y, and M_z about the x, y, and z axes may be written using Lagrange's Equation as

$$\begin{Bmatrix} M_x \\ M_y \\ M_z \end{Bmatrix} = \begin{bmatrix} I_x & -U_{xy} & -U_{xz} \\ -U_{xy} & I_y & -U_{zy} \\ -U_{xz} & -U_{zy} & I_z \end{bmatrix} \begin{Bmatrix} \ddot{\theta}_x \\ \ddot{\theta}_y \\ \ddot{\theta}_z \end{Bmatrix} \tag{53}$$

where I_x, I_y, and I_z are the moments of inertia about the x, y, and z axes, and U_{xy}, U_{xz}, and U_{zy} are the products of inertia with respect to the x and y axes, the x and z axes, and the y and z axes.

Equation 53 may be written in general notation as

$$\{M_q\} = \left[\frac{\partial M}{\partial \ddot{\theta}}\right] \{\ddot{\theta}\} \tag{54}$$

The $[\partial M/\partial \ddot{\theta}]$ matrix may be inverted to yield

$$\left[\frac{\partial M}{\partial \ddot{\theta}}\right]^{-1} \equiv \left[\frac{\partial \ddot{\theta}}{\partial M}\right] = \frac{1}{\Delta} \begin{bmatrix} I_y I_z - U_{zy}^2 & U_{xy} I_z + U_{zy} U_{xz} & U_{xy} U_{zy} + I_y U_{xz} \\ U_{xy} I_z + U_{zy} U_{xz} & I_x I_z - U_{xz}^2 & I_x U_{zy} + U_{xy} U_{xz} \\ U_{xy} U_{zy} + I_y U_{xz} & I_x U_{zy} + U_{xy} U_{xz} & I_x I_y - U_{xy}^2 \end{bmatrix} \tag{55}$$

where the determinant of the matrix is given by $\Delta = I_x I_y I_z - 2U_{xy} U_{zy} U_{xz} - U_{xy}^2 I_z - U_{zy}^2 I_x - U_{xz}^2 I_y$

Solving for the rotational accelerations and using the definition presented in Equation 55 yields

$$\{\ddot{\theta}\} = \left[\frac{\partial \ddot{\theta}}{\partial M}\right] \{M_q\} \tag{56}$$

The matrix $[\partial \ddot{\theta}/\partial M]$ represents the rigid-body acceleration coefficients of the rotational acceleration about any of the specified axes with respect to a moment about any of the given axes.

The linear accelerations of the points x_i, y_i, and z_i due solely to rotations or the rigid body may be expressed as

$$\begin{Bmatrix} \ddot{x}_i \\ \ddot{y}_i \\ \ddot{z}_i \end{Bmatrix} = \begin{bmatrix} 0 & z_i & -y_i \\ -z_i & 0 & x_i \\ y_i & -x_i & 0 \end{bmatrix} \begin{Bmatrix} \ddot{\theta}_x \\ \ddot{\theta}_y \\ \ddot{\theta}_z \end{Bmatrix} \tag{57}$$

Equation 57 may be written more generally using Equation 56,

$$\{q\} = [Q_i]\{\ddot{\theta}\} = [Q_i][\partial\ddot{\theta}/\partial M]\{M_q\} \tag{58}$$

The moments about the x, y, and z axes caused by orthogonal forces at any point are given by

$$\begin{Bmatrix} M_x \\ M_y \\ M_z \end{Bmatrix} = \begin{bmatrix} 0 & -z_F & y_F \\ z_F & 0 & -x_F \\ -y_F & x_F & 0 \end{bmatrix} \begin{Bmatrix} F_x \\ F_y \\ F_z \end{Bmatrix} \tag{59}$$

Equation 59 may be written as

$$\{M_q\} = [Q_F]\{F\} \tag{60}$$

Newton's Law relates the accelerations of the center of gravity of the body to the applied forces and the mass of the body:

$$\{\ddot{q}_o\} = \begin{Bmatrix} \ddot{x}_o \\ \ddot{y}_o \\ \ddot{z}_o \end{Bmatrix} = \begin{Bmatrix} F_x \\ F_y \\ F_z \end{Bmatrix} \frac{1}{M} = \{F\}\frac{1}{M} \tag{61}$$

The rigid-body acceleration coefficients describing rotational acceleration due to moment are given by Equation 55 and are written in matrix form as

$$[E_{\ddot{\theta}M}] = \left[\frac{\partial\ddot{\theta}}{\partial M}\right] \tag{62}$$

The rigid-body acceleration coefficients relating translational acceleration and moment are obtained from Equation 58:

$$[E_{\ddot{q}M}] \equiv [\partial\ddot{q}/\partial M] = [Q_i][\partial\ddot{\theta}/\partial M] = [Q_i][E_{\ddot{\theta}M}] \tag{63}$$

The rigid-body acceleration coefficients presenting rotational acceleration due to force are defined from Equations 56 and 60:

$$[E_{\ddot{\theta}F}] \equiv [\partial\ddot{\theta}/\partial F] = \left[\frac{\partial\ddot{\theta}}{\partial M}\right][Q_F] = [E_{\ddot{\theta}M}][Q_F] \tag{64}$$

The accelerations of a point on the rigid body result from the translational acceleration of the center of gravity and the linear acceleration due to pure rotations of the rigid body. The translational acceleration is obtained from Equations 58, 60, and 61 and is written as

$$\{\ddot{q}\} = \{F\}\frac{1}{M} + [Q_i][E_{\ddot{\theta}M}][Q_F]\{F\} \tag{65}$$

Equation 65 yields the rigid-body acceleration coefficients relating translational acceleration and force:

$$[E_{\ddot{q}F}] \equiv [\partial\ddot{q}/\partial F] = \left[\frac{1}{M}\right] + [Q_i][E_{\ddot{\theta}M}][Q_F] \tag{66}$$

A METHOD FOR THE EXPERIMENTAL DETERMINATION OF THE RIGID BODY ACCELERATION COEFFICIENTS

In some cases, where a commercial helicopter has been adopted for military use or where a military helicopter has undergone extensive modification, knowledge of the principal inertial axes and moments of inertia may be doubtful. If we determined the inertial properties (the gross weights and center of gravity location are known from weight and balance measurement) by swinging the ship, we could calculate the rigid body acceleration coefficients (RACs) by Equation 66, but accurately determining the inertial properties by swinging a fuselage is extremely difficult. We would determine each RAC from the low frequency response of each mobility run, or by the matrix inversion method of determining modal accelerations[11], or by subtracting $\sum A_{jki}\ddot{F}^R_{\omega i}$ from $\ddot{Y}^R_{\omega i}$ (Equation 22). However, these would not, in themselves, give us information about the RACs for stations at which the helicopter was not shaken in the ground test. But, if we use the method described below, we can experimentally determine all the RACs by shaking at only three points. Since the RACs derived from this test would be independent of those measured in the shake testing, they would serve as a physical property cross-check on that data. The method makes no assumptions about symmetry or principal axes.

[11] Klosterman and Lemon.

The engineer chooses three points on the aircraft; x_1, y_1, z_1; x_2, y_2, z_2; and x_3, y_3, z_3; measured from the center of gravity, with at least y_3, z_2, and y_1 not equal to zero. By any of the methods mentioned above, the engineer finds: $E_{x_1x_1}$, $E_{x_2x_1}$, $E_{z_3x_1}$, $E_{x_2x_2}$, $E_{z_3x_2}$, and $E_{z_3z_3}$. Let Ξ be the matrix of the partial derivatives of rotational accelerations with respect to applied moments, a 3 x 3 matrix. Then,

$$[\Xi] \equiv [\partial\ddot{\theta}/\partial M]$$

It is seen that

$$E_{x_1x_2} \equiv E_{x_2x_1} = \frac{1}{M} + \lfloor 0,\ z_1,\ -y_1 \rceil [\Xi] \begin{Bmatrix} 0 \\ z_2 \\ -y_2 \end{Bmatrix} \tag{67}$$

where M is the total mass of the ship.

Similarly,

$$E_{x_2z_3} \equiv E_{z_3x_2} = \lfloor 0,\ z_2,\ -y_2 \rceil [\Xi] \begin{Bmatrix} y_3 \\ -x_3 \\ 0 \end{Bmatrix} \tag{68}$$

and so on.

We therefore see that

$$\begin{bmatrix} 0 & z_1 & -y_1 \\ 0 & z_2 & -y_2 \\ y_3 & -x_3 & 0 \end{bmatrix}^{-1} \left(\begin{bmatrix} E_{x_1x_1} & E_{x_1x_2} & E_{x_1z_3} \\ E_{x_1x_2} & E_{x_2x_2} & E_{x_2z_3} \\ E_{x_1z_3} & E_{x_2z_3} & E_{z_3z_3} \end{bmatrix} - \begin{bmatrix} \frac{1}{M} & \frac{1}{M} & 0 \\ \frac{1}{M} & \frac{1}{M} & 0 \\ 0 & 0 & \frac{1}{M} \end{bmatrix} \right) \begin{bmatrix} 0 & 0 & y_3 \\ z_1 & z_2 & -x_3 \\ -y_1 & -y_2 & 0 \end{bmatrix}^{-1}$$

$$= [\Xi] \tag{69}$$

and

$$[Q]^{-1}\left([E'] - \left[\frac{1}{M'}\right]\right)[Q]^{-T} = [\Xi] \tag{70}$$

The three-dimensional, translational RAC's between points j and k are seen to be given by

$$\left[\frac{1}{M}\right] + \begin{bmatrix} 0 & z_j & -y_j \\ -z_j & 0 & x_j \\ y_j & -x_j & 0 \end{bmatrix} [Q]^{-1}\left([E'] - \left[\frac{1}{M'}\right]\right)[Q]^{-T} \begin{bmatrix} 0 & -z_k & y_k \\ z_k & 0 & -x_k \\ -y_k & x_k & 0 \end{bmatrix}$$

$$= \begin{bmatrix} E_{x_j x_h} & E_{x_j y_k} & E_{x_j z_k} \\ E_{y_j x_k} & E_{y_j y_k} & E_{y_j z_k} \\ E_{z_j x_k} & E_{z_j y_k} & E_{z_j z_k} \end{bmatrix} \tag{70a}$$

The rotational/moment RAC's are given by Equation 69. Equation 70a shows the common translation/force RACs. The translation/moment and rotation/force RACs may be obtained from Equations 63, 64, and 70 as follows:

$$[E_{\ddot{q}M}] = [Q_i][\Xi] \tag{70b}$$

$$[E_{\ddot{q}F}] = [\Xi][Q_F] \tag{70c}$$

METHODS OF OBTAINING MODAL ACCELERATION

PSEUDOINVERSE ITERATION METHOD AND MATRIX METHODS

A detailed description of the pseudoinverse iteration method for obtaining modal accelerations and an experimental verification of the method are given in Reference 2. Other methods using matrices may be found in Reference 6 and Reference 11. More recently developed methods, which are considerably simpler to use, are discussed below.

ANTIRESONANCE THEORY METHODS

Driving Point Check Method

The following develops the mathematical expression for modal acceleration which was presented without proof in Reference 2.

The proof is based upon antiresonance theory, and it is shown that modal acceleration can be determined if the resonances, the antiresonances, and the rigid-body acceleration coefficients are known.

In Equation 22, for a force at k, instead of at x, let g = 0, which is the case for an undamped system. This yields

$$\ddot{Y}_{jk} = E_{jk} - \sum_{i=Z+1}^{N} A_{jki} \frac{(\omega^2/\Omega_i^2)}{(1 - \omega^2/\Omega_i^2)} \tag{71}$$

where the superscript "R", indicating the real part, is dropped because there is no imaginary mobility in an undamped system. Similarly, for an undamped system (g = 0), Equation 29 becomes

$$\ddot{Y}_{jk} = E_{jk} \frac{\prod_{i=Z}^{N-1} (1 - \omega^2/a_{jki}^2)}{\prod_{i=Z+1}^{N} (1 - \omega^2/\Omega_i^2)} \tag{72}$$

---

2 Flannelly and Giansante.

6 Flannelly, Berman, and Giansante.

11 Klosterman and Lemon.

Equation 71 may be written in the form,

$$\ddot{Y}_{jk} = E_{jk} - \sum_{i=Z+1}^{N} A_{jki} \left(\frac{\omega^2}{\Omega_i^2}\right) \frac{\prod_{\substack{m=Z+1 \\ m\neq i}}^{N} (1 - \omega^2/\Omega_m^2)}{\prod_{i=Z+1}^{N} (1 - \omega^2/\Omega_i^2)} \tag{73}$$

Equating the two expressions for $\ddot{Y}_{jk}$ given by 72 and 73,

$$E_{jk} \prod_{i=Z}^{N-1} (1 - \omega^2/a_{jki}^2) = E_{jk} \prod_{i=Z+1}^{N} (1 - \omega^2/\Omega_i^2) - \omega^2 \sum_{i=Z+1}^{N} \frac{A_{jki}}{\Omega_i^2} \prod_{\substack{m=Z+1 \\ m\neq i}}^{N} (1-\omega^2/\Omega_m^2) \tag{74}$$

When $\omega = \Omega_m$, where m is one of the elastic modes and $(Z+1) \leq M \leq N$, Equation 74 becomes

$$E_{jk} \prod_{i=Z}^{N-1} (1 - \Omega_M^2/a_{jki}^2) = - \Omega_M^2 \frac{A_{jkM}}{\Omega_M^2} \prod_{\substack{m=Z+1 \\ m\neq i}}^{N} (1 - \Omega_M^2/\Omega_m^2) \tag{75}$$

Solving for A_{jkM} gives the expression reported without proof in Reference 2:

$$A_{jkM} = - E_{jk} \frac{\prod_{i=Z}^{N-1} (1 - \Omega_M^2/a_{jki}^2)}{\prod_{\substack{m=Z+1 \\ m\neq M}}^{N-1} (1 - \Omega_M^2/\Omega_m^2)} \tag{76}$$

The antiresonant frequencies of a driving point are all real, and this equation may be used directly as an independent, hand-calculator check on the driving point modal accelerations whenever the damping is low enough to detect the approximate antiresonant frequencies.

Vector Angle Method for Transfer and Driving Points

Now we will show that the undamped mobility may be found using the rigid body acceleration coefficient, the natural frequencies, and the anti-resonant frequencies. However, the antiresonant frequencies are not necessarily all real in a transfer mobility plot; there may be anti-resonant roots in the imaginary frequency spectrum. Equation 76 cannot be solved without all the antiresonant frequencies, and imaginary anti-resonances cannot be found in testing. It will be shown that undamped mobilities may be obtained using only the real antiresonances.

In the interest of notational simplicity, the elastic modes are numbered starting with "1", instead of Z+1, in Equation 29.

The damped mobility, with structural damping, in a free body is given exactly by Equation 29 for an infinite number of modes:

$$\ddot{Y}_{jk} = E_{jk} \frac{\prod_{i=1}^{\infty} (1 - \omega^2/a_{jki}^2 + ig_i)}{\prod_{i=1}^{\infty} (1 - \omega^2/\Omega_i^2 + ig_i)} \tag{29}$$

Each term in the numerator may be considered to be a vector of length $\left|(1 - \omega^2/a_{jki}^2)^2 + g_i^2\right|^{1/2}$ and angle $\nu_{i\omega} = \arctan\left[g_i/(1 - \omega^2/a_{jki}^2)\right]$.

Similarly, the denominator is the product of vectors of length $\left|(1 - \omega^2/\Omega_i^2)^2 + g_i^2\right|^{1/2}$ and angle $\delta_{i\omega} = \arctan\left[g_i/(1 - \omega_i^2/\Omega_i^2)\right]$.

Equation 29 may be expressed as

$$\ddot{Y}_{jk} = E_{jk} \left| \prod_{i=1}^{\infty} \frac{\left[(1 - \omega^2/a_{jki}^2)^2 + g_i^2\right]^{1/2}}{\left[(1 - \omega^2/\Omega_i^2)^2 + g_i^2\right]^{1/2}} \right| \exp. i \sum_{i=1}^{N} (\nu_{i\omega} - \delta_{i\omega}) \tag{77}$$

Or, in vector notation,

$$\ddot{Y}_{jk} = E_{jk} \left| \prod_{i=1}^{\infty} \frac{\left[(1 - \omega^2/a_{jki}^2)^2 + g_i^2\right]^{1/2}}{\left[(1 - \omega^2/\Omega_i^2)^2 + g^2\right]^{1/2}} \right|, \quad \sum_{i=1}^{N} (\nu_{i\omega} - \delta_{i\omega})$$

Note that the absolute amplitude of the mobility in terms of the sign of E_{jk} is

$$E_{jk}\left|\prod_{i=1}^{\infty}\frac{[(1-\omega^2/a_{jki}^2)^2+g_i^2]^{1/2}}{[(1-\omega^2/\Omega_i^2)^2+g_i^2]^{1/2}}\right| = (\text{SGN } E_{jk})|\ddot{Y}|$$

$$\ddot{Y}_{jk} = (\text{SGN } E_{jk})|\ddot{Y}|, \quad \sum_{i=1}^{N}(\nu_{i\omega}-\delta_{i\omega}) \tag{78}$$

where SGN x = + for x > 0

= - for x < 0

The undamped mobility is

$$\ddot{Y}_{jk}^{U} = E_{jk}\prod_{i=1}^{\infty}\frac{1-\omega^2/a_{jki}^2}{1-\omega^2/\Omega_i^2} = (\text{SGN } E_{jk})|\ddot{Y}|\prod_{i=1}^{\infty}\frac{1-\omega^2/a_{jki}^2}{1-\omega^2/\Omega_i^2}\sqrt{\frac{(1-\omega^2/\Omega_i^2)^2+g_i^2}{(1-\omega^2/a_{jki}^2)^2+g_i^2}}$$

$$= (\text{SGN } E_{jk})|\ddot{Y}|\prod_{i=1}^{\infty}\sqrt{\frac{1+g_i^2/(1-\omega^2/\Omega_i^2)^2}{1+g_i^2/(1-\omega^2/a_{jki}^2)^2}} = (\text{SGN } E_{jk})|\ddot{Y}|\prod_{i=1}^{\infty}\sqrt{\frac{1+\tan^2\delta_{i\omega}}{1+\tan^2\upsilon_{i\omega}}}$$

$$= (\text{SGN } E_{jk})|\ddot{Y}|\prod_{i=1}^{\infty}\frac{\cos\nu_{i\omega}}{\cos\delta_{i\omega}} \tag{79}$$

The cosine terms concerned with antiresonances are

$$\cos\nu_{i\omega} = \frac{1-\omega^2/a_i^2}{\left|\sqrt{(1-\omega^2/a_i^2)^2+g_i^2}\right|} = \pm\frac{1}{\sqrt{1+g_i^2/(1-\omega^2/a_2)^2}} \tag{80}$$

If the antiresonance is imaginary, then ω^2/a^2 is always positive and the value of $\cos\nu_i = +1/\sqrt{1+g^2}$, which, considering that g is always much

less than one, is always approximately unity. The minimum value of cos ν is approached as the antiresonant frequency becomes very large compared to the forcing frequency in the case of an imaginary or real antiresonance, but this is also seen to be the case when cos δ is in the denominator. Because there is necessarily the same number of real or imaginary antiresonances in a free system as natural frequencies (one less in a constrained system), it is readily appreciated that the cosine terms of real and imaginary antiresonances that are far from the forcing frequency are canceled by the cosine terms of the natural frequencies that are also far from the forcing frequency. The antiresonant cosine terms near the forcing frequency are very nearly one for imaginary antiresonances.

Figure 6 shows a plot of the cosine terms for real antiresonances and natural frequencies versus the nondimensional forcing frequencies and damping coefficients. It will be noted that natural frequencies and antiresonances have significant effects on the cosine terms only in the vicinity of the forcing frequency. That is, the magnitude of the undamped mobility differs from that of the absolute mobility only to the extent that the cosine terms differ from unity.

These cosine terms are cosines of ν and δ, not phase angles. The angles ν and δ are not physically realizable quantities in themselves, as is a phase angle, but are the angles of numerator vectors of Equation 77, $\sqrt{(1 - \omega^2/a^2)^2 + g^2}$, relative to the undamped axis of frequency, and similarly, for the denominator. Although not directly measurable, they are easily calculated from test data.

Consider a plot of $\ddot{Y}^R_{jx}$, which is the real part of $\partial \ddot{y}_j/\partial f_x$ - the mobility - and of $\ddot{Z}^R_{jk}$, which is the real part of $1/(\partial \ddot{y}_j/\partial f_k)$ - the system impedance.

Here the system is real impedance, the real part of the reciprocal of the complex mobility. Undamped antiresonances are obtained from the impedance plot by the method of Equation 43 for natural frequencies. The damping is found by the techniques of Equation 44. It is extremely important to note that Equation 43 can be applied to the impedance to obtain only the real antiresonances and that only the real antiresonances are required in this method.

Having found the real antiresonances, we may form for each real antiresonance and forcing frequency the cosine of ν by Equation 80. Similarly, the cosines of δ are formed from:

$$\cos \delta_{i\omega} = \frac{(1 - \omega^2/\Omega_i^2)}{\left|\sqrt{(1 - \omega^2/\Omega_i^2)^2 + g_i^2}\right|} \qquad (81)$$

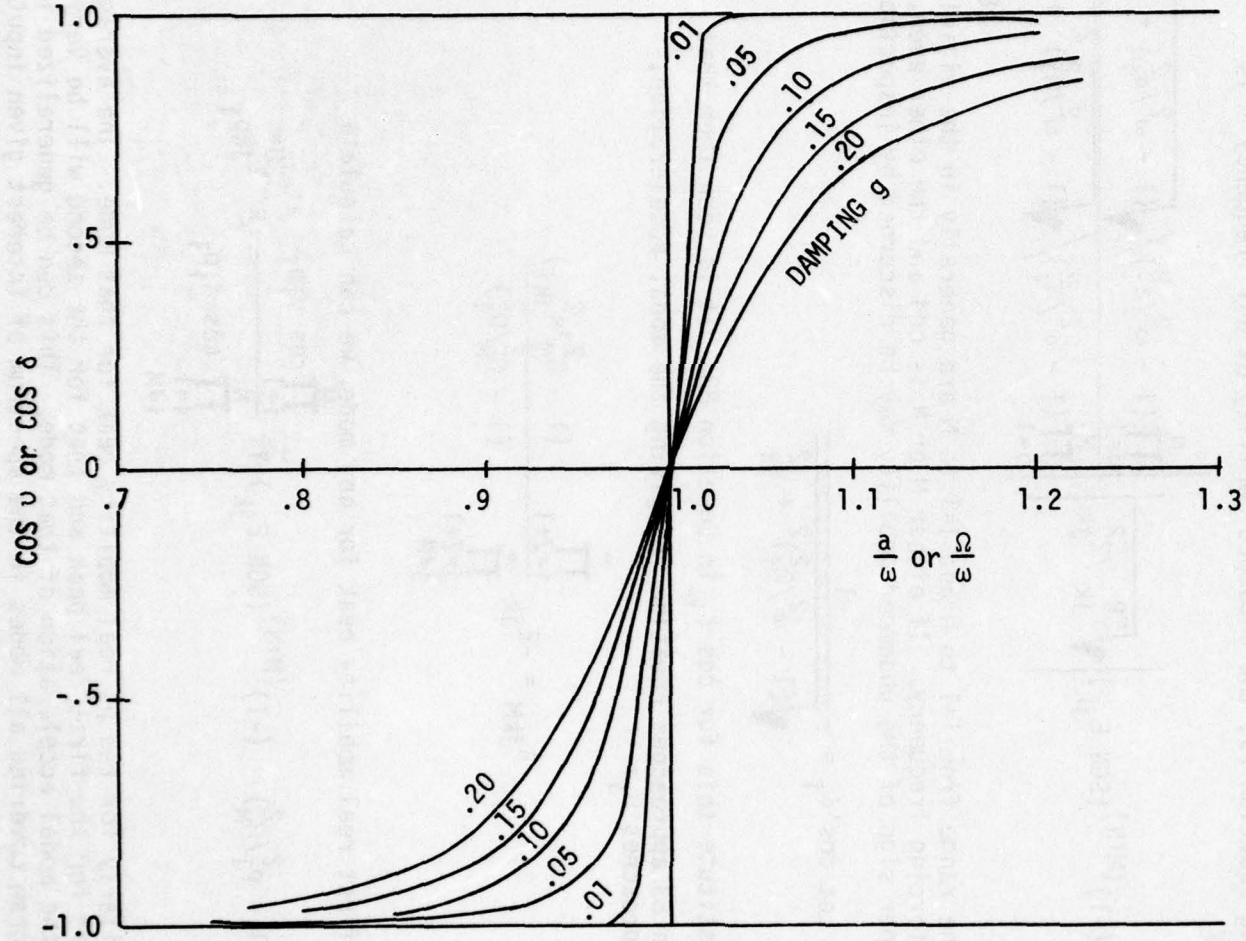

Figure 6. Cosines of Antiresonant and Natural Frequency Vector Angles

The absolute mobility is given by

$$|\ddot{Y}| = \left|\sqrt{\ddot{Y}^R/\ddot{Z}^R}\right| \tag{82}$$

Following Equation 79, the undamped mobility at any frequency ω is given by

$$\ddot{Y}^U_{jk} = (-1)^{(M+N)}(\text{SGN } E_{jk})\left|\sqrt{\ddot{Y}^R_{jk}/\ddot{Z}^R_{jk}}\right| \left| \frac{\prod_{i=1}^{N}(1 - \omega^2/a_i^2)\Big/\sqrt{(1 - \omega^2/a_i^2) + g_i^2}}{\prod_{i=1}^{M}(1 - \omega^2/\Omega_i^2)\Big/\sqrt{(1 - \omega^2/\Omega_i^2)^2 + g_i^2}} \right| \tag{83}$$

where the range from i=1 to N and i=1 to M are generally in the vicinity of the forcing frequency. If either M or N is odd and the other even, the proper sign of the undamped mobility may be discerned by inspection of $\ddot{Y}^R$. Let $\cos'\delta_i = \dfrac{-1}{\sqrt{(1 - \omega^2/\Omega_i^2)^2 + g_i^2}}$

and substitute this for $\cos \delta_{i\omega}$ in Equation 83. It is seen then that Equation 83 approaches Equation 76, giving the modal acceleration, as ω approaches Ω_i:

$$A_{jkM} = -E_{jk} \frac{\prod_{i=Z+1}^{\infty}(1 - \Omega_M^2/a_{jki}^2)}{\prod_{\substack{j=Z+1 \\ j\neq M}}^{\infty}(1 - \Omega_M^2/\Omega_i^2)}$$

At the first real mobility peak for any mode, we can calculate

$$\ddot{Y}^U_{jkp_1}(1 - p_1^2/\Omega_M^2) = (-1)^{(M+N)}(\text{SGN } E_{jk})|\ddot{Y}| \frac{\prod_{i=1}^{M}\cos \nu_i p_1}{\prod_{\substack{i=1 \\ i\neq M}}^{N}\cos \delta_i p_1} \equiv \ddot{Y}^{U*}_{jkp_1}$$

and similarly for the p_2 real mobility peak for that mode. The average of the Y* for the first real peak and that for the second will be very nearly the modal acceleration of that mode. This can be generalized into one program covering all modes in the spectrum of interest given inputs of the peak real acceleration mobility, the frequencies of these peaks, the frequencies of the real acceleration impedance peaks, the sign of the RAC (E), and the peak real acceleration impedance.

LOCAL SPECTRUM METHOD

The real mobility against frequency plot shows two peaks in the vicinity of a given mode.[2] Let the amplitudes and frequencies of these peaks be, respectively, $\ddot{Y}^R_{jkp_1}$, $\ddot{Y}^R_{jkp_2}$, p_1 and p_2 where $p_1 > p_2$. Let the peak imaginary mobility be $\ddot{Y}^I_{jk\Omega}$. From Equations 12 and 13, for the M-th mode,

$$\ddot{Y}^R_{jkp_1} - \ddot{Y}^R_{jkp_2} + \ddot{Y}^I_{jkM}$$

$$= -A_{jkM} \left[\frac{(p_1^2/\Omega_M^2)(1 - p_1^2/\Omega_M^2)}{(1 - p_1^2/\Omega_M^2) + g_M^2} - \frac{(p_2^2/\Omega_M^2)(1 - p_2^2/\Omega_M^2)}{(1 - p_2^2/\Omega_M^2)^2 + g_M^2} - \frac{1}{g_M} \right]$$

$$- \sum_{\substack{i=1 \\ i \neq M}}^{N} A_{jki} \left[\frac{(p_1/\Omega_i)^2(1 - p_i^2/\Omega_i^2)}{(1 - p_1^2/\Omega_i^2)^2 + g_i^2} - \frac{(p_2/\Omega_i)^2(1 - p_2^2/\Omega_i^2)}{(1 - p_2^2/\Omega_i^2)^2 + g_i^2} \right.$$

$$\left. - \frac{g_i(\Omega_M/\Omega_i)^2}{(1 - \Omega_M^2/\Omega_i^2)^2 + g_i^2} \right] \qquad (84)$$

where

$$p_1^2/\Omega_M^2 = \frac{1}{2}(1 + p_1^2/p_2^2) \qquad (85)$$

---

[2] Flannelly and Giansante.

$$p_2^2/\Omega_M^2 = \frac{1}{2}\,(1 + p_2^2/p_1^2) \tag{86}$$

and

$$g_M = \frac{p_1^2 - p_2^2}{2p_1p_2} \tag{87}$$

Substitute Equations 85, 86, and 87 into the terms not under the summation sign of Equation 84, and drop the terms under the summation sign as they will later be shown to be negligible. Define

$$\ddot{Y}^R_{jkp_1} - \ddot{Y}^R_{jkp_2} = \Delta\ddot{Y}^R_{jk}$$

then,

$$\Delta\ddot{Y}^R_{jk} + \ddot{Y}^I_{\Omega}$$

$$\cong -A_{jkM}\left[\frac{(1 + p_1^2/p_2^2)(1 - p_1^2/p_2^2)}{(1 - p_1^2/p_2^2)^2 + 4g_M^2} - \frac{(p_1^2 + p_2^2)(p_1^2 - p_2^2)}{(p_1^2 - p_2^2)^2 + \frac{p_1^2}{p_2^2}\,(p_1^2 - p_2^2)^2} - \frac{1}{g_M}\right]$$

$$\cong -A_{jkM}\left[\frac{p_1^2 + p_2^2}{p_2^2 - p_1^2}\left(\frac{1}{1 + p_2^2/p_1^2} + \frac{1}{1 + p_1^2/p_2^2}\right) - \frac{1}{g_M}\right] \tag{88}$$

But $\dfrac{1}{1 + p_2^2/p_1^2} + \dfrac{1}{1 + p_1^2/p_2^2} = 1$. Therefore, using this result and Equation 87 in Equation 88,

$$\Delta\ddot{Y}^R_{jk} + Y^I_M \cong A_{jkM}\,\frac{(1 + p_2/p_1)^2}{1 - (p_2/p_1)^2} \tag{89}$$

or

$$A_{jkM} \cong (\Delta\ddot{Y}^R_{jk} + \ddot{Y}^I_{\Omega M})\,\frac{1 - p_2^2/p_1^2}{(1 + p_2/p_1)^2} = (\Delta\ddot{Y}^R_{jk} + \ddot{Y}^I_M)\,\frac{(1 - p_2/p_1)}{(1 + p_2/p_1)} \tag{90}$$

assuming terms under the summation sign of Equation 84 are negligible.

Next, consider the terms inside the summation sign of Equation 84, and designate their sum as T. Let $\beta_i \equiv \Omega_M^2/\Omega_i^2$, and note that for $g^2 << g$, it can be shown from Equations 85, 86 and 87 that $p_1^2/\Omega_M^2 \cong (1 + g_M)$ and $p_2^2/\Omega_M^2 \cong (1 - g_M)$. Then:

$$T = -\sum_{\substack{i=1 \\ i\neq M}}^{N} A_{jki} \left\{ \frac{\beta_i(1 + g_M)[1 - \beta_i(1 + g_M)]}{[1 - \beta_i(1 + g_M)]^2 + g_i^2} - \frac{\beta_i(1 - g_M)[1 - \beta_i(1 - g_M)]}{[1 - \beta_i(1 - g_M)]^2 + g_i^2} \right.$$

$$\left. - \frac{\beta_i g_i}{(1 - \beta_i)^2 + g_i^2} \right\} \qquad (91)$$

It is convenient to represent $g_i = g_M = g$. For $1 >> g >> g^2$ and $(1 - \beta)^2 >> g^2$, it is seen that $T << 1$ and the terms are negligible.

ELECTRONIC MASS

Discussion

This section describes the theory of the Kaman Electronic Mass (E-MASS) and its application to improved vibration testing. The E-MASS is used in conjunction with all the information derivable from impedance tests with speed and accuracy heretofore unobtainable. The E-MASS method of testing simplifies the calibration of impedance measuring equipment, requires only the coincident response, and eliminates the measurement of all quantities except frequency. E-MASS is the only method capable of obtaining undamped mobility at any frequency in the spectrum for any specified mobility response. The E-MASS is expected to contribute significantly to dramatic reductions in the developmental costs of new helicopters, airplanes, and spacecraft.

The E-MASS electronically creates the dynamic effects of positive or negative mass between the excitation and any response point of a structure in real time, a situation not physically realizable with actual weights.

The E-MASS device and its associated software enable the engineer to determine all three parameters necessary and sufficient to define the true mobility response of a structure:

(1) The true (undamped) natural frequencies used in analysis

(2) The structural damping mode-by-mode for each mobility response

(3) The modal accelerations for each mode and mobility response

The ratios of modal accelerations determine the elements in the modal eigenvectors, and the reciprocal of a driving point modal acceleration is the "generalized mass" referred to that coordinate.[2] An accurate knowledge of the three parameters listed above enables the engineer to determine, at any point on the structure he places an accelerometer, the true complex response at that point resulting from the shaking of the structure at any other single point. He can then perform system identification, obtain static influence coefficients for arbitrary restraints, determine maneuver inertial loads, and accomplish other necessary analyses requiring known physical structural parameters.[2,6]

In actual practice, the engineer need only use the E-MASS system for one mobility response, along with conventional approximations to the normal modes (e.g. ratios of imaginary mobility peaks) if they are sufficiently accurate, to obtain all the necessary information. In addition, E-MASS can be used at other points to determine only those modes which are too closely coupled or influenced by extremely large or extremely small structural damping for accurate approximation by conventional methods. Alternatively, E-MASS may be used on all responses, eliminating conventional approximations entirely. With the flexibility of E-MASS, a variety of data acquisition methods can be employed while obtaining all three parameters and retaining on-site data control The engineer has the opportunity to optimize the amount of information obtained per unit of data recorded in a test.

Electronic Mass (E-MASS) Theory

The unrestrained jk-th acceleration mobility for zero structural damping is expressed in Equation 71:

$$\ddot{Y}_{jk} = E_{jk} - \sum_{i=Z+1}^{N} A_{jki} \frac{\omega^2/\Omega_i^2}{(1 - \omega^2/\Omega_i^2)} \qquad (71)$$

---

[2] Flannelly and Giansante.

[6] Flannelly, Berman, and Giansante.

Consider a constant mobility, $\Delta\ddot{Y}_{jk}$, subtracted from the mobility, $\ddot{Y}_{jk}$. The intersection of $\ddot{Y}_{jk}$ and $\Delta\ddot{Y}_{jk}$ describes new natural frequencies of the system, as will be shown. Let ω_h be the frequency at which $\Delta\ddot{Y}_{jk}$ intersects the undamped mobility of the system. These frequencies are also the pseudo-antiresonances described in Reference 2. The new natural frequencies resulting from the intersection of $\ddot{Y}_{jk}$ and $\Delta\ddot{Y}_{jk}$ are obtained from:

$$\ddot{Y}_{jk} = \Delta\ddot{Y}_{jk} \tag{92}$$

It is mathematically possible to simulate the addition or subtraction of mass in a damped real mobility plot so that the detrimental effects of damping on the engineer's ability to analyze shake test data are greatly lessened. This mathematical idealization is physically meaningless except for the case of a driving point mobility. However, as shown by the E-MASS device, a jk mass can be electronically added or subtracted to a linear system for producing new resonances.

If the impedance is changed by some amount ΔZ then,

$$Z' = Z + \Delta Z \tag{93}$$

or

$$Z' = Y^{-1} + \Delta Z = (I + \Delta ZY)Y^{-1} \tag{94}$$

and finally

$$(Z')^{-1} = Y' = Y(I + \Delta ZY)^{-1} \tag{95}$$

If only the jk-th element of the impedance matrix is changed, the new jk-th mobility is given by Equation 95 as

$$Y'_{jk} = \frac{Y_{jk}}{1 + \Delta Z_{jk} Y_{jk}} \tag{96}$$

Antiresonances are defined as the frequencies at which the undamped mobility is zero, and natural frequencies are defined as the frequencies at which the undamped mobility is infinite. From Equation 96, the addition of a mass to the jk-th element changes the natural frequencies but does not change the antiresonant frequencies. The new natural frequencies occur when the denominator of Equation 96 goes to zero or

$$Y_{jk} = -\frac{1}{\Delta Z_{jk}} \tag{97}$$

---

[2] Flannelly and Giansante.

From Equation 97, it is seen that the new natural frequencies are exactly equal to the frequency of the intersection of $-1/\Delta Z_{jk}$ with the undamped real mobility. This unique phenomenon explains why the E-MASS device successfully determines the undamped modal accelerations. The new natural frequencies introduced by the E-MASS device are identical to the pseudo-antiresonances described in Reference 2.

Since the E-MASS adds or subtracts mass, Equation 92 becomes

$$\ddot{\Delta Y}_{jk} = -\frac{1}{\Delta m} \tag{98}$$

Combining Equations 71 and 92 gives

$$\ddot{Y}_{jk} = E_{jk} - \sum_{i=Z+1}^{N} A_{jki} \frac{1}{(\Omega_i^2/\omega_h^2 - 1)} \tag{99}$$

where $\ddot{\Delta Y}_{jk}$ is the E-MASS setting, E_{jk} is the rigid-body acceleration coefficient, A_{jki} is the i-th modal acceleration, Ω_i is the undamped resonance, and ω_h is the undamped pseudo-antiresonance.

In matrix form, Equation 99 becomes

$$\left\{E_{jk} - \ddot{\Delta Y}_{jk}\right\} = \left[\frac{1}{(\Omega_i^2/\omega_h^2 - 1)}\right] \left\{A_{jki}\right\} \tag{100}$$

The modal accelerations can be obtained independently of knowing the rigid-body acceleration coefficient using Equation 100 and two different E-MASS settings, $\ddot{\Delta Y}_{jk(1)}$ and $\ddot{\Delta Y}_{jk(2)}$.

$$\left\{E_{jk} - \ddot{\Delta Y}_{jk(1)}\right\} = \left[\frac{1}{(\Omega_i^2/\Omega_{(1)_h}^2 - 1)}\right] \left\{A_{jki}\right\} \tag{101}$$

$$\left\{E_{jk} - \ddot{\Delta Y}_{jk(2)}\right\} = \left[\frac{1}{(\Omega_i^2/\Omega_{(2)_h}^2 - 1)}\right] \left\{A_{jki}\right\} \tag{102}$$

---

[2] Flannelly and Giansante.

where $\Omega_{(1)_h}$ and $\Omega_{(2)_h}$ are the natural frequencies appearing in the mobility plot for the corresponding E-MASS settings. Subtracting Equation 101 from Equation 102 gives

$$\left\{\ddot{\Delta Y}_{jk_{(1)}} - \ddot{\Delta Y}_{jk_{(2)}}\right\} = \left[F_{hi}\right]\left\{A_{jk_i}\right\} \tag{103}$$

where

$$\left[F_{hi}\right] = \left[\frac{1}{(\Omega_i^2/\Omega^2_{(2)_h} - 1)} - \frac{1}{(\Omega_i^2/\Omega^2_{(1)_h} - 1)}\right]$$

Since the rigid body acceleration coefficient can be obtained from either calculation or measurement, the accuracy of determining the modal accelerations is enhanced by eliminating the rigid-body acceleration coefficient from the calculations required by Equation 100. If $\ddot{\Delta Y}_{jk_{(1)}}$ and $\ddot{\Delta Y}_{jk_{(2)}}$ are of opposite sign, the frequency expressions for the diagonal terms of F_{hi} add while those for the off-diagonal terms subtract. This mathematical feature serves to make F_{hi} more diagonal, and consequently, better conditioned than the matrix in Equation 100. The E-MASS settings and the resulting shifts of the natural frequencies determine the modal accelerations from Equation 103.

$$\left\{A_{jk_i}\right\} = \left[F_{hi}\right]^{-1}\left\{\ddot{\Delta Y}_{jk_{(1)}} - \ddot{\Delta Y}_{jk_{(2)}}\right\} \tag{104}$$

It is not necessary to have the same E-MASS setting throughout the entire frequency spectrum since only frequency shifts are of interest. A change in the E-MASS setting, mode-by-mode, gives larger or smaller frequency shifts, allowing for more efficient and convenient operation of the E-MASS device.

The E-MASS device and Equation 104 are used to determine for specified response and excitation coordinates the one parameter not obtained by present state-of-the-art testing methods.

The preceding development and discussion have concentrated on the measurement of acceleration mobility and unrestrained systems. However, the E-MASS device is equally applicable to restrained systems. The only difference between restrained and unrestrained structures is the interpretation of the rigid-body acceleration coefficient E_{jk}. For restrained systems, E_{jk}, is zero and the aforementioned methods remain unchanged. Since Equation 103 is independent of the rigid-body acceleration coefficient, it does not matter whether E_{jk} has some finite value or is zero, as in the case of restrained structures.

E-MASS Calibration Procedure

The most critical and perhaps the most important phase of any test program concerns the calibration procedure necessary for relating electrical responses to physically-meaningful responses. The E-MASS device can be used to eliminate most of the work now required for calibrating mobility response data in terms of g/lb, since the E-MASS output is physically calibrated as a direct measure of mass (lb/g). The calibration of E-MASS and its applications in system calibration are necessary here.

The physical calibration of the E-MASS device is dependent upon a known input condition. A static mass of known magnitude is mounted on an impedance head of known calibration in terms of lb/volt and g/volt and coupled to an electronic exciter.

The outputs of the E-MASS include a force signal of the form

$$f_{out} = f_{in} \pm \Delta m \ddot{y} \tag{105}$$

and an acceleration, $\ddot{y}$. The E-MASS real impedance response

$$\Delta \ddot{Z}^R = \frac{f_{in}}{\ddot{y}} \pm \Delta m \tag{106}$$

is obtained from the automatic mechanical impedance analysis system and recorded on the analog X-Y recorder, yielding a calibration line for the E-MASS device in terms of lb/g versus the E-MASS setting, ΔS. A typical plot of the E-MASS impedance response is illustrated by Figure 7.

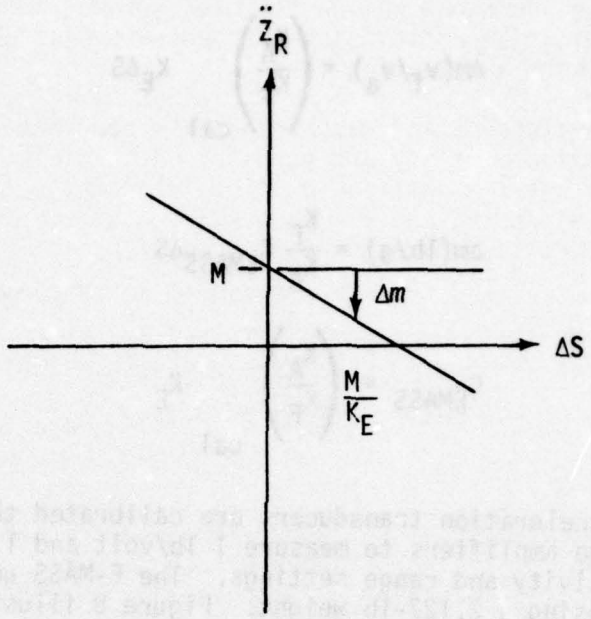

Figure 7. E-MASS Impedance Response

where

$$\ddot{Z}^R = M - \Delta m = M - K_E \Delta S \tag{107}$$

To facilitate a general calibration constant for the E-MASS device, say C_{EMASS}, consider the following development.

$$\Delta m(lb/g) = K_E \Delta S \tag{108}$$

where K_E is the slope of the E-MASS calibration line for known transducer calibrations. In

$$\Delta m(lb/g) = \frac{K_F(lb/v_f)}{K_A(g/v_a)} \Delta m(v_f/v_a) \tag{109}$$

K_F and K_A are the force and acceleration transducer calibration constants, respectively, obtained from specified sensitivity and range settings on the charge amplifiers. Therefore,

$$\Delta m(v_f/v_a) = \left(\frac{K_A}{K_F}\right)_{cal} K_E \Delta S \qquad (110)$$

and

$$\Delta m(lb/g) = \frac{K_F}{K_A} C_{EMASS} \Delta S \qquad (111)$$

where

$$C_{EMASS} = \left(\frac{K_A}{K_F}\right)_{cal} K_E \qquad (112)$$

The force and acceleration transducers are calibrated through their respective charge amplifiers to measure 1 lb/volt and 1 g/volt for specified sensitivity and range settings. The E-MASS unit described was calibrated using a 2.127-lb weight. Figure 8 illustrates this E-MASS calibration line, which directly relates the amount of mass electrically added or subtracted by the E-MASS. A calibration constant of

$$C_{EMASS} = .000097404(v_f/v_a)/\Delta S$$

was obtained for this particular E-MASS unit, which can electrically add or subtract a maximum of 50,000 pounds.

Transducer Calibration

Force and acceleration transducers are usually calibrated in terms of pico-coulomb/lb or pcb/g. The sensitivity and range settings on most charge amplifiers enable the user to relate the transducer outputs as lb/volt or g/volt. The accelerometers can be appropriately calibrated to match a "master" accelerometer in terms of g/volt. The accelerometers are matched by selecting a specified charge-amplifier range setting and adjusting the charge-amplifier sensitivity control until the required g/volt is obtained. The recorded range and sensitivity settings serve to calibrate the transducers.

For example, suppose a "master" accelerometer is calibrated to measure 1g/volt. For an acceleration of 1 g (using the "master" accelerometer) and a specified charge amplifier range setting, the sensitivity is adjusted until the filtered accelerometer signal measures .707 volt rms. Similarly, if a 2-pound weight is excited at 1 g, then the sensitivity is adjusted until the filtered force signal measures 1.414 volts rms. The force transducer is therefore calibrated to measure 1 lb/volt. The transducers used to calibrate the E-MASS device have the following characteristics for a 2.127-lb weight:

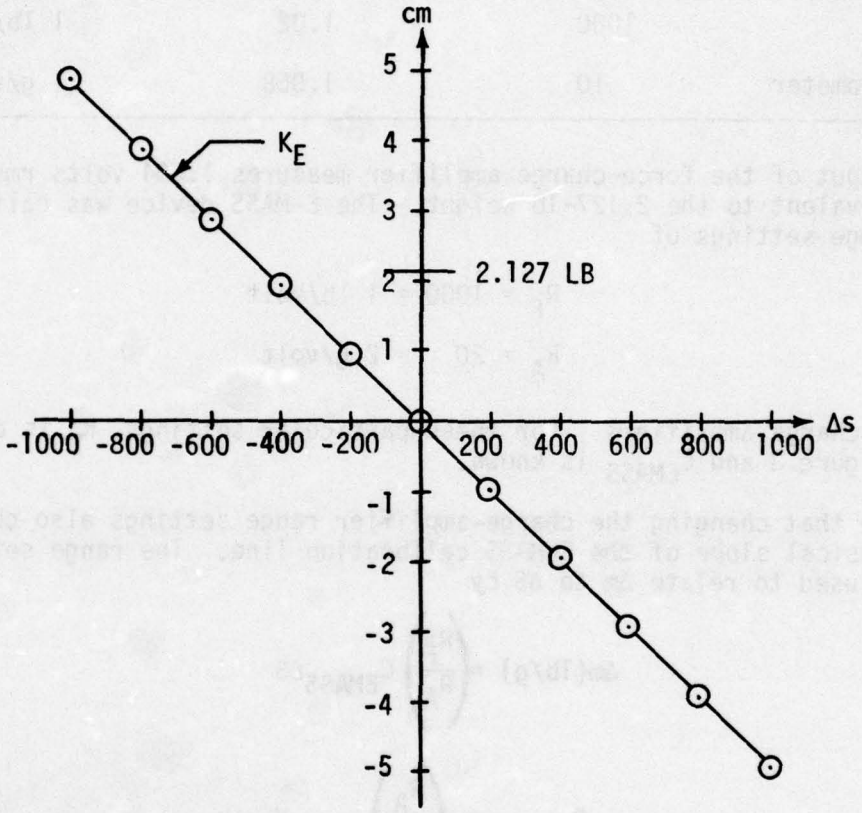

$R_A = 20$, $R_F = 1000$

$K_E = .0048703$ lb/g/ΔS

$C_{EMASS} = .000097404\ v_f/v_a/\Delta S$

Figure 8. Electronic Mass Calibration

CHARGE AMPLIFIER SETTINGS AND OUTPUT			
Transducer	Range	Sensitivity	Output
Force	1000	1.02	1 lb/volt
Accelerometer	10	1.058	1 g/volt

The output of the force-charge amplifier measures 1.504 volts rms, which is equivalent to the 2.127-lb weight. The E-MASS device was calibrated for range settings of

$$R_F = 1000 = 1 \text{ lb/volt}$$

$$R_A = 20 \quad = 2 \text{ g/volt}$$

on the charge amplifiers. For these particular settings, K_E is obtained from Figure 8 and C_{EMASS} is known.

Observe that changing the charge-amplifier range settings also changes the physical slope of the E-MASS calibration line. The range settings can be used to relate Δm to ΔS by

$$\Delta m(\text{lb/g}) = \left(\frac{R_F}{R_A}\right) C_{EMASS} \Delta S \tag{113}$$

where

$$C_{EMASS} = \left(\frac{R_A}{R_F}\right)_{cal} K_E \tag{114}$$

If $(R_A/R_F)_{cal}$ changes, then K_E automatically compensates to give the same E-MASS calibration constant, C_{EMASS}.

This behavior of the impedance versus E-MASS setting is illustrated as follows (Figure 9):

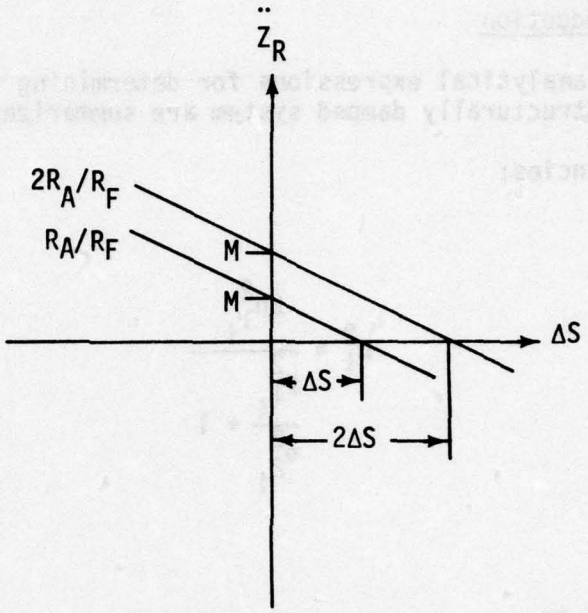

Figure 9. Impedance Vs E-MASS Setting

and

$$C_{EMASS} = R_A/R_F \frac{M}{\Delta S}$$

or

$$C_{EMASS} = 2R_A/R_F \frac{M}{2\Delta S}$$

System Calibration

The calibrated E-MASS device serves as an excellent system calibration method for shake testing of restrained and unrestrained structures. The jk-th acceleration mobility defined by the E-MASS output is

$$\ddot{Y}_{jk} = \frac{\ddot{y}}{f \pm \Delta m \ddot{y}} \qquad (115)$$

If the true force signal, f, is nulled for any convenient E-MASS setting, Δm, then the calibration of the measured acceleration mobility simply becomes

$$(\ddot{Y}_{jk})_{cal} = \pm \frac{1}{\Delta m} \text{ (g/lb)} \qquad (116)$$

This procedure is sufficient to calibrate the entire mobility response for known charge amplifier settings and transducer calibrations.

E-MASS Data Reduction

The necessary analytical expressions for determining the modal parameters of a linear, structurally damped system are summarized here.

Natural Frequencies:

$$\Omega_i^2 = \frac{2p_{1_i}^2}{\frac{p_{1_i}^2}{p_{2_i}^2} + 1} \tag{117}$$

Structural Damping:

$$g_i = \frac{1}{2}\left(\frac{p_{2i}}{p_{1i}} - \frac{p_{1i}}{p_{2i}}\right) \tag{118}$$

Modal Accelerations:

$$\left\{A_{jk_i}\right\} = \left[\frac{1}{(\Omega_i^2/\Omega_{(2)_h}^2 - 1)} - \frac{1}{(\Omega_i^2/\Omega_{(1)_h}^2 - 1)}\right]^{-1} \left\{\ddot{\Delta Y}_{jk_{(1)}} - \ddot{\Delta Y}_{jk_{(2)}}\right\} \tag{119}$$

where p_{1_i} and p_{2_i} are the frequency peaks which occur in the real damping mobility. Recall that $\Omega_{(2)_h}$ and $\Omega_{(1)_h}$ are the undamped resonances created when mass is electrically added or subtracted by the E-MASS settings of $\ddot{\Delta Y}_{jk_{(2)}}$ and $\ddot{\Delta Y}_{jk_{(1)}}$, respectively.

Illustration of E-MASS Operation

Figure 10 shows the test setup used for the illustration of the E-MASS. Included in the photograph are the beam specimen, the automatic mechanical impedance analysis system, the E-MASS device, and the computer terminal used for test-site data reduction. Figure 11 isolates the E-MASS device. The beam specimen, more fully described in Reference 2, was excited at the 0.5-inch station, and the response was measured at the 25-inch station. The real damped transfer acceleration mobility was recorded on the analog X-Y recorder and calibrated by the E-MASS. The frequency spectrum of interest was a range of 10 Hz to 1200 Hz. Figures 12 and 13 illustrate the frequency response for the specimen with a zero setting on the E-MASS device. The physical calibration, frequency limits, and change amplifier settings are recorded on these figures. Figures 14 and 15 illustrate the frequency responses for various preselected E-MASS settings. The necessary frequency data is read as centimeters from Figures 14 and 15 and converted to Hertz through computer software. The E-MASS settings are also converted into g/lb using the E-MASS calibration constant and the charge amplifier settings. Table 1 summarizes the natural frequencies obtained for the E-MASS settings in g/lb, obtained from the mobility plots. Equations 117, 118, and 119 were used to reduce this data to obtain the natural frequencies, modal accelerations, and structural damping of the test specimen. Table 2 summarizes the modal parameters for the first six modes of the beam. These identified modal parameters were used in conjunction with Equations 15 and 16 to reproduce the shake test results. Figures 16 and 17 present the frequency responses identified by the computer simulation. Observe that the mobility amplitude, resonances, and antiresonances are in excellent agreement. The E-MASS device can be effectively used to obtain the necessary parameters which define acceleration mobility shake test data. Although this model has very little damping and is perhaps unrealistic for general structural dynamic applications, the E-MASS device has provided the engineer with an excellent tool for analytical testing. The ability to use the E-MASS for obtaining appropriate analytical models is confirmed. Application of this analytical model to other dynamic problems has been thoroughly discussed in Reference 2.

Summary of the E-MASS Operation

The application of the E-MASS in vibration testing is summarized as follows:

(1) To obtain the desired acceleration mobility response with a zero E-MASS setting.

(2) For any convenient E-MASS setting, to null the force charge amplifier output and record the pen position. The mobility response is calibrated in terms of g/lb.

---

[2] Flannelly and Giansante.

(3) To select appropriate intersections on the damped mobility response, and to change the E-MASS setting until the recorder matches the intersection.

(4) To obtain the modified acceleration mobilities for the desired modes, repeating for each E-MASS setting.

(5) To record the E-MASS settings and the corresponding frequency peaks. To input this data into the software reduction system and obtain the modal parameters.

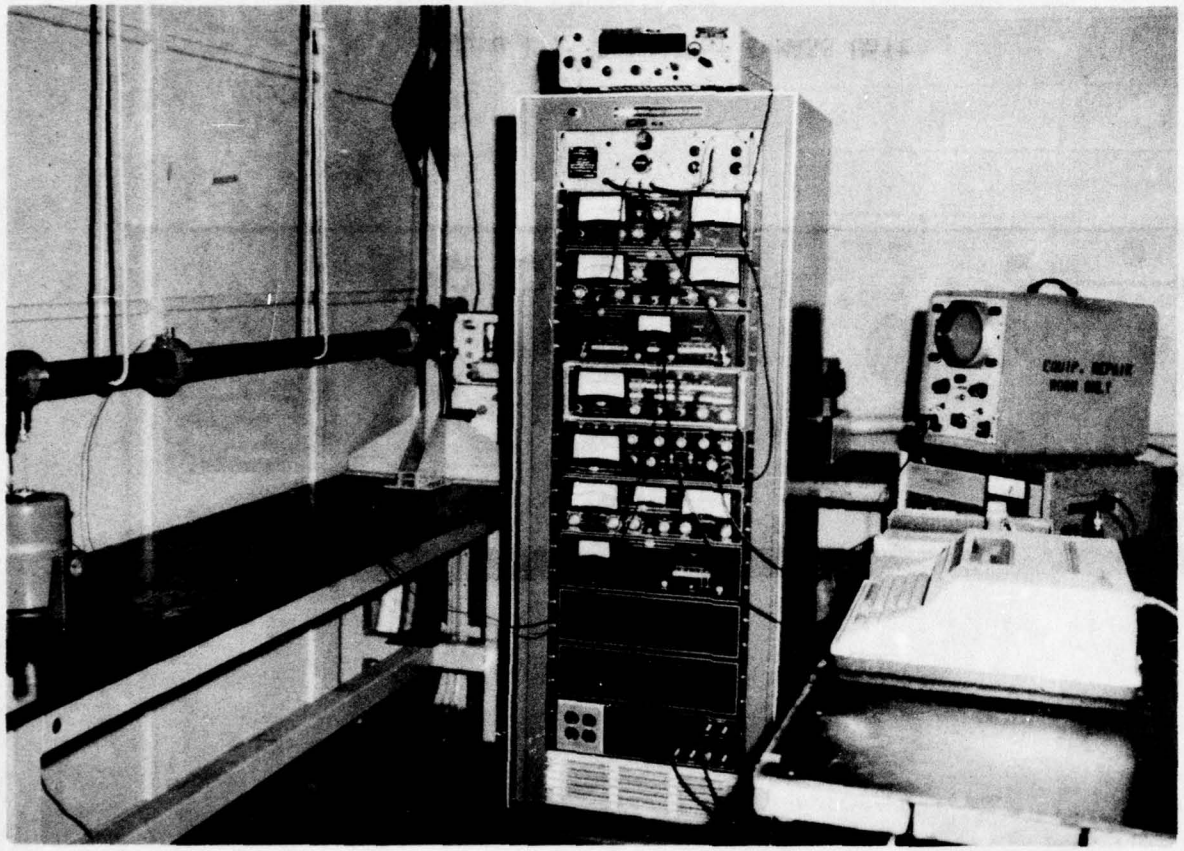

Figure 10. E-MASS Setup

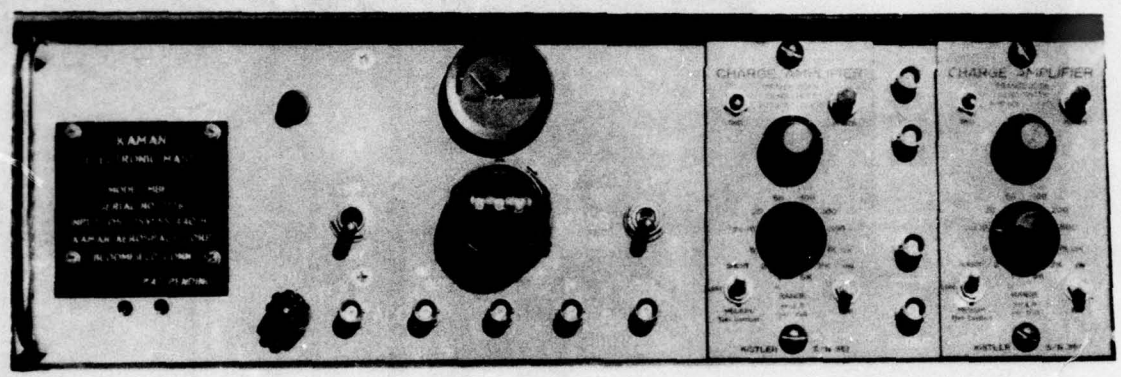

Figure 11. Detail of E-MASS Unit

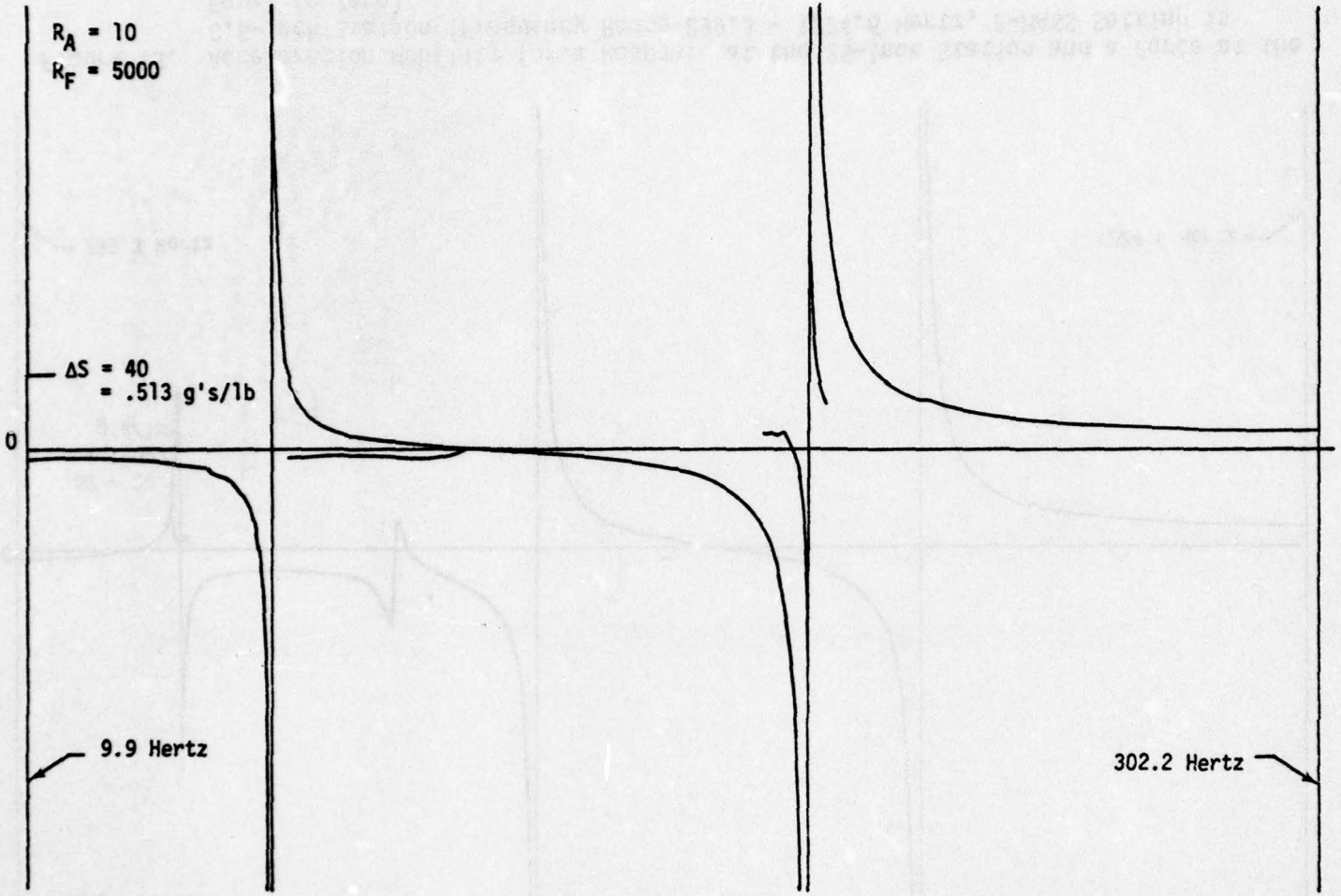

Figure 12. Acceleration Mobility for a Response at the 25-Inch Station and a Force at the 0.5-Inch Station (Frequency Range 9.9 - 302.2 Hertz, E-MASS Setting is Equal to Zero)

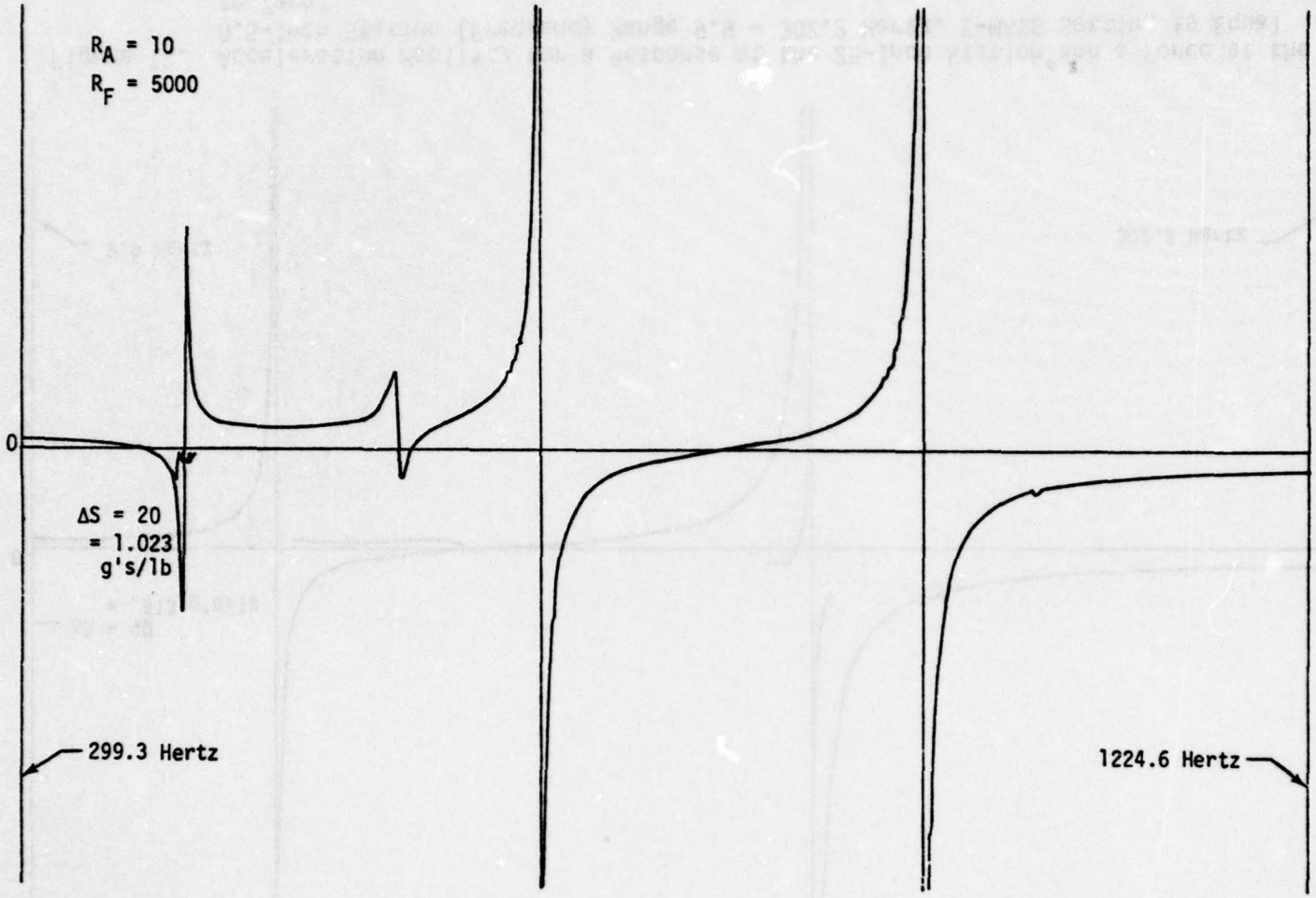

Figure 13. Acceleration Mobility for a Response at the 25-Inch Station and a Force at the 0.5-Inch Station (Frequency Range 299.3 - 1224.6 Hertz, E-MASS Setting is Equal to Zero)

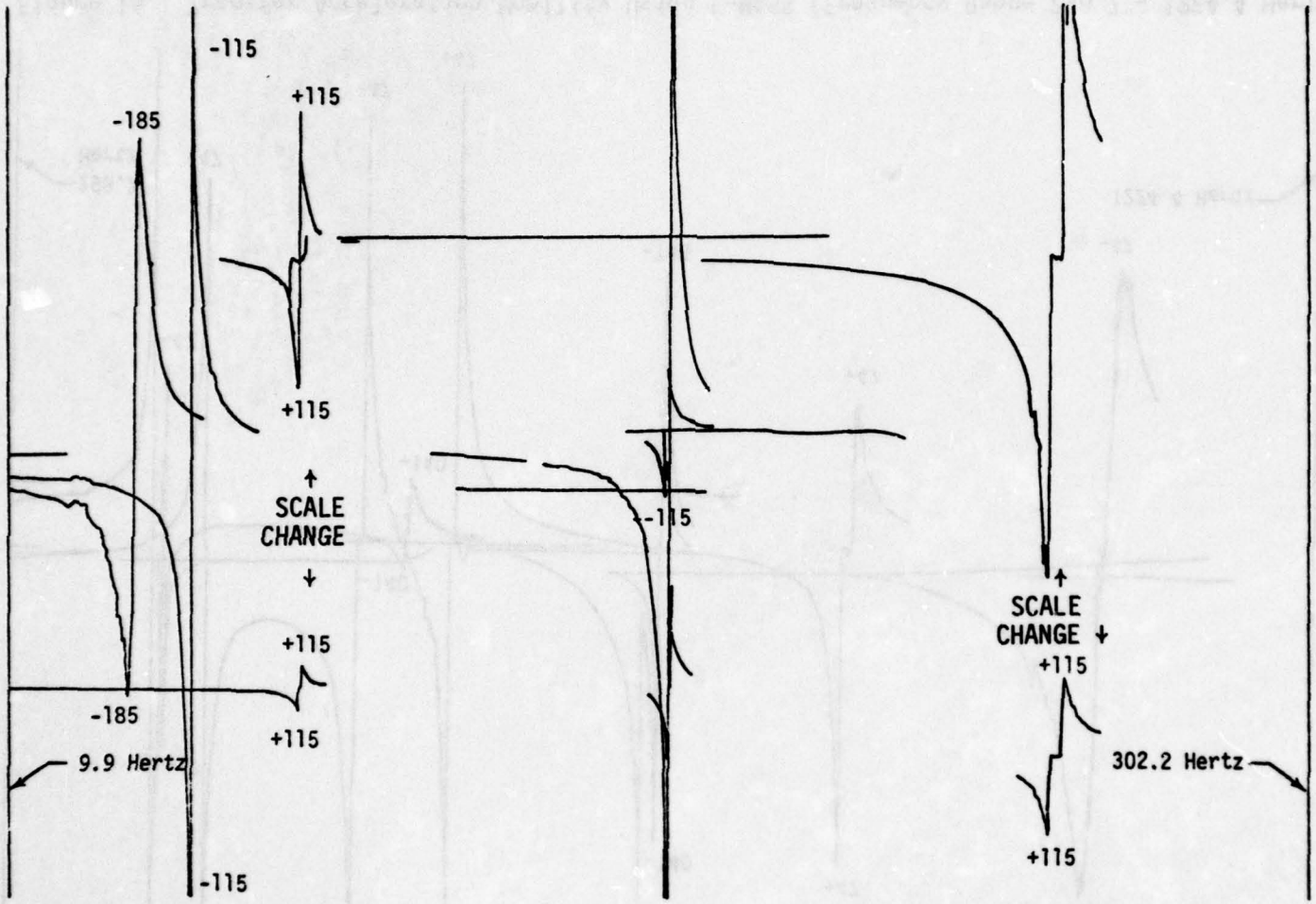

Figure 14. Transfer Acceleration Mobility Using E-MASS (Frequency Range 9.9 - 302.2 Hertz - The scale of the ordinate and ordinate position of the traces are immaterial.)

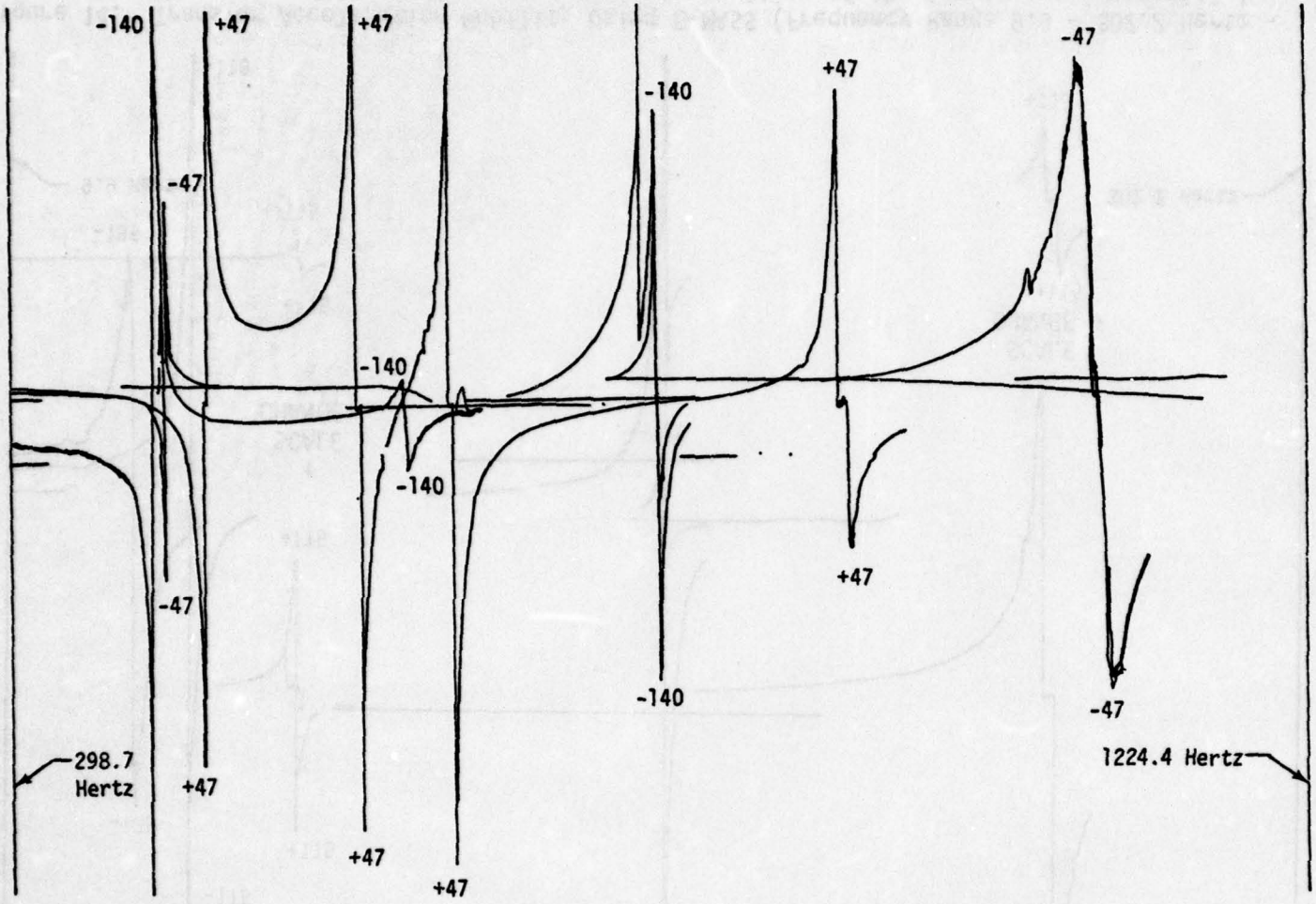

Figure 15. Transfer Acceleration Mobility Using E-MASS (Frequency Range 298.7 - 1224.4 Hertz - A typical run)

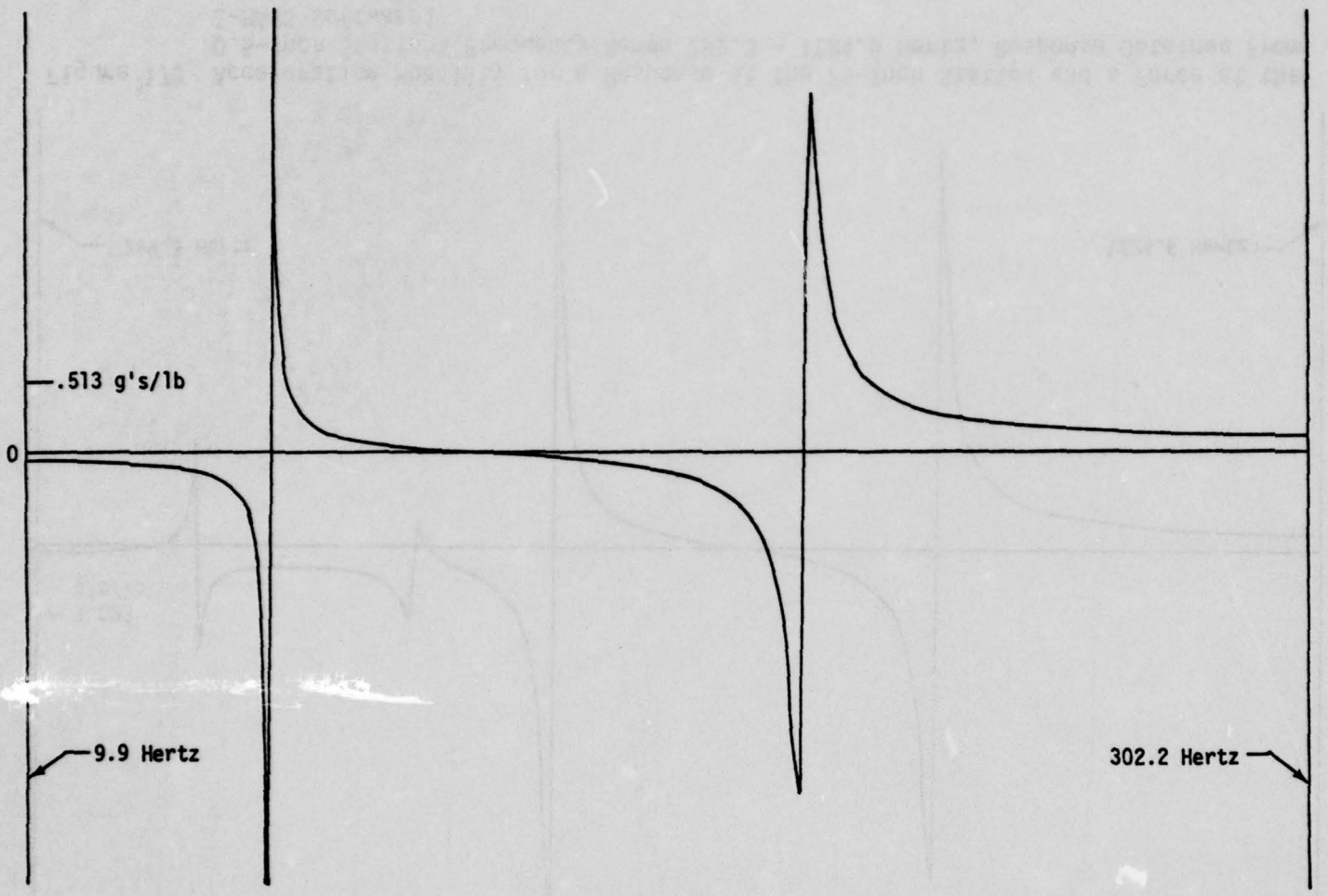

Figure 16. Acceleration Mobility for a Response at the 25-Inch Station and a Force at the 0.5-Inch Station (Frequency Range 9.9 - 302.2 Hertz, Response Obtained From E-MASS Software)

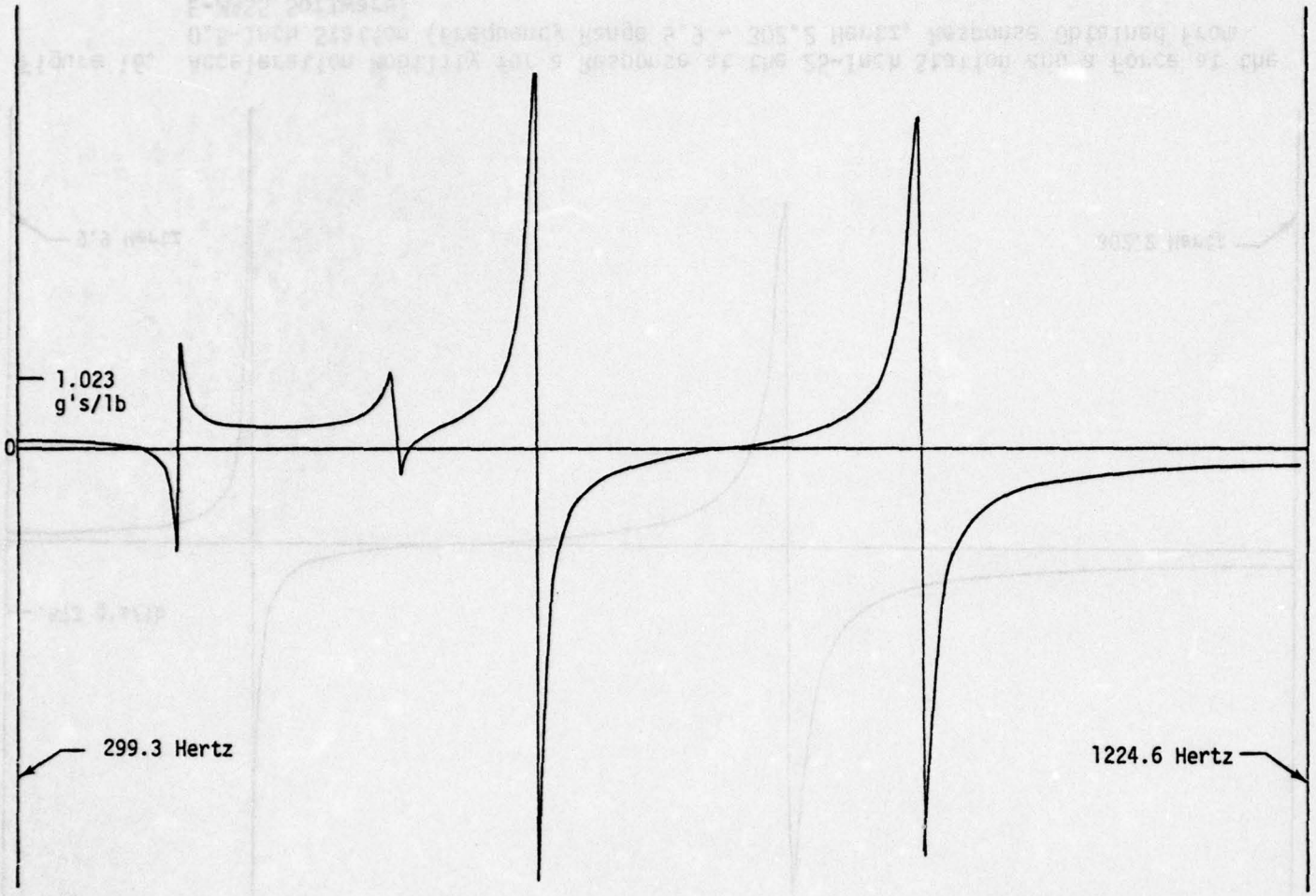

Figure 17. Acceleration Mobility for a Response at the 25-Inch Station and a Force at the 0.5-Inch Station (Frequency Range 299.3 - 1224.6 Hertz, Response Obtained From E-MASS Software)

TABLE 1. NATURAL FREQUENCIES OBTAINED FROM POSITIVE AND NEGATIVE E-MASS SETTINGS

Mode	E-MASS Setting Δs	E-MASS Setting $In/Sec^2/Lb$	Resonances (Hz)
I	0	0	65.4
II	0	0	187.54
III	0	0	415.25
IV	0	0	569.72
V	0	0	672.52
VI	0	0	948.95
I	115	68.99	75.28
II	115	68.99	245.05
III	47	168.8	436.83
IV	47	168.8	546.24
V	47	168.8	612.44
VI	47	168.8	894.07
I	-115	-68.99	50.87
II	-115	-68.99	158.57
III	-140	-56.67	400.75
IV	-140	-56.67	580.14
V	-140	-56.67	760.15
VI	-47	-168.8	1075.9

TABLE 2. SUMMARY OF MODAL PARAMETERS FOR A FORCE AT 0.5-INCH STATION AND A RESPONSE AT 25-INCH STATION

Mode	Natural Frequencies (Hz)	Modal Accelerations (In./Sec^2/Lb)	Structural Damping
I	65.4	25.133	.0058
II	187.54	28.348	.0134
III	415.25	9.076	.0067
IV	569.72	-6.439	.0105
V	672.52	-30.087	.0059
VI	948.95	-28.861	.0063

E_{jk} = -28.51 in./sec^2/lb

DYNAMIC MODEL FORCE DETERMINATION TESTS

DYNAMIC MODEL TEST FACILITY

Description of the Helicopter Dynamic Model

An experiment was undertaken to demonstrate the ability of force determination to determine a helicopter's hub loads directly from measured fuselage accelerations. Further, an investigation of the sensitivity of force determination to typical helicopter gross weight and center of gravity changes was desired. The principal objective of the test specimen was to have a dynamic model that realistically simulates the characteristics of typical helicopters. The dynamic characteristics, in order of importance, are: (1) an appropriate mass and stiffness distribution - a relatively stiff cockpit and cargo section with an elastically softer tail boom section; (2) a relatively low fundamental natural frequency; and (3) representative structural damping. As shown in Figure 18, a 5-foot-long dynamic model was designed to reflect the overall structural and mass characteristics of military utility helicopters. The model, constructed of riveted and bolted aluminum, has a large central fuselage with open sides, a longitudinal carry-through structure of small depth at the deck and roof, and "beefy" vertical members at the forward and aft ends of the main cabin. The flight deck is essentially a cantilevered keel, and the tail boom is a "bent" cantilever beam.

Steel weights (confined to a space of small depth) on the roof structure of the dynamic model simulate the masses of engines and transmission, while steel and aluminum weights simulate the tail rotor system and weight concentrations on the flight deck, as shown in Figure 18. Fuel and payload were simulated by layers of steel weights in the center cabin, designed to be removable to examine the effects of fuel burnoff and center of gravity shifts.

The first natural frequency of the dynamic model was made to be 18.1 Hz, in imitation of dynamic data showing 18 Hz on the Kaman HU2K Navy utility helicopter. Fore-and-aft adjustments of a flight deck mass and a tail boom mass allowed fine tuning of dynamic model natural frequencies. The measured natural frequencies of the dynamic model were 18.1, 19.6, 40.8, 65.9, 75.8 and 77.9 Hz. It will be noted that some of these modes are quite close together, reflecting a situation not uncommon in actual aircraft.

A unit weight and inertia breakdown of the model is shown in Table 3. Butt Line Zero is the plane of symmetry, the stations are measured from the nose, and the water lines are measured from the cargo deck area. These reference lines are shown in Figure 18.

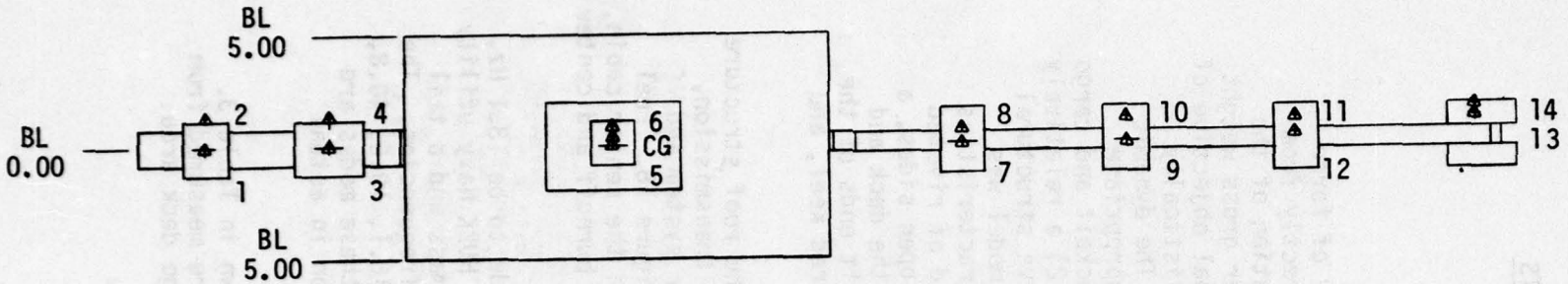

PLAN VIEW

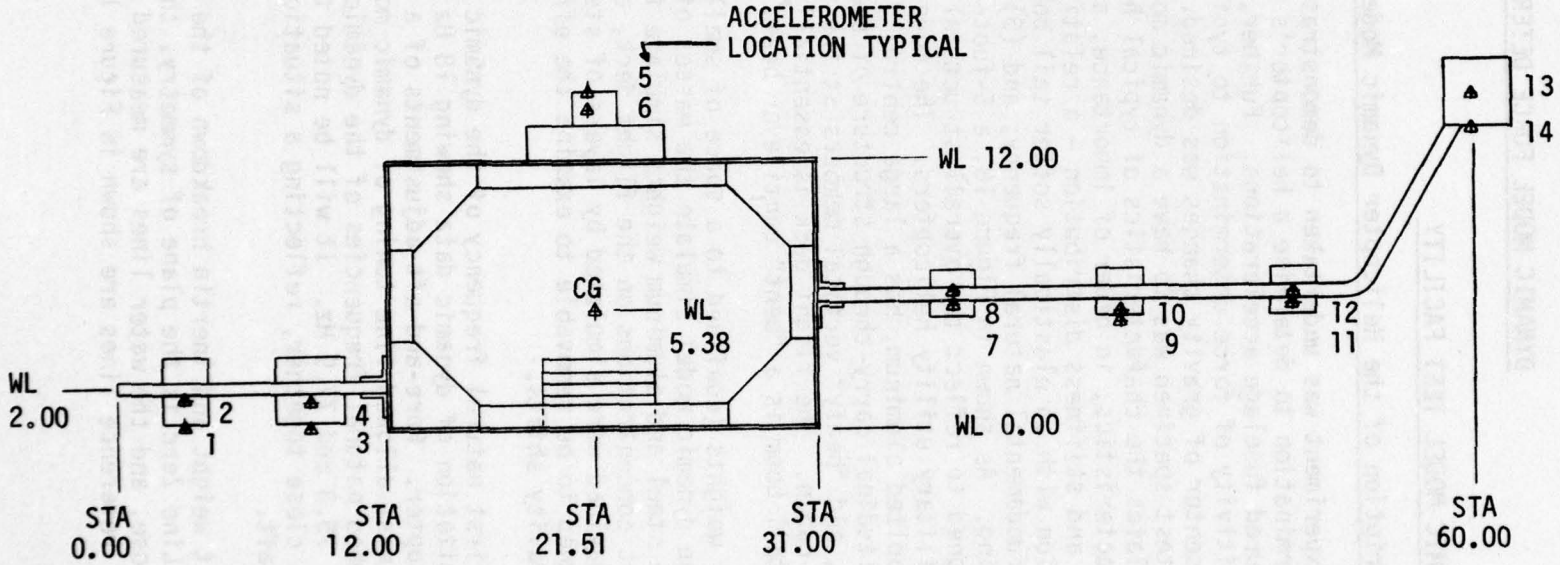

PROFILE VIEW

Figure 18. Schematic of Dynamic Test Model

TABLE 3. UNIT WEIGHTS AND MOMENTS OF INERTIA OF THE DYNAMIC MODEL

	Location			Moment of Inertia		
Weight (lb)	X Butt Line (in.)	Y Station (in.)	Z Water Line (in.)	I_{xx} Pitch ($lb\text{-}in.^2$)	I_{yy} Roll ($lb\text{-}in.^2$)	I_{zz} Yaw ($lb\text{-}in.^2$)
1.25	0.00	5.97	1.97	14.90	0.45	15.29
0.37	0.00	11.53	1.97	0.29	0.38	0.15
0.44	0.00	21.17	14.25	0.16	0.16	0.16
4.19	0.00	21.17	12.75	13.35	7.54	19.32
17.25	0.00	21.42	6.00	1396.54	646.72	1177.36
0.31	0.00	31.37	6.00	0.35	0.43	0.13
2.43	0.00	42.89	6.00	116.67	0.40	116.67
1.01	0.00	57.82	10.23	8.51	6.42	2.55
1.81	0.00	59.02	13.00	2.53	3.15	3.30
4.06	0.00	3.03	1.97	4.78	0.89	4.31
7.19	0.00	8.48	1.97	13.57	14.46	9.89
1.19	0.00	44.30	6.00	1.66	1.86	0.99
5.44	0.00	21.42	1.00	13.37	14.30	24.05
0.06	0.00	3.03	0.47	0.05	0.07	0.05
0.06	0.00	8.48	0.17	0.00	0.00	0.00
0.06	0.00	21.17	15.00	0.00	0.00	0.00
0.06	0.00	36.94	5.51	0.00	0.00	0.00
0.06	0.00	44.30	4.51	0.00	0.00	0.00
0.06	0.00	51.90	5.51	0.00	0.00	0.00
0.06	-1.00	59.02	14.42	0.00	0.00	0.00
0.06	-1.54	3.03	1.07	0.00	0.00	0.00
0.06	-1.50	8.48	0.92	0.00	0.00	0.00
0.06	-0.75	21.17	14.25	0.00	0.00	0.00
0.06	-0.50	36.94	6.00	0.00	0.00	0.00
0.06	-1.22	44.30	5.01	0.00	0.00	0.00
0.06	-0.50	51.90	6.00	0.00	0.00	0.00
0.06	-1.50	59.02	13.00	0.00	0.00	0.00
Center of Gravity	-.0107	21.51	5.38			

The total weight is 47.78 pounds. The moments of inertia and products of inertia about the center of gravity are I_{xx} = 11,280; I_{yy} = 1362; I_{zz} = 10,391; U_{xy} = -5.77; U_{xz} = -.839; and U_{yz} = 1445 lb-in. Butt plane zero is the plane of symmetry of the model. Station zero is the nose, and waterline zero is the cargo deck.

Suspension System

The dynamic model was suspended upside down, allowing a convenient hub shaker location, on bungee cords of a low spring rate. The shaker is much larger relative to the dynamic model than a full-scale shaker would be relative to an actual fuselage. This made it impossible to hang the model right-side-up with a realistic fore-and-aft spread of bungees. Further, the upside-down suspension simplified the work involved in the many shaker positions tested, thereby reducing costs.

A winch system for regulating the free length of the fore-and-aft bungee cords allowed the dynamic model to be trimmed in pitch during center of gravity changes. It also provided a simple fine adjustment of the height of the dynamic model, allowing the shaker armature to be quickly and easily positioned between the limit stops as the gross weight was changed. The winch system was used to elevate the model out of the way of the work table so that calibrations on the impedance-head, shaker checks, and other work not involving the dynamic model itself, could be done.

The inverted "U" support of the winch suspension system was attached to the work table and was of adjustable height so that the entire test set-up was independent of any fixed structure and could be moved for demonstration purposes with little adjustment or dismantling effort.

Such design features make the test setup and the dynamic model a convenient facility for inexpensive dynamic-model testing beyond the work done under this contract.

Instrumentation Provisions on the Dynamic Model

As shown in Figure 18, the dynamic model was fitted with 14 accelerometers, seven vertically and seven laterally. Concentrated weights on the model were drilled and tapped for mounting an impedance head laterally or vertically at positions the engineer might choose. The flat horizontal and vertical surfaces of the dynamic model allow an infinite number of positions at which additional fixed accelerometers can be bonded or at which a roving accelerometer can be wax mounted. The use of a roving accelerometer in dynamic model testing must be done with care to account for the mass of the accelerometer itself, as it is not scaled down from full size.

The stud-mounted fixed accelerometers were mounted with special precautions to avoid case distortion, which can produce physically meaningless signals. Great care was taken to assure the surface flatness, the verticality of the tapped hole, and the mounting torque, and that the stud design met the manufacturer's exacting specifications.

The connection of the impedance head from the dynamic model to the shaker had to be axially rigid but flexible in rotation and in the lateral directions so that restraints would not be introduced. The typical necked-down rod used in testing larger specimens is not suitable for scale model use, so a special connector consisting of orthogonal flat steel columns in series was designed for use on the dynamic model. The plates of the new sting were proportioned to carry axial loads much higher than required for shaking to preclude buckling and to have virtually zero restraint in torsion and in the slopes and deflections in the plane perpendicular to the shaking axis.

The positions of the accelerometers on the model are shown in Table 4. Odd-numbered accelerometers sense vertical vibration; even-numbered accelerometers sense lateral vibration.

With x, y and z measured from the center of gravity, the RACs are determined from Equation (66).

For j and k odd-numbered accelerometers,

$$E_{jk} = 8.0787 + .3323\, x_j x_k + 1.7349 \times 10^{-4}(x_j y_k + x_k y_j) + .03422\, y_j y_k \quad \text{in./lb-sec}^2$$

For j and k even numbered accelerometers,

$$E_{jk} = 8.0787 + .04357\, y_j y_k - .0462(y_j z_k + y_k z_j) + .3323\, z_j z_k \quad \text{in./lb-sec}^2$$

For accelerometers in which the indices sum, j + k, to an odd number,

$$E_{jk} = z_j(-1.7349 \times 10^{-4} y_k - .3323 x_k) + y_j(.04621 x_k + 2.6889 \times 10^{-5} y_k) \quad \text{in/lb-sec}^2$$

TABLE 4. ACCELEROMETER LOCATIONS

Accelerometer Number	X From Butt Line Zero (in.)	Y From Station Zero (in.)	Z From Waterline Zero (in.)
1	0	3.03	.47
2	-1.54	3.03	1.07
3	0	8.48	.17
4	-1.50	8.48	.918
5	0	21.17	15.00
6	-.75	21.17	14.25
7	0	36.94	5.51
8	-.50	36.94	6.0
9	0	44.3	4.51
10	-1.23	44.3	5.01
11	-1.00	51.9	5.51
12	-.50	51.9	6.00
13	-1.00	59.02	14.42
14	-1.50	59.02	13.0
C.G.	-.0107	21.51	5.38

Damping in the Dynamic Model

The damping characteristics of the dynamic model varied somewhat from those desired. However, the variations produced data on the conservative side, so that no significant degradation of the experiments resulted.

Structural damping coefficients in the 3-percent range were desired, but in spite of riveted joints, the coefficients were in the 1/2-percent to 1-1/2-percent range. Consideration was given to increasing the structural damping of the dynamic model by using thin rubber laminations and high-hysteresis coatings, but it was finally decided to leave the damping low and to err on the conservative side. Low damping is conservative because the lower the damping, the steeper the mobility curves near resonances, and hence, slight variations in the forcing frequency in these spectral regions result in large changes in mobility. Therefore, the calibration error is greater near resonances. With more damping, the calibration errors near resonances would be smaller, giving greater accuracy in force determination. If the damping treatment of the dynamic model were to increase the damping to a level greater than that which would be experienced on a full-size aircraft, the accuracy of force determination shown in these experiments would be unrealistically good. It was, therefore, conservative to keep the model damping on the low side.

Originally the tail boom was constructed of bolted, aluminum laminations. This boom failed to give the desired level and type of damping; the laminations produced ankylosis instead. Ankylosis (Reference 12) is a condition of "sticking" and "unsticking" which sometimes occurs in small-scale models with bolted structure of the degrees of freedom. It was first noticed in wind tunnel experiments at the National Physics Laboratory in England in 1933 (Reference 12). In that instance, the ankylotic effect of friction made an otherwise stable airplane wind tunnel model unstable. This phenomenon is apparently confined to models since there are no known references to its occurring in actual aircraft.

Ankylosis in this experiment was corrected by replacing the bolted, laminated tail boom with a tail boom of solid cross-section. With the solid tail boom, the model was more representative of a helicopter with a typical dynamically well-behaved semi-monocoque closed tail section.

Some in-house research at Kaman on nonmetallic damping, which does not bear on the work in this contract, indicates that the hysteretic damping levels of the dynamic model could be increased by controlled amounts, should that be desired in the future use of the model. Its modular construction would also allow the replacement of major portions of the structure with units of composite material with various damping and dynamic characteristics.

---

[12] Frazer, Duncan and Collar.

DESCRIPTION OF THE TESTS

The dynamic model helicopter was shaken to obtain the 14x2 mobility matrix $[\ddot{Y}]$. The first column of this mobility matrix is the complex ratios of the accelerations at each of the fourteen fuselage accelerometers to unit vertical forces at the hub. The second column of the mobility matrix is the complex ratios of the accelerations at each of the fourteen fuselage accelerometers to unit lateral forces at the hub. This mobility matrix was obtained in two ways: (1) by direct shaking at the hub with only one shaker at a time, and (2) by shaking at the nose, and not at the hub, and using modal accelerations. The results of the tests, comparing the two mobility matrices, are given below.

Next, the dynamic model helicopter was "flown" by using vertical and lateral shakers at the hub simultaneously. Different flight speeds and maneuvers were represented by different magnitudes and phasings of the shaker forces at the hub. For each flight condition, the amplitudes and relative phasings of the fourteen fuselage accelerometers were recorded.

Having obtained the mobility matrix $[\ddot{Y}]$ from the shake tests and the "in-flight" accelerations of the fourteen accelerometers $\{\ddot{y}\}$ from "flight", the real and imaginary vertical and lateral forces at the hub were calculated using the complex pseudoinverse of the mobility, $[\ddot{Y}]^+$:

$$\{f\}^R + i\{f\}^I = [\ddot{Y}]^+ \{\ddot{y}\} \tag{121}$$

The calculated magnitudes and phase angles of these forces were then compared with the magnitudes and phase angles of the forces measured on the shakers in the "flight". This was done for 81 test cases covering 54 combinations of vertical and lateral forces over phase angles ranging from 0° to 180°. Included in these are cases representing calibration errors due to fuel burnoff effects on the center of gravity and the gross weight.

SUMMARY OF FORCE DETERMINATION TEST RESULTS

Table 5 summarizes the average absolute errors found in 81 tests of force determination. The term "error" defines the percentage difference between applied hub loads measured by a force transducer and the hub loads predicted by force determination. In general, the errors are within the achievable limits of accuracy of the measurements of the applied loads.

TABLE 5. SUMMARY OF FORCE DETERMINATION

Configuration	Average Absolute Percent Error in Vertical Force Amplitude	Average Absolute Percent Error in Lateral Force Amplitude	Average Absolute Degree Error in Phase
Direct Hub Shake - Correct Calibration			
Nominal 15 Hz Calibration	2.49	16.61	3.45
Nominal 17 Hz Calibration	4.08	7.69	3.44
Nominal 25 Hz Calibration	2.36	4.47	4.78
Mass Change 25 Hz Calibration	6.18	1.76	2.76
CG Change 25 Hz Calibration	5.59	2.74	4.64
Modal Acceleration Test - Correct Calibration			
Nominal 25 Hz Calibration	5.19	3.69	4.40
Direct Hub Shake - Flight Configuration Different From Calibration Configuration			
Mass Change Nominal 25 Hz Calibration	24.1	1.97	3.49
CG Change Nominal 25 Hz Calibration	22.4	3.02	4.64

The results indicate that force determination of a configuration is a precise method of measuring the magnitudes and phasings of hub forces. It is indicated by the test results that force determination calibration of a nominally configured aircraft with vertical and lateral hub excitations may have errors of up to 24 percent for flights with 60-percent fuel burnoff and extreme center of gravity shift, which suggests that a force determination calibration in a ground shake test should be done for several increments of fuel burnoff and longitudinal shifts of center of gravity.

Caution should be observed in extrapolating from the results obtained with these model tests to conclusions about the usefulness of force determination on full-scale aircraft, in spite of the excellent results obtained by force determination in flights of the DAVI-modified UH-1H. Many helicopters have more interaction among hub forces than could be investigated in this limited project, scale effects cause some degree of unrealism in model testing, and the model did not simulate the dynamics of such things as secondary structures or structural doors.

DIRECT SHAKE FORCE DETERMINATION TEST RESULTS

25 Hz Case - Table 6

25 Hz lies between the second and third modes of the helicopter dynamic model, which are at 19.6 Hz and 40.8 Hz, and represents a fuselage which is reasonably well detuned from resonance with blade passage frequency.

17 Hz Case - Table 7

17 Hz is only 6.1 percent below the 18.1-Hz natural frequency of the helicopter dynamic model and represents a fuselage that is <u>not</u> well detuned from resonance with blade passage frequency.

15 Hz Case - Table 8

The 16.6-percent error in the lateral force at 15 Hertz was of some interest. Why did this condition show more error than the others? Also we might ask "How accurate is accurate?" The 6- or 7-percent error obtained for the other forces is certainly within measurement error and requires no further examination. However, the 16.6-percent error is a significant change (not necessarily high) and was explained by some additional testing. Recall that the dynamic calibration of the model was performed by independent force application at the hub to simulate actual operating conditions. The calibration matrix was obtained from the acceleration mobility data for each accelerometer. When hub forces were simultaneously applied to the model, new hub boundary conditions were introduced by the shaker attachment. The forces are applied at the simulated hub through "soft" flexure units that introduce a resonance of the system near 7.0 Hertz. If the hub calibration is again performed with the shakers connected, then the acceleration mobilities (and

TABLE 6. CALIBRATION AT NOMINAL GROSS WEIGHT AND CENTER OF GRAVITY, FLIGHT AT NOMINAL GROSS WEIGHT AND CENTER OF GRAVITY

25 Hz

Vertical Force Magnitude			Lateral Force Magnitude			Phase Angle		
Measured "Flight" Input (lb)	Calculated by Force Determination (lb)	Error (%)	Measured "Flight" Input (lb)	Calculated by Force Determination (lb)	Error (%)	Measured "Flight" Input (deg)	Calculated by Force Determination (deg)	Error (deg)
15	15.466	3.107	10	9.726	2.74	120	125.14	5.14
10	10.067	.67	10	9.51	4.9	180	188.16	8.16
10	9.977	.23	15	14.134	5.773	180	187.587	7.587
15	15.314	2.093	10	9.4	6.0	180	186.935	6.935
15	15.211	1.407	10	9.584	4.16	180	187.233	7.233
15	15.553	3.687	10	9.558	4.42	45	43.558	1.442
15	15.459	3.06	10	9.751	2.49	90	87.882	2.118
15	15.413	2.753	10	9.577	4.23	0	-1.932	1.932
15	15.634	4.227	10	9.452	5.48	0	-2.514	2.514
Average Error		2.36%			4.47%			4.78°

TABLE 7. CALIBRATION AT NOMINAL GROSS WEIGHT AND CENTER OF GRAVITY, FLIGHT AT NOMINAL GROSS WEIGHT AND CENTER OF GRAVITY

17 Hz

Vertical Force Magnitude			Lateral Force Magnitude			Phase Angle		
Measured "Flight" Input (lb)	Calculated by Force Determination (lb)	Error (%)	Measured "Flight" Input (lb)	Calculated by Force Determination (lb)	Error (%)	Measured "Flight" Input (deg)	Calculated by Force Determination (deg)	Error (deg)
2.5	2.349	6.04	5.0	5.394	7.88	180	183.384	3.384
2.5	2.374	5.04	5.0	5.365	7.3	90	91.336	1.336
2.5	2.324	7.04	5.0	5.474	9.48	45	46.845	1.845
5.0	4.746	5.08	5.0	5.452	9.04	0	4.731	4.731
5.0	4.79	4.2	5.0	5.46	9.2	0	3.403	3.403
2.5	2.333	6.68	5.0	5.384	7.68	0	3.104	3.104
5.0	4.767	4.66	2.5	2.712	8.48	45	46.553	1.553
5.0	4.821	3.58	2.5	2.684	7.36	90	92.672	2.672
5.0	4.863	2.74	2.5	2.793	11.72	180	183.285	3.285
5.0	4.846	3.08	2.5	2.7	8.0	0	1.538	1.538
5.0	4.979	.42	2.5	2.596	3.84	90	100.87	10.87
5.0	4.972	.56	2.5	2.622	4.88	180	185.457	5.457
5.0	4.807	3.86	2.5	2.706	5.15	0	1.537	1.537
Average Error		4.08%			7.693%			3.44°

TABLE 8. CALIBRATION AT NOMINAL GROSS WEIGHT AND CENTER OF GRAVITY, FLIGHT AT NOMINAL GROSS WEIGHT AND CENTER OF GRAVITY

15 Hz

Vertical Force Magnitude			Lateral Force Magnitude			Phase Angle		
Measured "Flight" Input (lb)	Calculated by Force Determination (lb)	Error (%)	Measured "Flight" Input (lb)	Calculated by Force Determination (lb)	Error (%)	Measured "Flight" Input (deg)	Calculated by Force Determination (deg)	Error (deg)
10	10.177	1.77	5	5.903	18.06	180	182.221	2.221
10	10.033	.33	5	5.854	17.08	90	95.7125	5.713
10	9.95	.5	5	5.732	14.64	0	3.559	3.559
10	9.732	2.68	5	5.952	19.04	0	2.838	2.838
10	9.921	.79	5	5.708	14.16	45	50.171	5.171
5	4.613	7.74	10	11.474	14.74	0	2.563	2.563
5	4.818	3.64	2.5	2.964	18.56	0	2.087	2.087
Average Error		2.49%			16.61%			3.45°

consequently the calibration) are different. As the forcing frequency becomes much greater than the lower resonance introduced by the shakers, the acceleration mobilities converge to the same measurement. One can conclude that the percent error for the 15-Hertz calibration can be greater than for the 17-Hertz calibration, which, in turn, can be greater than the 25-Hertz calibration. This is confirmed by observing that the errors in the lateral forces at 15 Hertz, 17 Hertz, and 25 Hertz are 16.61 percent, 7.69 percent, and 4.47 percent, respectively.

A comparison of acceleration mobilities with and without the shakers attached to the model showed a greater difference for the lateral force than for the vertical force. An accelerometer on the tail section was selected for comparison purposes. This difference in mobility measurements explains why, at 17 Hertz, the vertical force calculations are biased on the low side while the lateral force calculations are biased on the high side. The calibrations for the vertical forces are higher with the shakers attached, and the calibrations for the lateral forces are lower. At 25 Hertz, this bias of the calculated forces is not nearly as noticeable since the effects of the lower resonance are no longer significant.

The influence of the shaker attachments on the method of force determination is primarily of academic interest. Under actual operating conditions, this boundary condition effect will not be present. The agreement between the known applied forces and the forces obtained via force determination is excellent, and consequently, a recalibration of the model to account for these artificial boundary conditions does not appear beneficial. It is immaterial whether the error is 7 percent or 4 percent since these differences are well within the range of measurement error. Of course, if this boundary condition anomaly had been worse, additional testing would have been recommended.

In order to minimize the effects of the shaker attachments, the 25-Hertz condition was selected for purposes of comparison between the nominal configuration and the mass change and center-of-gravity change configurations. At 25 Hertz, the acceleration mobilities of the suspended model and the acceleration mobilities with the shakers attached appear to be identical.

Weight Change Case - Tables 9 and 10

Any aircraft used in force determination would be dynamically calibrated by ground shake tests for the configuration to be flown. However, fuel burnoff in flight causes mass and vertical center-of-gravity changes that affect the dynamics of the ship. To help evaluate how much fuel burnoff can be tolerated for a given calibration, fuel burnoff was simulated by removing 3.75 pounds of steel weights from the lower fuselage near the center-of-gravity station. This represents a 7.8-percent change in the fuselage weight (without rotors). With 10 percent of a helicopter's total gross weight being the weight of the rotor and 12 percent of a typical helicopter's gross weight being the weight of the fuel, this

TABLE 9. CALIBRATION AT NOMINAL GROSS WEIGHT AND CENTER OF GRAVITY, FLIGHT AT CHANGED GROSS WEIGHT AND VERTICAL CENTER OF GRAVITY

25 Hz

Vertical Force Magnitude			Lateral Force Magnitude			Phase Angle		
Measured "Flight" Input (lb)	Calculated by Force Determination (lb)	Error (%)	Measured "Flight" Input (lb)	Calculated by Force Determination (lb)	Error (%)	Measured "Flight" Input (deg)	Calculated by Force Determination (deg)	Error (deg)
10	12.741	27.41	10	9.659	3.41	180	172.384	7.616
10	12.858	28.58	15	14.829	1.14	180	173.074	6.926
15	18.567	23.78	10	9.782	2.18	120	118.11	1.89
15	18.824	25.49	10	9.716	2.84	180	173.857	6.143
15	18.484	23.23	10	9.859	1.41	90	89.314	.686
15	18.219	21.46	10	10.182	1.82	45	45.989	.989
15	17.849	18.99	10	10.049	.99	0	.169	.169
Average Error		24.13%			1.97%			3.49°

TABLE 10. CALIBRATION AT CHANGED GROSS WEIGHT AND VERTICAL CENTER OF GRAVITY, FLIGHT AT CHANGED GROSS WEIGHT AND VERTICAL CENTER OF GRAVITY

25 Hz

Vertical Force Magnitude			Lateral Force Magnitude			Phase Angle		
Measured "Flight" Input (lb)	Calculated by Force Determination (lb)	Error (%)	Measured "Flight" Input (lb)	Calculated by Force Determination (lb)	Error (%)	Measured "Flight" Input (deg)	Calculated by Force Determination (deg)	Error (deg)
10	10.803	8.03%	10	9.774	2.26	180	175.796	3.412
10	10.821	8.21%	15	15.004	0	180	176.249	3.175
15	15.885	5.9%	10	9.769	2.31	120	120.834	2.724
15	16.023	6.82	10	9.814	1.86	180	177.534	3.677
15	15.893	5.95	10	9.835	1.65	90	91.531	2.217
15	15.774	4.96	10	10.229	2.29	45	47.922	1.933
15	15.51	3.4	10	10.198	1.98	0	2.378	2.209
Average Error		6.18%			1.76%			2.76°

weight change in the dynamic model represents about a 60-percent fuel burnoff.

Table 10 shows the results obtained with the calibration corrected for the change in weight due to fuel burnoff.

Center-of-Gravity Change Case - Tables 11 and 12

To give an indication of how much center-of-gravity shift should be allowed without calibrating for the shift in the shake test, the center of gravity of the dynamic model was shifted from the nominal 21.52-inch station to the 20.83-inch station for the same gross weight. This 3.25-percent change in the center-of-gravity station represented a shift from the nominal position to one of the extreme center-of-gravity positions in a typical helicopter and is more severe than one would actually allow without accounting for it in the shake test calibration. When the corrected calibration for the center-of-gravity shift was used, the results of Table 12 were obtained.

MODAL ACCELERATION FORCE DETERMINATION TEST RESULTS - NOSE SHAKING

Discussion

The purpose of these sets of tests was to demonstrate that force determination can be successfully accomplished without shaking at the conventional point of excitation, i.e, the hub. With modal acceleration testing, the engineer can calibrate the fuselage for any number of external forces by shaking at only one point, although it is advantageous to choose two or three shaking points to check the data's reliability, improve accuracy, and simplify the data reduction.

The shaking point or points for modal acceleration testing is a choice of convenience for the engineer. In the interests of maximum accuracy, the shaking point or points should have high driving point mobilities for the modes of consequence, a condition which also allows the use of relatively small shakers. Such points are commonly near the nose or tail of a helicopter.

Procedure

The nose of the helicopter dynamic model was chosen as the shaking point, although testing showed that the tail would have been almost equally suitable. The helicopter dynamic model was shaken both laterally and vertically to take advantage of the high degree of decoupling resulting from symmetry. The first and third modes showed up very strongly in the vertical driving point mobility plot at the nose, while the second mode was negligible. The second, fourth, fifth, and sixth modes had strong driving point responses at the nose in lateral shake, while the first and third modes were negligible.

AD-A035 960 KAMAN AEROSPACE CORP BLOOMFIELD CONN F/G 20/11
LABORATORY VERIFICATION OF FORCE DETERMINATION, A POTENTIAL TOO--ETC(U)
JAN 77 W G FLANNELLY, F D BARTLETT DAAJ02-75-C-0004
UNCLASSIFIED R-1457 USAAMRDL-TR-76-38 NL

2 OF 2
AD
A035960

END

DATE
FILMED
3-77

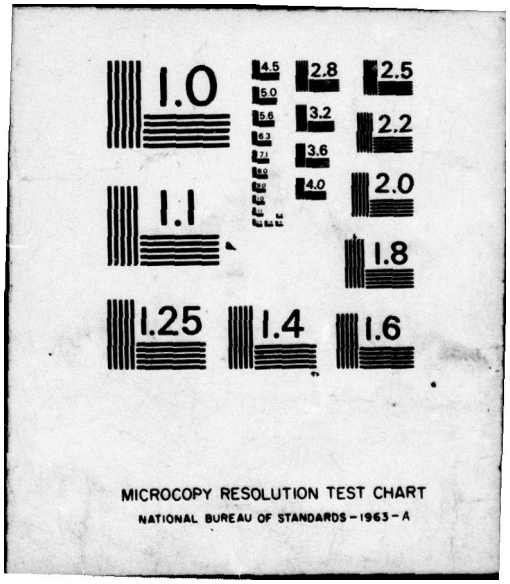
1.0
1.1
1.25
1.4
1.6
1.8
2.0
2.2
2.5
2.8
3.2
3.6
4.0
4.5
5.0
5.6
6.3
7.1
8.0
9.0
MICROCOPY RESOLUTION TEST CHART
NATIONAL BUREAU OF STANDARDS-1963-A

TABLE 11. CALIBRATION AT NOMINAL CENTER OF GRAVITY AND GROSS WEIGHT, FLIGHT AT SHIFTED CENTER OF GRAVITY AND NOMINAL GROSS WEIGHT

25 Hz

Vertical Force Magnitude			Lateral Force Magnitude			Phase Angle		
Measured "Flight" Input (lb)	Calculated by Force Determination (lb)	Error (%)	Measured "Flight" Input (lb)	Calculated by Force Determination (lb)	Error (%)	Measured "Flight" Input (deg)	Calculated by Force Determination (deg)	Error (deg)
10	12.487	24.87	10	10.001	0	180	173.819	6.181
10	12.601	26.0	15	14.67	2.2	180	173.416	6.584
15	18.603	24.02	10	10.186	1.86	120	114.585	5.415
15	18.386	22.57	10	9.509	4.91	180	174.216	5.784
15	18.213	21.42	10	10.18	1.8	90	85.788	4.212
15	18.100	20.67	10	10.416	4.16	45	42.152	2.848
15	17.584	17.23	10	10.623	6.23	0	-1.434	1.434
Average Error		22.4%			3.02%			4.64°

TABLE 12. CALIBRATION AT SHIFTED CENTER OF GRAVITY AND NOMINAL GROSS WEIGHT, FLIGHT AT SHIFTED CENTER OF GRAVITY AND NOMINAL GROSS WEIGHT

25 Hz

Vertical Force Magnitude			Lateral Force Magnitude			Phase Angle		
Measured "Flight" Input (lb)	Calculated by Force Determination (lb)	Error (%)	Measured "Flight" Input (lb)	Calculated by Force Determination (lb)	Error (%)	Measured "Flight" Input (deg)	Calculated by Force Determination (deg)	Error (deg)
10	10.716	7.2	10	9.654	3.46	180	173.819	6.181
10	10.766	7.7	15	14.458	3.60	180	173.416	6.584
15	16.05	7.0	10	9.838	1.62	120	114.585	5.415
15	15.80	5.4	10	9.447	5.53	180	174.216	5.784
15	15.753	5.0	10	10.057	0	90	85.788	4.212
15	15.687	4.58	10	10.18	1.80	45	42.152	2.848
15	15.335	2.23	10	10.318	3.18	0	-1.434	1.434
Average Error		5.59%			2.74%			4.64°

The modal accelerations for all 14 accelerometers, including the two at the hub, were determined using E-MASS for the vertical and lateral shake. The ratios of each to its driving point were compared to the other as a check on the validity of the data. For each of the 14 accelerometers, the modal accelerations and RACs (rigid body acceleration coefficients known from weight data) were fed into a Hewlett-Packard 2000F time-share computer using a telephone line. The mobility curves calculated by the computer using the modal accelerations and RACs were plotted on the time-share plotting terminal and compared to the actual test plot for each accelerometer as a check on the testing. The low-frequency asymptote of the measured mobility curve on the test x-y recorder was compared to the RAC, calculated from weights data, as still another check. Agreement was excellent for each case. These were done for both the vertical shake and the lateral shake during the course of the testing. In every mobility plot, the hysteretic damping coefficient, g, and the undamped natural frequency were determined for each mode.

The importance of using the on-site data checks described above was demonstrated early in these tests by the detection through these methods of seriously distorted signals from two of the 14 accelerometers. With conventional methods of testing, it is impossible to detect such false signals. The problem with the two accelerometers was corrected, and the tests on the helicopter dynamic model were continued.

Orthonormal Modes and Mobility Matrix

The orthonormal modal vector for each mode was formed using either the modal accelerations from the nose vertical shake or those from the nose lateral shake, depending on which had the larger driving point modal acceleration. In the first mode, for example, the vertical nose shake had a driving point modal acceleration of 11.69 in./lb-sec^2 while the lateral nose shake had a driving point modal acceleration of only 0.17 in./(lb-sec^2), so the vertical shake modal accelerations were used. The nose vertical station was designated "1". The first mode (I) orthonormal vector for any accelerometer j was found from Equation 20:

$$\psi_{jI} = \frac{A_{j1I}}{\sqrt{A_{11I}}} \quad \text{in.}^{1/2}/(\text{lb}^{1/2}\text{-sec})$$

As another example, the lateral driving point modal acceleration for the second mode was 13.05 in./(lb-sec^2) while the vertical was .227 in./(lb-sec^2), and of course, the modal accelerations for lateral nose shake were used in forming the orthonormal mode vector for the second mode:

$$\psi_{jII} = \frac{A_{j2II}}{\sqrt{A_{22II}}} \quad \text{in.}^{1/2}/(\text{lb}^{1/2}\text{-sec})$$

for the j-th accelerometer with nose lateral being designated as 2.

The orthonormal mode vectors for the first six modes in the helicopter dynamic model are shown in Table 13.

Of the 14 accelerometers, two were positioned for hub excitations, giving a 12x2 matrix of mobilities if the hub accelerometers were removed for flight. In an actual helicopter one would use as many as, but not more than, six accelerometers at the rotor hub during shake tests. The hub accelerometers would be removed before flight.

After calibration in the above manner, the helicopter dynamic model was "flown" as described earlier with simultaneous vertical and lateral hub forces of varying magnitudes and phasings, and the fuselage accelerations were recorded. These "flight" accelerations, premultiplied by the pseudo-inverse of the mobility matrix as shown above, give the force determinations of the magnitudes and phases of the forces applied to the hub in "flight". The force determination results are compared to the actual magnitudes and phasings of the hub forces applied in the "flights" in Table 14.

TABLE 13. ORTHONORMAL MODES

$(IN./LB\text{-}SEC^2)^{1/2}$

Mode Designation	I	II	III	IV	V	VI
Natural Frequency (Hz)	18.1	19.6	46.8	65.9	75.8	77.9
Accelerometer						
1	3.419	.562	-5.840	-.199	-.116	-.068
2	-.537	3.613	-1.873	4.254	1.683	2.833
3	1.174	.132	.429	0.000	.088	-.061
4	-.454	1.574	.043	-.320	-.055	-.359
5	-1.696	-.329	.799	.038	-.832	.538
6	.171	-1.837	-.126	.081	-.136	-.287
7	-1.956	-.045	-1.840	-.155	1.180	-.694
8	.626	-4.747	-.327	2.941	.027	.309
9	.088	-.081	-1.415	-.039	3.960	-3.009
10	.058	-.379	-.265	5.075	-.772	-5.160
11	2.291	.247	-.441	.025	3.422	-2.342
12	-.188	1.825	-.154	6.327	-1.455	-6.888
13	6.638	.883	1.463	-1.105	0.000	2.109
14	-.520	4.478	.307	-3.802	2.779	1.936

TABLE 14. MODAL ACCELERATION CALIBRATION AT NOMINAL GROSS WEIGHT AND CENTER OF GRAVITY, FLIGHT AT NOMINAL GROSS WEIGHT AND CENTER OF GRAVITY

Vertical Force Magnitude			Lateral Force Magnitude			Phase Angle		
Measured "Flight" Input (lb)	Calculated by Force Determination (lb)	Error (%)	Measured "Flight" Input (lb)	Calculated by Force Determination (lb)	Error (%)	Measured "Flight" Input (deg)	Calculated by Force Determination (deg)	Error (deg)
23.8	23.37	1.7	15.8	15.14	4.2	270	273.9	3.9
17.5	18.12	3.5	14.0	14.05	0.4	57	64.03	7.03
10.05	10.01	0	13.3	12.91	2.9	37	40.76	3.76
16.6	17.36	4.6	17.0	15.37	9.6	222	216.0	6.0
13.7	14.31	4.45	19.6	18.97	3.2	65	69.76	4.76
19.75	21.24	7.5	14.0	13.01	7.1	155	151.87	3.13
22.1	23.93	8.3	18.2	17.04	6.4	140	136.71	3.29
11.2	10.92	2.5	18.1	17.88	1.2	30	37.21	7.21
17.4	18.70	7.5	14.6	14.04	3.9	133	131.41	1.59
15.0	15.67	4.5	10.0	9.90	1.0	90	88.72	1.0
11.1	9.63	15.2	19.0	18.78	1.1	320	316.21	3.79
26.5	28.03	5.8	11.9	11.09	6.8	136	131.03	4.97
14.1	13.89	1.5	21.2	19.88	6.2	255	246.67	8.33
20.1	18.29	9.0	23.1	23.04	0.2	324	330.15	6.15
14.9	13.27	10.9	22.6	22.10	2.2	325	326.35	1.35
20.0	20.02	0	15.1	15.18	0.5	35	37.13	2.13
24.0	24.68	2.8	18.1	17.81	1.6	60	60.45	.45
18.9	21.83	14.7	24.4	23.31	4.5	149	142.5	6.5
13.0	14.02	7.9	13.1	12.2	6.9	195	186.38	8.62
23.1	22.72	1.6	11.4	11.18	2.0	290	295.15	5.15
11.4	11.50	0	16.5	15.97	3.2	56	59.35	3.35
20.1	20.42	1.6	15.3	14.57	4.8	256	256.5	0.5
14.6	15.7	7.5	16.3	16.06	1.5	71	75.95	4.95
21.0	21.38	1.5	22.8	21.15	7.2	240	232.2	7.80
Average		5.19%			3.69%			4.40°

The two columns of the matrix of mobilities at frequency ω relating the accelerometers to the hub in these dynamic model tests are given by:

$$\{\ddot{Y}_{j5}\} = \{E_{j5}\} + \sum_{i=Z+1}^{6} -\frac{\omega^2}{\Omega_i^2}\left[\frac{1 - \omega^2/\Omega_i^2 - ig_i}{(1 - \omega^2/\Omega_i^2)^2 + g_i^2}\right]\{\psi_j\}_i \psi_{5i}$$

and

$$\{\ddot{Y}_{j6}\} = \{E_{j6}\} + \sum_{i=Z+1}^{6} -\frac{\omega^2}{\Omega_i^2}\left[\frac{1 - \omega^2/\Omega_i^2 - ig_i}{(1 - \omega^2/\Omega_i^2)^2 + g_i^2}\right]\{\psi_j\}_i \psi_{6i}$$

for hub excitations designated 5 and 6.

FLIGHT APPLICATION OF FORCE DETERMINATION TO THE UH-1H

Force determination was used as an adjunct to another project, the flight evaluation of Kaman's Dynamic Antiresonant Vibration Isolator (DAVI). This project was also performed under contract for the Eustis Directorate, USAAMRDL. This particular application of force determination was necessarily rather crude, but the results were very revealing.

Prior to the installation of the DAVI rotor isolation system, the UH-1H test vehicle was flown for baseline vibration data, and the magnitudes and phases of accelerations in the fuselage were recorded. The standard UH-1H was also shake tested to obtain baseline mobility data. Six vertical and six fore-and-aft accelerometers were used in the baseline shake test and flight test to determine the two-per-rev vertical and longitudinal forces at the hub using the force determination method. Pitching and rolling moments were considered to be negligible because the UH-1 has a teetering rotor.

When the DAVI rotor isolation system was installed, the ship was shaken to determine the mobilities using the direct shake technique. The hub forces found through force determination for the standard UH-1H were then applied to the shake test mobilities on the DAVI-modified ship to predict the new flight vibrations with the DAVI. The comparison of these force determination predictions to actual flight results of the DAVI UH-1 is shown in Figure 19.

The force determination predictions correlate very well with flight data for the pilot's seat and the tail at all flight speeds from 20 to 120 knots. The correlations at the pilot's seat and the nose are excellent up to 80 knots. Beyond 80 knots, the force determination prediction and the flight measurements diverge. Force determination theory would suggest that this divergence is caused by a two-per-rev vertical vibratory force acting on the fuselage in flight. The copilot's seat and nose curves given by force determination prediction and by flight measurement indicate that this unknown, two-per-rev fuselage force becomes effective at about 80 knots and is a function of the forward speed of the ship. This suggests an aerodynamic excitation other than downwash.

These predictions from force determination led to the suspicion that the horizontal stabilizer, mounted on the tail boom and actuated by motions of the swashplate, was the excitation source. There is a two-per-rev relative motion on the horizontal stabilizer pitch control in both the DAVI-equipped aircraft and the conventional aircraft.

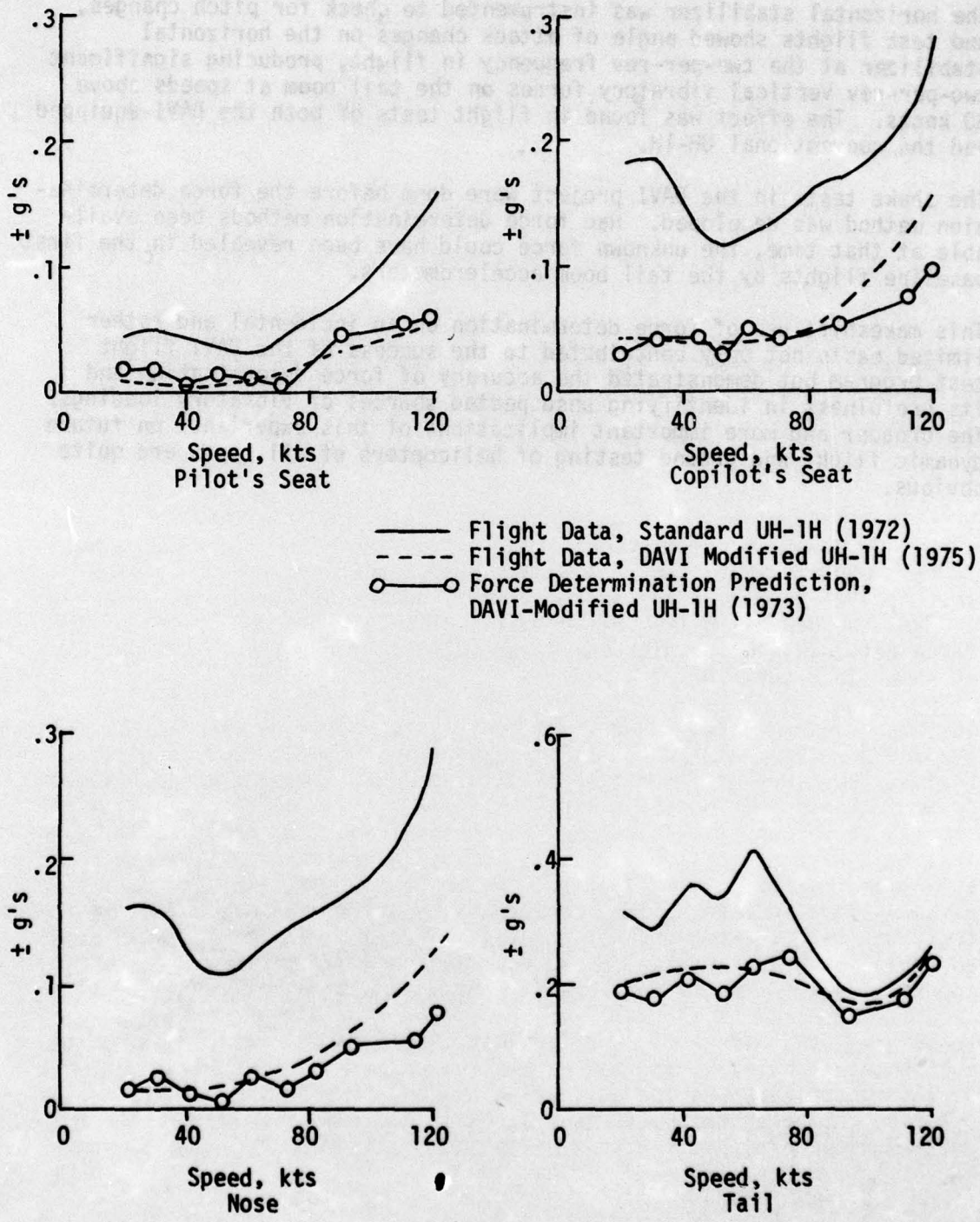

Figure 19. Two-Per-Rev Vertical Vibration on the UH-1H

The horizontal stabilizer was instrumented to check for pitch changes, and test flights showed angle of attack changes on the horizontal stabilizer at the two-per-rev frequency in flight, producing significant two-per-rev vertical vibratory forces on the tail boom at speeds above 80 knots. The effect was found in flight tests of both the DAVI-equipped and the conventional UH-1H.

The shake tests in the DAVI project were done before the force determination method was developed. Had force determination methods been available at that time, the unknown force could have been revealed in the first baseline flights by the tail boom accelerometers.

This makeshift use of force determination on an incidental and rather limited basis not only contributed to the success of the DAVI flight test program but demonstrated the accuracy of force determination and its usefulness in identifying unsuspected sources of vibratory loadings. The broader and more important implications of this experience on future dynamic flight and ground testing of helicopters of all types are quite obvious.

CONCLUSIONS

1. Force determination technology is sufficiently established to allow it to be fully demonstrated on a full-size helicopter to determine in-flight vibratory main rotor loads, tail rotor loads, aerodynamic surface loads and loads from external stores using only fuselage accelerometer data.

2. Using force determination flight test results, accelerated reliability testing on helicopter airframe and equipment in ground vibration tests can be done.

3. Force determination can be used to correlate the rotor loads predicted by rotor analysis computer programs with the rotor loads and ship vibrations actually measured in flight.

4. The methods of force determination can be employed in conjunction with rotor analysis computer programs to predict the vibration effects of a proposed new rotor on the fuselage and fuselage-mounted equipment, including engines and gearboxes. This may be done using flight test data on an existing aircraft or analytical mobility data on a proposed new aircraft fuselage.

5. In a ground vibration survey, it is not necessary to shake a helicopter at the hub or to apply moments at the hub. The data required can be acquired by shaking at one or more convenient points using modal acceleration testing.

6. Modal acceleration testing can be done with relatively small shakers and negligible tare positioned at high mobility points, commonly the nose and tail. This yields as much information as would shaking at every accelerometer location.

7. Modal acceleration testing yields the classical analytical normal modes and undamped natural frequencies needed for practical comparison to theory, as opposed to mere mobility ratios ordinarily found from shake tests.

REFERENCES

1. Veca, Angelo C., VIBRATION EFFECTS ON HELICOPTER RELIABILITY AND MAINTAINABILITY, Sikorsky Division, United Technologies Corporation; USAAMRDL Technical Report 73-11, Eustis Directorate, U. S. Army Air Mobility Research and Development Laboratory, Fort Eustis, Virginia, April 1973, AD 766307.

2. Flannelly, W. G., and Giansante, N., EXPERIMENTAL VERIFICATION OF SYSTEM IDENTIFICATION, Kaman Aerospace Corporation; USAAMRDL Technical Report 74-63, Eustis Directorate, U. S. Army Air Mobility Research and Development Laboratory, Fort Eustis, Virginia, August 1974, AD 784190.

3. Ormiston, R. A., COMPARISON OF SEVERAL METHODS FOR PREDICTING LOADS ON A HYPOTHETICAL HELICOPTER ROTOR, Proceedings of the Meeting of Specialists on Rotorcraft Dynamics, American Helicopter Society and Ames Research Center, Sponsors, 13-15 February 1974.

4. Coleman, R. P., and Feingold, A. M., THEORY OF SELF-EXCITED MECHANICAL OSCILLATIONS OF HELICOPTER ROTORS WITH HINGED BLADES, National Advisory Committee for Aeronautics Technical Note 3844, February 1957.

5. Cransdale, R., Gaukroger, D. R., and Skingle, C. W., A TECHNIQUE FOR MEASURING IMPEDANCES OF A SPINNING MODEL ROTOR, Royal Aircraft Establishment Technical Report 71092; Ministry of Defence, Farnborough Hants, England, May 1971.

6. Flannelly, W. G., Berman, A., and Giansante, N., RESEARCH ON STRUCTURAL DYNAMIC TESTING BY IMPEDANCE METHODS, Kaman Aerospace Corporation; USAAMRDL Technical Report 72-63A, B, C &D, U. S. Army Air Mobility Research and Development Laboratory, Fort Eustis, Virginia, November 1972, AD 756389, AD 756390, AD 756391, & AD 756392.

7. Rosanoff, R. A., and Ginsburg, T. A., MATRIX ERROR ANALYSIS FOR ENGINEERS, Proceedings of the Conference Held at Wright-Patterson Air Force Base, Ohio, 26-28 October 1965.

8. Singh, Jagjit, GREAT IDEAS IN INFORMATION THEORY, Language and Cybernetics, New York, Dover Publications, 1966.

9. Moore, E. H., GENERAL ANALYSIS, PART I, Social Security Administration, American Philosophical Society, Philadelphia, 1935.

10. Penrose, R., A GENERALIZED INVERSE FOR MATRICES, Proceedings of the Cambridge Philosophical Society, 51, 1955, pp 406-413.

11. Klosterman, A. L., and Lemon, J. R., DYNAMIC DESIGN ANALYSIS VIA THE BUILDING BLOCK APPROACH, Shock and Vibration Bulletin, 42(4), January 1972, pp 97-104.

REFERENCES (Continued)

12. Frazer, R. A., Duncan, W. J., and Collar, A. R., ELEMENTARY MATRICES, Cambridge, England, Syndics of the Cambridge University Press, 1938, reprinted 1965.

13. Soroka, W. W., NOTE ON THE RELATIONS BETWEEN VISCOUS AND STRUCTURAL DAMPING COEFFICIENTS, Journal of the Aeronautical Sciences, Volume 16, No. 7, July 1949, p 409.

14. Bartlett, Jr., F. D., and Flannelly, W. G., APPLICATION OF ANTI-RESONANCE THEORY TO HELICOPTERS, Journal of the American Helicopter Society, Volume 19, No. 1, January 1974, pp 11-15.

LIST OF SYMBOLS

a_i	i-th antiresonant frequency
a_{jxi}	i-th antiresonant frequency for response at j due to force at x
A_{jki}	modal acceleration of the i-th mode for response at j due to force at k - in./sec^2/lb
C_{EMASS}	E-MASS calibration constant defined in Page 60
E_{jk}	jk-th rigid-body acceleration coefficient - in./lb-sec^2
f	force - lb
g	structural damping coefficient; also acceleration of gravity - in./sec^2
g_i	structural damping coefficient of the i-th mode
i	imaginary operator, $\sqrt{-1}$
I	moment of inertia - lb-in.-sec^2
K	stiffness - lb/in.
K_A	accelerometer transducer calibration constant - g/volt
K_E	slope of E-MASS calibration curve - lb/g/Δs
K_F	force transducer constant - lb/volt
K_i^*	generalized stiffness of the i-th mode - lb/in.
Δm	mass - lb-sec^2/in.
M	mass - lb-sec^2/in.
M_x	moment around x axis - lb-in.
M_i^*	generalized mass of the i-th mode - lb-sec^2/in.
N	number of modes
p_{1_i}, p_{2_i}	frequency peaks defined in Page 36

LIST OF SYMBOLS (Continued)

R_A	accelerometer charge amplifier range setting
R_F	force charge amplifier range setting
ΔS	E-MASS potentiometer setting
U	product of inertia - lb-in.-sec^2
v_a	output voltage of accelerometer charge amplifier - volts
v_f	output voltage of force charge amplifier - volts
y	displacement - in.
$\ddot{y}$	vibratory acceleration - in./sec^2
$\ddot{Y}_{jk}$	acceleration mobility - in./lb-sec^2
$\ddot{Y}$	acceleration mobility - in./lb-sec^2
ΔY_{jk}	E-MASS acceleration mobility setting - in./lb-sec^2
Z	displacement impedance - lb-sec^2/in.
$\ddot{Z}$	acceleration impedance - lb-sec^2/in.
ΔZ_{jk}	impedance change - lb/in.
ϕ_{ji}	j-th element in the i-th normal mode
Φ	normal mode
ψ	orthonormal mode (in./lb-sec^2)$^{1/2}$
$\ddot{\theta}$	rotational acceleration - rad/sec^2
ψ_{ji}	j-th orthonormal mode element for i-th mode
ω	forcing frequency - rad/sec, Hz
Ω_i	i-th natural frequency - rad/sec, Hz

LIST OF SYMBOLS (Continued)

BRACKETS

[ ]	matrix
[↘]	diagonal matrix
[I]	identity matrix
{ }	column or row matrix

SUPERSCRIPTS

R	real
I	imaginary
-1	inverse
T	transpose
-T	inverse transpose
+	pseudoinverse
*	a modal parameter

SUBSCRIPTS

i	modal index
j	accelerometer index
k	accelerometer index
x	accelerometer index forcing station
q	generalized index
I,II & III	used as subscripts to modal accelerations

LIST OF SYMBOLS (Continued)

OTHER INDICES

N	number of degrees of freedom
J	number of generalized coordinates
HxF	capital letters under matrices indicate the number of rows and columns, respectively
..	dots over a quantity indicate differentiation with respect to time or a parameter related to differentiation with respect to time
Σ	summation symbol - indicates the sum of the indexed terms
Π	product symbol - indicates multiplication of the indexed terms